

**Flexural and Shear Response of Deteriorated Prestressed Concrete Girders Taken from a
Decommissioned Bridge in Alberta**

by

Zhaohan Wu

A thesis submitted in partial fulfillment of the requirements for the degree of

Master of Science

in

STRUCTURAL ENGINEERING

Department of Civil and Environmental Engineering

University of Alberta

© Zhaohan Wu, 2021

ABSTRACT

Prestressed concrete (PC) bridges are a major component of North America's transportation network. As this network ages, the response of deteriorated PC bridge girders is of interest since rehabilitation and repairs are constrained by limited infrastructure budgets. Bridges are often evaluated using a largely qualitative rating system which results in differences in opinions between evaluators. As part of a larger initiative to develop reliability-based bridge management tools for deteriorated structures, this thesis presents results and analysis from a series of full-scale destructive tests on a 28-year old PC bridge removed from service near Barrhead, Alberta.

There are many studies on PC girders, but these studies are limited to non-deteriorated systems, systems with accelerated deterioration (corrosion, debonding), non-destructive testing, and normal density concrete. The impact of deterioration on semi-lightweight PC girders subject to real-world environmental effects is rarely studied. Destructive testing was carried out on four 11 m single span, semi-lightweight PC voided slab girders taken from a decommissioned bridge with different types and degrees of deterioration. Both flexural and shear testing was conducted to provide insight on the deteriorated behaviour of the girders. Four-point bending was used for flexural test. Shear tests were conducted using three-point bending with different shear spans (1.0 m and 1.5 m). Modifications on some girders simulated further damage. Flexure tests indicated that all girders resisted the design factored load based on CSA S6:19 but no girders satisfied live load deflection limits of span/800. Deterioration significantly affected the flexural strength of the girders with a 23% decrease in strength for the most deteriorated girder relative to the baseline girder. More concerning, corrosion led to undesirable strand rupture failure prior to yielding which greatly reduced failure deflection. Material tests confirmed that strand corrosion greatly affected the strength and ductility of the strands.

Shear tests showed that shear span-to-depth ratio affected failure mode. All specimens with 1.0 m load scheme failed by strut crushing. For 1.5 m load scheme, girders in fair condition failed by shear compression. However, when stirrups were corroded, diagonal tension failure occurred leading to excessive yielding and wide cracks. Anchorage failure may occur when anchorage is inadequate leading to sudden failure from reinforcement or strand pull out. All girders performed well above design ULS loadings; deterioration did not greatly impact the peak load for the tested girders. However, deterioration affected events leading up to failure. Struts formed at a 29% lower load for 1.0 m load scheme and 32% lower load for 1.5 m load scheme due to induced prestressed strand loss, but the ultimate load only decreased by 9.6% and 9.9% for 1.0 and 1.5 m respectively. Anchorage failure resulted in the lowest peak load and sudden unexpected failure away from load point. Corrosion that leads to anchorage issues, such as end cracking, needs to be carefully examined by bridge inspectors.

After testing, forensic investigation found the average as-built concrete strength was 51% larger than the design value; four extra 25M bars were also discovered that were not included in the stock drawings for this bridge. These bars were initially added for camber control but served as a major backup system since corrosion was much more present in the strands. With updated material properties, CSA S6:19 accurately predicted the baseline girder capacity within 5% of the test value for flexure. CSA S6:19's sectional approach based on MCFT was conservative in predicting the shear capacity of the girders for both load schemes due to the assumption of plane sections remaining plane. Considering both flexural and shear results, it was concluded that the deteriorated PC girders were flexure dominant and safely resisted the design load at the time of testing.

ACKNOWLEDGEMENTS

The completion of this thesis would not have been possible without the support and guidance of many parties. Deepest gratitude for the support, help and guidance I received during this process and making the completion of this thesis possible.

First and foremost, I would like to acknowledge my **parents, Xiaoling Yao and Jiang Wu**. Everything that I am today would not be possible if it weren't for your endless sacrifices and unconditional love. You have worked tirelessly to support me in every way possible and helped me to achieve my dream of getting a higher education. You have put everything else second in order for me to study abroad and for that I can never repay you.

To my **grandfather**, who never saw this adventure, I have always carried your university dream with me deep in my heart. No matter how hard the times are, I can always pick myself up with you in my heart. This is for you and I hope you are proud.

To my **partner, Lucas Green**, thank you for being the most hardworking editor any writer can ask for. This thesis would not be possible without your late night revisions and endless reassurance and encouragement that all will be okay.

To my **loyal friend, K.O.**, thank you for your loving companion. I would never be able to finish this process in the brutal quarantine without you by my side.

To Alberta Transportation, thank you so much for funding my research (AT CON0020571) and providing this once in a lifetime opportunity for me to learn and grow. Thank you, John Alexander, the Director of Bridge Engineering at AT and Mike Tokar for your patient feedback and wise knowledge. This for sure has been quite a journey. I would also like to acknowledge our structural lab technicians, **Greg Miller and Cameron West**. My work would not have been possible without their help.

Most importantly, I want to thank my incredible **supervisors, Dr. Carlos Cruz Noguez and Dr. Douglas Tomlinson**. The journey had begun much before this master's degree. Because of your passion for teaching and structural engineering, I fell in love with the structural discipline which led me to this extraordinary opportunity. To Dr. Douglas Tomlinson, your endless structural knowledge has provided me guidance throughout the whole process. You are a living breathing design code; you always have an answer when I ask you difficult questions and for that I am forever thankful. Your passion in experimental research and good sense of humour have made this journey enjoyable. To Dr. Carlos Cruz Noguez, I am forever grateful for your reassurance, life advice, and endless encouragements; I would not have been able to complete this journey without them. You have built me up with your wise words and guided me through multiple hardships with your expertise. Thank you for always taking a couple minutes asking how I am doing. Thank you both for taking a chance on an international student fresh out of her undergraduate degree.

TABLE OF CONTENTS

ABSTRACT.....	ii
ACKNOWLEDGEMENTS.....	iv
TABLE OF CONTENTS.....	vi
LIST OF FIGURES	x
LIST OF TABLES.....	xv
CHAPTER 1 : INTRODUCTION	1
1.1 Background.....	1
1.2 Problem Statement and Motivation	2
1.3 Research Objective	4
1.4 Research Scope	5
1.5 Thesis Organization	5
CHAPTER 2 : LITERATURE REVIEW	6
2.1 Girder Bridge	6
2.1.1 Concerns	6
2.1.1.1 Concrete deterioration.....	7
2.1.1.2 Steel deterioration	10
2.2 Life and Safety	11
2.3 Prestressed Concrete	14
2.3.1 Service limit state.....	15
2.3.2 Ultimate limit state.....	16
2.4 Bridge Testing.....	17
2.4.1 Testing method: flexural test	18

2.4.2	Testing method: shear test	24
2.5	Research Gaps.....	29
CHAPTER 3	: FLEXURAL RESPONSE	30
3.1	Introduction.....	30
3.2	Experimental Program	35
3.2.1	Bridge description.....	35
3.2.2	Test girders.....	37
3.2.3	Materials	41
3.2.3.1	Concrete	41
3.2.3.2	Non-prestressed steel	44
3.2.3.3	Prestressing strands.....	47
3.2.4	Test setup and instrumentation	49
3.3	Results and Discussion	54
3.3.1	Load-deflection relationship.....	54
3.3.2	SLS performance and initial cracking.....	56
3.3.3	ULS performance.....	58
3.3.4	Failure	59
3.3.5	Comparison to design code predictions	61
3.4	Chapter conclusions	65
CHAPTER 4	: SHEAR RESPONSE	67
4.1	Introduction.....	67
4.2	Experimental Program	69
4.2.1	Testing rationale.....	69

4.2.2	Test girders.....	73
4.2.2.1	Girder LD-1	76
4.2.2.2	Girders HD-1 and HD-1.5.....	76
4.2.2.3	Girders MD-1.5 and MD-1.5S.....	78
4.2.2.4	Girders ID-1 and ID-1.5.....	79
4.2.3	Test setup and instrumentation	80
4.3	Results and Discussion	82
4.3.1	Load-deflection relationship.....	82
4.3.2	1.0 m load scheme.....	85
4.3.2.1	Initial cracking	85
4.3.2.2	Strut formation.....	85
4.3.2.3	Peak load.....	86
4.3.2.4	1.0-m loading scheme – summary of experimental performance.....	87
4.3.3	1.5 m load scheme.....	88
4.3.3.1	Initial cracking	88
4.3.3.2	Strut formation.....	88
4.3.3.3	Peak load.....	90
4.3.3.4	1.5-m loading scheme – summary of experimental performance.....	93
4.3.4	Comparison to design code predictions	93
4.4	Chapter Conclusion.....	97
CHAPTER 5 : SUMMARY AND CONCLUSIONS		100
5.1	Summary.....	100
5.2	Flexural Testing	100

5.3	Shear Testing	101
5.4	Recommendations.....	103
	REFERENCES	104

LIST OF FIGURES

Figure 2- 1: AASHTO/PCI standard products: box girder (left), voided slab (right) (PCI Design Manual,2011).....	6
Figure 2- 2: ASR within the concrete (darkened rim on granite gneiss and chert particles by ASR) (Lane, 1994).....	8
Figure 2- 3: ASR cracking on a bridge built in Czech Republic (Lukschová et al., 2008).	9
Figure 2- 4: Collapsed I-35W bridge in Minneapolis, MN (Gash, 2007).....	12
Figure 2- 5: Collapse of Lake View Drive bridge girder in 2005 (Panchak, 2005).	13
Figure 2- 6: The collapse of de la Concorde overpass (Mahoney, 2006).	14
Figure 2- 7: Four-point bending test setup (Pettigrew et al. 2016).	18
Figure 2- 8: The deterioration on the Walnut Street Bridge (a) Spalling of concrete cover (b) Ruptured prestressing strands hanging under the bridge into river (Shenoy and Frantz, 1991)...	19
Figure 2- 9: Load deflection curves (solid curves was the prediction calculated by strain compatibility method; factored and service load were calculated using 1989 AASHTO specification) (Shenoy and Frantz, 1991). Note: 1 kip = 4.45 kN, 1 in. = 25.4 mm.	19
Figure 2- 10: Load versus midspan deflection of the damaged and undamaged beams (Miller and Parekh, 1994).	21
Figure 2- 11: Accelerated corrosion setup and steel configurations for test beams (Malumbela et al., 2010).	22
Figure 2- 12: Three-point bending setup (Floyed et al., 2016).	24
Figure 2- 13: Shear failure of the prototype cantilever using the as built properties of the de la Concorde overpass (Johnson et al., 2007).	25
Figure 2- 14: Three- point bending test setup (Osborn et al., 2012).....	26

Figure 3- 1: Pitting corrosion of steel reinforcement used in concrete (Bertolini et al., 2004). ...	31
Figure 3- 2: Concrete section loss due to freeze and thaw damage (AT, 2017).	31
Figure 3- 3: Test setup used by Pessiki et al (1996) to determine cracking and decompression loads in prestressed ‘I’ girders. 1 foot = 305 mm, 1 inch = 25.4 mm (Pessiki et al., 1996).	32
Figure 3- 4: Four-point bending test setup (Pettigrew et al., 2016).	33
Figure 3- 5: Experimental and predicted load deflection curves from prestressed concrete girders tested by (Shenoy and Frantz, 1991). 1 kip = 4.45 kN, 1 inch = 25.4 mm.	34
Figure 3- 6: (a) Bridge being taken apart, (b) photo of heavily deteriorated girder.	36
Figure 3- 7: Cross section of test girders showing (a) general geometry and (b) reinforcement details. Stirrups not shown for clarity. All dimensions in mm.	37
Figure 3- 8: Girder conditions (a)Girder LD with no visible damage (b) Girder HD with severe concrete loss and steel corrosion (c)Girder MD with moderate deterioration (d) Girder ID with moderate deterioration and induced corrosion	39
Figure 3- 9: Deterioration mapping on the bottom of the specimens (a) Girder LD without any visible deterioration at 0% concrete spall (b) Girder HD had 70% overall concrete spall with both reinforcement and strand corrosion (c)Girder MD had 20% concrete loss with rebar corrosion and light strand corrosion (d) Girder LD had 20 % concrete loss with rebar corrosion and light strand corrosion.	40
Figure 3- 10: Induced (cut) strands loss in Girder ID.	40
Figure 3- 11: Stress Strain Curves from concrete cylinders extracted from the tested girders. ...	42
Figure 3- 12: (a) Extraction of rebar from Girder LD (b) Failed Girder MD with both types of bars visible (c) ‘X’ ribbing in Girder LD’s 25M bars and (d) ‘bamboo’ ribbing on 25M bars from other girders.	44

Figure 3- 13: Stress and strain curve from 10M bars (a)full curve for bamboo ribbed bars (b) zoomed in curve for bamboo ribbed bars showing elastic region and yield plateau (c) full curve for ‘x’ ribbed bars (d) zoomed in curve for ‘x’ ribbed bars showing elastic region and yield plateau, (b) X-ribbed. 46

Figure 3- 14: Stress and strain curves from longitudinal 25M bars (a) entire curve (b) zoomed in region showing elastic region and yield plateau. 47

Figure 3- 15: Stress and strain curve for prestressing seven wire strands. 48

Figure 3- 16: Test setup and instrumentation (a) Elevation view of test setup showing location of load points and instrumentation (b) Photo showing placement of sensors (c) photo showing overall girder in place. 50

Figure 3- 17: CL-W truck load (CSA S6:14, 2014)..... 51

Figure 3- 18: possible critical midspan moment cases using truck load (a) first three axle numbers of the truck are on the bridge girder (b) the heaviest axle (no.4) is located at midspan of the girder (Huang, 2020). 51

Figure 3- 19: Lane load considered (a) CL-W lane load (CSA S6:14,2014) (b) possible critical midspan moment (Huang, 2020)..... 52

Figure 3- 20: Load deflection curves. 54

Figure 3- 21: Deflected shapes at (a) SLS, (b) ULS, (c) failure. 55

Figure 3- 22: Failure modes of tested girders (a) Girder LD – concrete crushing, (b) Girder HD– strand rupture, and (c) Girder MD – concrete crushing, (d) Girder ID – strand rupture. 60

Figure 4- 1: Three- point bending test setup (Osborn et al., 2012)..... 68

Figure 4- 2: Three- point bending test setup. Dimensions in parenthesis are in mm. (Saqan and Frosch, 2009). 68

Figure 4- 3: Three- point bending test setup (Floyed et al., 2016).	69
Figure 4- 4: Truss analogy (Wight and MacGregor, 2012).	70
Figure 4- 5: Different types of shear failures (Sinha, 2002).	71
Figure 4- 6: A strut and tie model of a deep beam (Sinha, 2002).	72
Figure 4- 7: A strut and tie model of a deep beam (Kuo et al., 2010).	72
Figure 4- 8: Flexural girder cutting.....	74
Figure 4- 9: Shear girders from the original flexural girders and their deterioration mapping (a) LD-1 (b) HD-1.5 and HD-1.0 (c) MD-1.5S and MD-1.5 (d) ID-1.5 and LD-1.0.....	75
Figure 4- 10:Stirrups layout on the girder up to 1.5m load point.	75
Figure 4- 11: Girder LD-1 with no visible deterioration damage (a) tested shear span region (b) other end.....	76
Figure 4- 12: (a) Girder HD-1 and (b) Girder HD-1.5.....	77
Figure 4- 13: Location of deterioration on the tension side of Girder HD (a) midspan region of girder with most severe corrosion (b) strands in midspan region showing evidence of pitting corrosion (c) photo of single strand showing damage at midspan (d) significant spalling and reinforcement corrosion but limited strand corrosion for Girder HD-1 (e) significant spalling and reinforcement corrosion but limited strand corrosion for Girder HD-1.5.	78
Figure 4- 14: (a) Girder MD-1.5S (b) Girder MD-1.5.....	79
Figure 4- 15: Cut stirrups (cuts circled) on girder MD-1.5S. These stirrups had limited deterioration as evidenced by their colour and lack of pitting corrosion.	79
Figure 4- 16: (a) Girder LD-1, (b) Girder LD-1.5, and (c) Cut strands for Girder ID for induced deterioration.	80

Figure 4- 17: Test setup and instrumentation (a) Elevation view of test setup showing location of load points and instrumentation (b) Photo of test specimen.	81
Figure 4- 18: Grouting of girder end with damage (a) before grouting (b) after grouting.	81
Figure 4- 19: Load deflection curves for (a) tests with 1.0 m shear span and (b) tests with 1.5 m shear span.	83
Figure 4- 20: Strut formation on shear girders with diagonal cracking indicated with arrows (a) Girder LD-1 (b) Girder HD-1.	86
Figure 4- 21: Failure modes of shear girder with 1.0 m load scheme.	87
Figure 4- 22: Strut formation with crack location indicated by arrows (a) Girder MD-1.5S (b) Girder ID-1.5 (c) Girder HD-1.	90
Figure 4- 23: Failure modes of shear girders with 1.5m load scheme.	92

LIST OF TABLES

Table 2- 1: Normalized predicted capacity by different methods (Floyed et al., 2016).	27
Table 3- 1: Bridge condition rating system (AT, 2008).....	34
Table 3- 2: Bridge inspection rating and explanations (AT, 2016).	36
Table 3- 3: Test specimens.	39
Table 3- 4: Material properties of concrete for each specimen.	43
Table 3- 5: Material properties of rebar.	47
Table 3- 6: Material properties of prestressing 7 wire strands.....	49
Table 3- 7: General test results for each specimen.	55
Table 3- 8: Uncracked stiffness of each specimen and percentage of baseline.	56
Table 3- 9: Deflection of each specimen and percentage increase to the deflection limit.....	57
Table 3- 10: Girder ductility.	61
Table 3- 11: Test predictions comparison of crack and peak load compared to Girder LD.....	63
Table 3- 12: Test predictions comparison of uncracked stiffness.....	64
Table 4- 1: Test specimens for shear loading.	74
Table 4- 2: General test results.	84
Table 4- 3: Peak load of the shear girders and ratios to designed ULS.	88
Table 4- 4: Strut formation of the shear girders and ratios to designed ULS.	89
Table 4- 5: Peak load of shear girder and ratio to Designed ULS.	93
Table 4- 6: Material properties of the as tested shear girder.....	96
Table 4- 7: Shear resistances of different load schemes using CSA S6:19 (2019).....	97
Table 4- 8: Test prediction comparison.	97

CHAPTER 1 : INTRODUCTION

1.1 Background

The market share of prestressed concrete in bridges has grown from zero to about 50% since the 1950s (PCI, 2011) which makes prestressed concrete one of the major construction materials used for highway bridges. However, highway bridges are susceptible to both chemical attacks and extreme weather. The Canadian Infrastructure Report Card (CIRC) (2019) reported that 12% of Canadian bridges are in ‘poor’ or ‘very poor’ condition. This means that many of these bridges have deteriorated below acceptable limits and are approaching the end of their service life. About a quarter of the bridge inventory in Canada (26.3%) shows signs of deficiency due to deterioration and needs immediate attention (CIRC, 2019). The burden of maintenance, rehabilitation and placement of deteriorated bridges are a drain on the economy. For instance, an estimated \$123 billion was spent on bridge rehabilitation in the United States for 9.1% of their structural deficient bridges (ASCE, 2017).

Deteriorated bridges that are not properly maintained may fail catastrophically, causing loss of life and property, and hindering the operation of emergency and critical services in the case of collapse. The sudden collapse of de la Concorde highway bridge in Laval, Quebec killed five people and injured six in 2006. This bridge failed due to a combination of deterioration, faulty design, and construction (Johnson et al., 2007). The 2018 collapse of the Morandi Bridge in Genoa Italy killed 43 people and caused economic damage that took years to restore. The cause of failure was due to improper maintenance which overlooked corrosion of one of the cables (IDVIA, 2020). These incidents highlight the extreme importance of maintenance and the impact that deterioration has on bridges.

There is a large body of literature on experimental investigations of deteriorated prestressed concrete bridge girders. This non-exhaustive list includes Cullington and Raggett (1991), Shenoy and Frantz (1991), Rinaldi et al. (2010), Pape and Melchers (2013), Dasar et al. (2016), and Pettigrew (2016). Cullington and Raggett (1991) conducted destructive shear test on 30-year-old pretensioned without shear links I-beams. The authors found for regions without shear reinforcement, I-beams were more likely governed by web cracking failure. Shenoy and Frantz (1991) studied the remaining capacity of two 27-year-old PC box girders by conducting destructive flexural tests. The results showed ACI (1989) could accurately predict the behaviour of the girders using tested material properties. Rinaldi et al. (2010) tested nine artificially corroded prestressed concrete beams with different percentages of strand loss under four-point bending. The authors found the failure for corroded beams is governed by strand rupture and that corrosion significantly decreased the ultimate bearing capacity of the corroded beams. Pape and Melchers (2013) tested three prestressed concrete girders with different degrees of deterioration (two with corroded tendons and one with no visible damage) that were exposed to marine conditions in service. The results indicated that all girders failed below the expected design load and the capacity reduced linearly as tendon corrosion loss increased which led to the conclusion that the possibility of progressive collapse should be considered for older prestressed concrete bridge girder under marine conditions. Pettigrew (2016) found that deck thickness affects the accuracy of the design prediction by testing the remaining flexural capacity of double tee light weight prestressed concrete bridge girders.

1.2 Problem Statement and Motivation

Albertan bridges are inspected by bridge evaluators and they are assigned a rating on a 1-9 numerical system. A rating of 1 means the bridge needs immediate action and 9 means the bridge

is in pristine condition (Alberta Transportation, 2008). Using visual procedures to assign ratings is highly variable since inspections are affected by multiple factors such as the physical condition of the inspector (e.g. rest, peripheral visual acuity) affecting how they can complete the job, environmental factors (e.g. wind, noises, snow), and management factors where the inspection speed, and social pressure (working in pairs) have direct correlation of how well the inspection is completed (Moore et al., 2001). This variability means that visual inspections alone are not likely to identify or detect deterioration for which the inspection is prescribed, and it is challenging to detect deterioration that beyond the ones that already been identified or easily visualized (Moore et al., 2001); therefore, inspections may not be enough to truly reflect the remaining capacity. Studying deterioration effects on these bridges can help correlate the types of damages to how they affect bridge capacity which helps transportation ministries better evaluate bridges with similar deterioration.

There have been many studies focused on the experimental testing of prestressed concrete girders (Cullington and Raggett (1991), Shenoy and Frantz (1991), Rinaldi et al. (2010), Pape and Melchers (2013), Dasar et al. (2016), and Pettigrew (2016)). The majority of the studies investigated the remaining capacity of girders by destructive testing and comparing experimental results with values predicted by design codes. There was rarely a control girder from the same bridge examined to investigate the behaviour change from deterioration effect. Most studies also focused on normal density concrete and hollow boxed girders, but there are no studies, to my knowledge, that investigates semi-lightweight voided slab prestressed concrete bridge girders.

Recently, a prestressed concrete bridge (called the “Tiger Lily Bridge”) built in 1990 and located near Barrhead, Alberta was decommissioned in 2018 due to severe concrete spalling and steel corrosion. The bridge consisted of nine, 11 m long, rectangular semi-lightweight prestressed

concrete voided slab girders without topping, connected by five steel shear connectors on either side of the girders. The rapid deterioration of the Tiger Lily Bridge raises concerns on whether similar bridges will soon face similar structural deficiencies. The girders from the Tiger Lily Bridge constitute a valuable opportunity to investigate the deterioration effects experimentally, in terms of the residual girder strength, which led to the decommissioning of the bridge at such an early age.

1.3 Research Objective

The goal of this research project is to evaluate the current load carrying capacity and failure modes of single span, voided slab, prestressed concrete bridge girders with different types and degrees of deterioration to provide insight on the cause and effects of deterioration on the Tiger Lily Bridge.

To achieve the objective, the following tasks and subtasks need to be completed:

Task 1: Conduct a literature review on relevant studies of the flexural and shear response in deteriorated prestressed and reinforced concrete girders;

Task 2: Design a test setup to perform flexural and shear tests on full size bridge girders.

Task 3: Conduct flexural and shear tests on bridge girders with different degrees of deterioration to record and analyze the relationship between deterioration, girder capacity, and failure mode.

Subtask 3.1: Collect samples of concrete, reinforcement, and prestressing steel from each girder and test these samples according to relevant ASTM standards.

Subtask 3.2: Evaluate the flexural performance of the girders using destructive testing.

Subtask 3.3: Evaluate the shear performance of the girders using destructive testing.

Subtask 3.4: Compare experimental results to predictions from the S6:19 bridge code

1.4 Research Scope

The scope of this thesis is limited to the static experimental assessment of the corroded girders taken from the Tiger Lily Bridge, in terms of the flexural and shear response. Other researchers are completing analytical and reliability analyses of this bridge. Specific measurements of chemical attack such as chloride contents in concrete were not investigated. This study's results and conclusions are limited to bridges with similar design with similar concrete and steel material properties. Suggestions for repair and maintenance of these bridge girders are not included in this thesis. The behaviour of prestressed concrete bridges with similar designs is uncertain if the material properties (for instance concrete density) of the bridge are different.

1.5 Thesis Organization

This thesis consists of chapters as follows:

Chapter 1: Introduction to the research program and outline of objective and scope.

Chapter 2: A review of literature on flexural and shear testing of corroded prestressed and reinforced concrete beams and girders. Chapter 2 discusses Task 1.

Chapter 3: Experimental data and analysis from a series of flexural tests on the girders that investigates the deterioration effect on girder stiffness, cracking moment, capacity, and failure mode. Chapter 3 discusses part of Task 2 and 3, Task 4.1, Task 4.2, and part of Task 4.4.

Chapter 4: Experimental data and analysis from a series of shear tests on the girders that investigates the deterioration effect on girder capacity and failure mode under two different loading arrangements. Chapter 4 discusses the remainder of Tasks 2 and 3, Task 4.3, and part of Task 4.4.

Chapter 5: Conclusions of the research program are presented.

CHAPTER 2 : LITERATURE REVIEW

2.1 Girder Bridge

Reinforced/prestressed concrete roadway bridges are an important component of North America's transportation network. Girder bridges are the most common highway bridge in the United States. The majority of bridges span less than 50 m, rarely exceeding 150 m. Girder bridges are popular because they have greater stiffness and subject to fewer vibrations (Barker and Puckett, 2013). In North America, most highway bridges have spans less than 30 m. In the United States, 90% of roadway bridges have spans less than 30.5 m and 67% of these bridges have spans ranging between 6.1 m to 18.3 m (Hurd, 1985). There are several types of short-span concrete bridge girders in terms of their cross-section geometry – such as box shaped, voided slab, or solid rectangular. Box-shaped and voided slab girders are primarily used as prestressed members in small span bridges (Figure 2-1). These girders are placed side by side and connected with shear keys that allow for transverse load sharing.

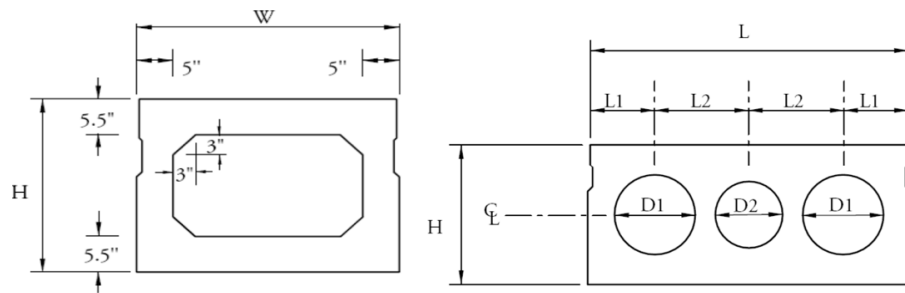


Figure 2- 1: AASHTO/PCI standard products: box girder (left), voided slab (right) (PCI Design Manual,2011).

2.1.1 Concerns

Since bridges are required to withstand the environment they are in for decades, quantifying the remaining service life of a bridge is of great concern to transportation ministries to keep the pedestrians or drivers using the bridge safe. Deterioration is inevitable over the service life of bridges, especially in regions like Canada where the climate is cold, and salts and other adverse

chemicals are often used to reduce ice formation. Over 30% of the existing bridge inventory in the United States is well past its service life and maintenance/repair needs of these structures are growing exponentially (Federal Highway Administration, 2018). An estimated \$267 billion per year (3.1% of the 1998 U.S. Gross Domestic Product) is required, according to the United States Department of Transportation, to repair deteriorated bridges (Koch et al., 2002). Based on 2019 data, 12.4 % of Canadian bridge stock is in ‘poor’ or ‘very poor’ condition, which means that many bridges are near or beyond their service life (CIRC, 2019). Another 26.3% are in fair condition, meaning these bridges require rehabilitation due to deterioration and deficiencies in the medium to long term (CIRC, 2019). Bridge deterioration is an urgent issue because of the pressure on public safety and the sometimes limited financial resources of jurisdictions where these bridges are located.

2.1.1.1 Concrete deterioration

Concrete acts as a both a physical and chemical protective layer to reinforcement. Concrete has a notable strength under compression, but it is relatively weak in tension. Multiple factors affect concrete properties and promote crack formation/development, such as weather or chemical attacks. Once cracks form, corrosion agents can penetrate concrete and reach reinforcement easier which leads to deterioration.

Temperature change is a highly adverse factor for concrete durability. The freeze/thaw durability of reinforced concrete is closely related to its pore structure. As water and moisture enter into concrete pores, the volumetric expansion of water (9%) when it freezes exerts pressure on pore walls. Once the transverse stress from this pressure exceeds the concrete tensile strength, the pore will crack and rupture. This leads to a cascading effect where water further infiltrates pores and eventually causes larger scale damage such as scaling or spalling with multiple

freeze/thaw cycles. Freeze/thaw cycles are of particular concern in structures located in cold regions such as Canada.

Alkali aggregate reactions occur when the reactive silica in concrete aggregates react with alkali hydroxides in the mix, causing expansion and cracking over time. There are two types of alkali aggregate reactions: alkali-silica reaction (ASR) and alkali-carbonate reaction (ACR). ASR is common when aggregates contain reactive silica materials. These silica materials react with alkali hydroxide in the concrete to form gel around the aggregates. This occurs when water from the cement paste or overall environment (humidity, rain) is absorbed. If the aggregate is composed entirely with reactive silica, the surface of the aggregate may quick react with the alkaline pore solution to form ASR gel (darkened rim) at the surface as indicated in Figure 2-2 (Rajabipour et al., 2015).



Figure 2- 2: ASR within the concrete (darkened rim on granite gneiss and chert particles by ASR) (Lane, 1994).

Gel formed around aggregates swells and causes the concrete to expand and eventually form a map-like cracking pattern. Figure 2-3 shows Lukschová et al. (2008) inspected a bridge that was repaired in the late 1990s due to extensive signs of ASR, finding severe map-like cracking by ASR.

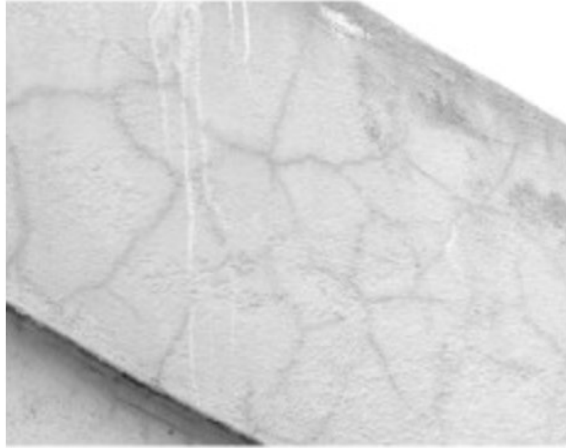


Figure 2- 3: ASR cracking on a bridge built in Czech Republic (Lukschová et al., 2008).

Alkali carbonated reaction (ACR) is a reaction between dolomitic limestone aggregate, and hydroxide ions called dedolomitization. The alkali reacts with dolomite in the aggregates causing production of brucite and calcite. Brucite production is responsible for the volume expansion due to absorption of water which leads to concrete cracking. ACR is not as common as ASR and less understood, although it is known that the time frame for damage caused by ACR is much shorter than ASR (Thomas et al., 2013).

Both ASR and ACR are identified by petrographic identification performed by examining the chemical and physical features of concrete samples from a thin slice retrieved from the specimen. This could both be done macro or microscopically. Lukschová et al (2009) investigated samples from ASR affected bridges built between 1924 and 1982 in the Czech Republic. They used optical microscopy to observe thin sections of the bridges. Alkali silica gel was clearly formed by microcracks forming reaction rims when aggregate fragments contact the cement paste. They also found quartzite and greywacke, two different types of coarse aggregates that are critical to control ASR. Lahdensivu et al. (2018) found that ASR affected the tensile strength of the concrete; 33%

of the tested materials had varied tensile strength from 0.27 to 3.50 MPa instead of the required 1.50 MPa. Authors stated that advanced ASR affects the bearing capacity of the bridge over time.

2.1.1.2 Steel deterioration

Concrete initially protects reinforcement from damage, but the concrete's permeability allows harmful ions such as chloride to penetrate and reach the reinforcement over time. In colder countries such as Canada, chlorides are often introduced via de-icing salts. De-icing salts normally contain chlorides as a freezing point depressant. According to the U.S. Geological Survey (Bolen and Barnes, 2016), the United States used 20.3 million tons of de-icing salt in 2016. The most common de-icing salt is sodium chloride. Chloride ions from these salts penetrate into concrete over time with this rate increased when combined with freeze/thaw cracking. Chloride ingress initiates corrosion when it reaches the reinforcement. The passivity of steel reinforcement initially prevents corrosion through an oxidation layer that forms on the reinforcement perimeter due to the concrete's alkaline environment. However, once chloride ions reach the reinforcement, they 'eat away' the passive layer, producing an acid that eventually corrodes (oxidizes) reinforcement. Oxidation creates iron oxide (i.e., rust) which has a larger volume than the original steel. This increased volume creates tensile stress on surrounding concrete and eventually causes concrete spalling. After concrete spalls, steel is increasingly exposed and susceptible to even more severe corrosion. Eventually, section loss of steel reinforcement leads to significant loss of strength which requires costly replacement or repair.

There are methods that help to prolong the life of bridges by delaying the deterioration effect on the girders. Corrosion resistant reinforcement such as fibre reinforced polymer (FRP) bars or stainless steel is often implemented in delaying the corrosion effect; However, due to the relatively

high cost of these materials (Nürnberg, 1996), they are almost never used for construction of short span prestressed concrete girder bridges.

2.2 Life and Safety

As time goes by, bridges in service deteriorate due to environmental exposures and their capacities will be affected by the damage. Deterioration effects on bridge girders need to be addressed properly or the potential failure due to structural deficiency could lead to loss of life or financial burden.

On August 1, 2007, the I-35W Bridge over the Mississippi River in Minneapolis collapsed killing 13 people and injured 145. There were many factors contributing to the failure of this eight-lane concrete deck steel truss arched bridge which includes insufficient design where the gusset plate had inadequate capacity due to incorrect calculation and deterioration which eventually caused the bridge's collapse when one of the gusset plates failed due to inadequate capacity (National Transportation Safety Board, 2008). In addition to the lives lost, the collapse of the bridge interrupted 140,000 daily traffic crossings and disturbed traffic flow in the area which generated significant economic loss due to longer traffic hours, distance, and higher congestion volumes (Zhu and Levinson, 2010). \$400,000 daily were estimated to be lost by the Minnesota Department of Transportation due to rerouting travellers and commercial vehicles alone. Goodwin (1977) argued that previous experience is crucial for traveller decisions, so the collapse of the I-35W could potential cause travel pattern change which eventually results ongoing capital loss from disturbed traffic flow. Zhu and Levinson (2010) indicated that total number of river crossing trips dropped 6.3% and that only 3.1% were restored after a replacement bridge was opened.



Figure 2- 4: Collapsed I-35W bridge in Minneapolis, MN (Gash, 2007).

In 2005, a 16.2 m long prestressed concrete girder weighing 60 tons of the Lake View Drive Bridge in Pennsylvania failed under service. This bridge was built in the late 1950s and, before one of its beams failed, an inspection team gave this overpass a score of 4 out of 10 indicating structural deficiency. Post-failure inspections showed that 39 out of 60 prestressing strands had corrosion-induced failure. There was also heavy concrete spalling and strand corrosion on the bottom flange of the voided box girder. Naito et al. (2006) evaluated the failed beam and found that the construction generally met design requirements, but the bottom flange cover was 60% thinner than required and the thickness of the bottom flange 15% was smaller than the designed value. Inadequate cover could have induced premature strand corrosion. Additionally, vent holes in the girder's top flange were not indicated on shop drawings and did not align with drain holes used for rainfall drainage leading to half of the void being filled with water, adding significant superimposed loading on the girder. Additionally, high chloride levels were measured in the water which would induce reinforcement corrosion. Due to the thinner cover, the chloride was able to

corrode the bottom strand layer. Fortunately, only minor injuries were sustained during the failure but an estimated 60,000 vehicles per day were redirected due to the collapse.



Figure 2- 5: Collapse of Lake View Drive bridge girder in 2005 (Panchak, 2005).

The infamous collapse of de la Concorde overpass in Laval that killed five people and injured six was investigated by the Commission of Quebec (Johnson et al., 2007). They found that bridge collapsed via shear failure because of a combination of faulty design, deterioration, and construction errors. Rebar in the failure region was misplaced and the concrete strength of the 36-year old bridge was barely 27.6 MPa at the time of collapse which suggest strength at 28 days back in 1970 was most probably lower due to the fact that concrete keeps on gaining strength over time. This bridge was built in 1970s using an innovative technique by resting the box girders on a beam seat continuously over the entire width of the bridge without intermediate support; However, this resulted the beam seat being directly under the expansion joints which makes the seats vulnerable to water runoff, debris, and road salt. The worst part of the design was that the seat was impossible to access without lifting the girder meaning that inspections could not evaluate deterioration and that these seats could not be repaired without major expense. These seats are not allowed under the current CSA S6 bridge code. Rebar on the upper part near the end of the cantilever did not prevent propagation of the crack plane. Researchers later tested a cantilever girder with the same

properties as the failed one, under the same load at the time of collapse, finding that even with these design and construction errors the cantilever would have safely resisted the load without deterioration (Johnson et al., 2007). The collapse of the de la Concorde was a tragedy and is an important lesson that teaches engineers and researchers how deterioration and inadequate design can have catastrophic effect.

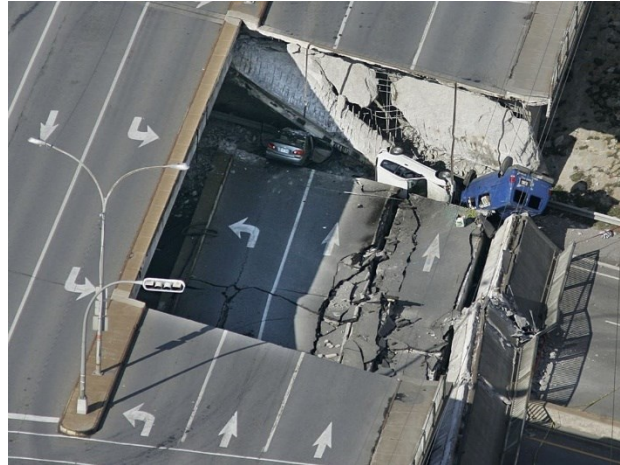


Figure 2- 6: The collapse of de la Concorde overpass (Mahoney, 2006).

2.3 Prestressed Concrete

Prestressed concrete is often preferred for bridge girders over typical reinforced concrete due to its enhanced serviceability performance and service life. Prestressing allows for a reduction of concrete volume used in construction and makes prestressed concrete more cost-effective than typical reinforced concrete. Once in service, prestressed concrete bridges should require very little operating cost when designed according to the Canadian Bridge Design Code specification (CPCI, 2017); Comparing with steel bridges, the repainting of a steel bridge alone would cost 10 to 20% of the initial cost (CPCI, 2017).

In prestressed concrete members, compression stresses are induced through the use of special reinforcement types and processes before the external loads are applied, with the purpose (usually)

of ensuring that the concrete section remains uncracked under service loads. A common form of prestressing is by tensioning high strength steel strands within the concrete member. Prestressed concrete is grouped into two categories. Pretensioning consists of stressing strands in tension in formwork before casting concrete. Concrete is poured and once it hardens, the strand ends are cut from their supports and compression is transferred into concrete, which prevents the strands from relaxing. Post-tensioning consists of tensioning steel tendons that are installed inside a hollow duct left in an already hardened member.

2.3.1 Service limit state

Serviceability limit states (SLS) are in place to ensure that structures have a satisfactory performance in terms of the limit states that they encounter under typical loads in their service life (such as deformation, vibration, etc.). Serviceability often controls when prestressed concrete bridges are properly designed (Nowak and El-Hor, 1995); therefore, being able to assess the deflection and camber of a prestressed member are very important. Time dependent creep and shrinkage are major influences on the deflection and camber of prestressed concrete. Creep is the gradual increase of strain in concrete when it is subjected to compressive stress over of time. Shrinkage is the contraction occurring in concrete as it dries and hardens due to moisture loss from evaporation. Like creep, shrinkage also increases with time but is related more so to environmental effects like humidity.

Camber control is important for prestressed concrete members. Camber deformations occur immediately upon the transfer of the prestressing force. After prestress transfer, the camber increases with time, primarily caused by concrete creep of the concrete. Excessive camber can cause cracking therefore the cracking can give water borne contaminants a route to deteriorate the concrete and steel reinforcement (Jayaseelan and Russell, 2007). To control camber and cracking

of prestress concrete girders, additional non-prestressed reinforcement can be placed into the section of the girder that experiences compression from the camber.

Deflection is another serviceability concern. Deflection of a bridge is a combination of short and long term effects from eccentric prestressing force, self-weight, sustained, and live load. Creep and shrinkage affect the long term deflection of a bridge since it is a time dependent phenomenon. Long term deflection can be predicted using design specifications to prevent excessive deflection; however, the design codes tend to underestimate the result due to the fact that the behaviour of creep and shrinkage is complicated and sometimes the effect of the creep and shrinkage is overlooked by the codes (Birhane et al., 2020). Excessive deflections can cause cracking which leads to loss of stiffness, causing a larger deflection at mid span and eventually leading to corrosion. Tsukiyono Bridge, a prestressed concrete hinged bridge with hollow cross section in Gunma Prefecture, Japan had deflections three times larger than predicted by the design code after 25 years in service. Ohno et al. (2012) modelled the Tsukiyono Bridge, along with three other bridges with similar shapes and spans to investigate the cause of the excessive deflection. The authors found the long-term time dependent deflection caused by delayed drying shrinkage of the concrete accounted approximately 25 to 45% of the total deflection of the bridge and hence must not be neglected in design. The excessive creep deflection was due to design predicted deflection by Japan Road Association Code grossly underestimated the deflection as it did not consider the coupling between different types of creeps (mechanical and hygro-thermal creep).

2.3.2 Ultimate limit state

Ultimate limit states include material or stability failures that compromise the safety of the member when the structure is subjected to overloading at some point in its life. For prestressed concrete girders, the main failure modes to consider are flexural and shear failures. Flexural failure occurs

when internal bending moments cause material failure from either concrete crushing or reinforcement rupture. In well-designed reinforced concrete members, reinforcement yields before concrete reaches its ultimate failure strain (i.e. crushes) to ensure that there is adequate ductility and warning of failure. Compared to flexural failures, shear failures are far more sudden. Therefore, well-designed members should have a higher capacity to resist shear than flexure.

An important factor that affects the mechanism of shear in a member is the span to depth (a/d) ratio. As the a/d ratio decreases, so-called “deep beam” behaviour governs member response. CSA S6:19 (2019) considers a structure a deep beam when the a/d ratio is less than two. For deep beams, a large amount of load is transferred to supports by compression struts connecting the load and the support reaction. This means that the strain distribution is no longer linear, and shear typically dominates within the region. Shear failure of a deep beam is often caused by diagonal compression failure or by strut crushing. In diagonal tension failure, an inclined crack first forms along the line joining the support and the load point. Later, cracks form parallel to the first crack and finally the structure fails when the concrete between the two cracks crushes. Strut crushing consists of the development of high compressive forces in the concrete struts, which eventually exceeding their compressive capacity. Another failure type not exclusive for deep beam but often occurring is anchorage failure due to the high stress near the support. CSA S6 Clause 8.10.3.2 (2019) indicates where anchorage condition is influenced by the cross-sectional area of the strut; However, if the design is inadequate, the longitudinal reinforcement and strands could pull out and cause anchorage failure.

2.4 Bridge Testing

Destructive testing can be used to better understand how deterioration affects the structural response of bridges and to assess their residual load-carrying capacity. These tests may study the

material properties of concrete and reinforcement used in the bridge in addition to studying their response under flexure and shear demands.

2.4.1 Testing method: flexural test

Flexural tests are widely used to analyze the response of bridge girders under bending moments. A typical 4-point bending setup is shown in Figure 2-7. A stiff spreader beam distributes load from an actuator to the test specimen to create a region under constant moment and zero shear near midspan. Flexural testing determines the moment resistance of the test specimen, related failure modes (e.g. concrete crushing in compression, reinforcement rupture or pulling out), member properties (e.g. flexural stiffness), and also how deterioration affects different part of the member.

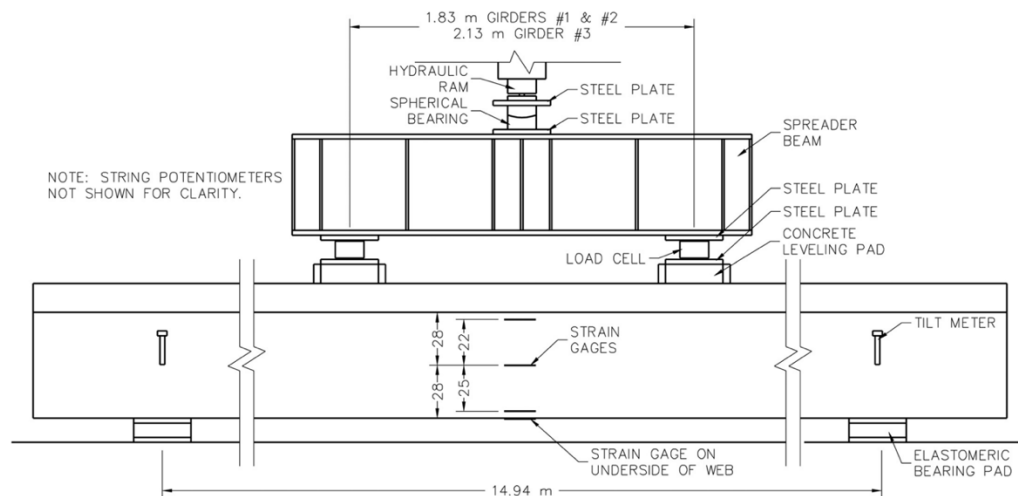


Figure 2- 7: Four-point bending test setup (Pettigrew et al. 2016).

Shenoy and Frantz (1991) studied 27-year old prestressed concrete bridge girders from the Walnut Street Bridge built in 1960 in East Hartford, Connecticut. Bridges from this era were built without waterproofing membranes and at risk of corrosion in the from de-icing salt run-off penetrating into concrete. The beams in the worst condition had significant concrete spalling and exhibited ruptured prestressing strands due to corrosion (Figure 2-8)

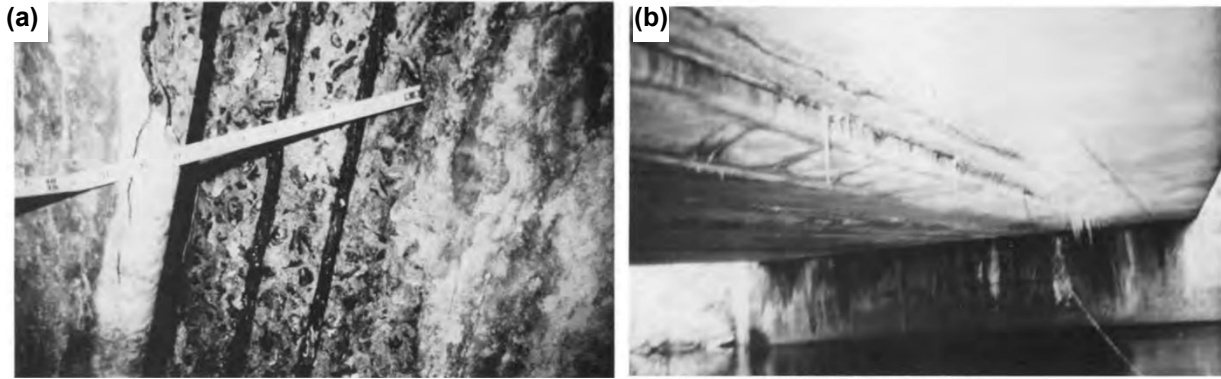


Figure 2- 8: The deterioration on the Walnut Street Bridge (a) Spalling of concrete cover (b) Ruptured prestressing strands hanging under the bridge into river (Shenoy and Frantz, 1991).

Two 17-m long box beams were tested under four-point bending at third points, monitoring load, and midspan deflection. One beam had moderate staining on both sides from water leakage from shear keys without visible damage. The other beam had severe staining and sign of minor cracking and spalling on one side while the other side only showed moderate staining. For both beams, despite the deterioration, flexural cracking was first observed at approximately twice the 1989 AASHTO service limit and the ultimate load of the two beams (223 kN and 213kN) also greatly exceeded the required factored load (156 kN) using 1989 AASHTO specification (Figure 2-9). The higher strength is attributed to these members being designed to carry a heavier live load of 80% of an HS-20 truck wheel load which is different than the AASHTO specification in 1989, but the strain compatibility method could accurately the behaviour as shown in Figure 2-9.

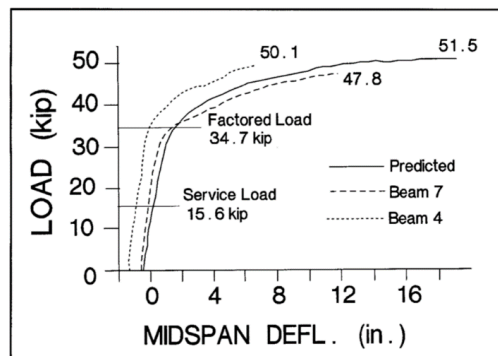


Figure 2- 9: Load deflection curves (solid curves was the prediction calculated by strain compatibility method; factored and service load were calculated using 1989 AASHTO specification) (Shenoy and Frantz, 1991). Note: 1 kip = 4.45 kN, 1 in. = 25.4 mm.

Pettigrew et al. (2016) investigated the behaviour of a 48-year-old double-tee lightweight concrete (1790 kg/m^3) bridge girders taken from a decommissioned 15.5 m, single-span bridge in Utah. Part of the study focused on evaluating the remaining flexural strength of these girders using destructive four-point loading (Figure 2-7). The girders were simply supported on top of elastomeric bearing pads with a span of 14.94 m, the point loads on the girder was spaced 1.83 m apart. All girders had the same failure mode: web concrete cracking followed by deck crushing in the constant moment region. The authors further investigated the effect of deck deterioration by calculating the flexural capacity using the entire deck thickness and then repeated using half-deck thickness. The AASHTO LRFD approximate method (2012) overestimated flexural capacity by 26.2% and 12.5% respectively for nominal full- and half- deck thickness comparing to the measured capacity. This difference was reduced to 24.1% and 11.6% when strain compatibility method was used. The authors believe that overestimation is due to the deck deterioration reducing the capacity of the compressive block.

Miller and Parekh (1994) conducted a destructive test on a deteriorated sidewalk support beam from a bridge over the Maumee River in Ohio. The deteriorated corner of the beam had concrete spalling from strand corrosion. Three of 18 strands had severe corrosion: one strand was broken and missing along most of the beam length while the other two had broken at various places. The authors also cast a beam with same dimension and cross section as the deteriorated beam and tested it under the same setup to investigating the effect of deterioration. The 23.3 m long beams were tested under four point bending with loads applied 8.5 m from either end. The undamaged beam failed with steel yielding, no strands ruptured, and no lateral deflection noted. The damaged beam failed very suddenly and the exact cause of failure could not be determined. The deteriorated beam had lower pre-cracked stiffness and a 20% lower cracking load compared to the undamaged beam

(Figure 2-10). The authors believed the lower values were due to a combination of prestress loss and loss of cross-sectional area due to corrosion, but prestress loss could not be estimated because of the sudden failure. The damaged beam also experienced a relatively large (28 mm) lateral deflection because the deterioration caused asymmetry of the strands and cross section. The authors recommended adding transverse post tensioning which ties the beams together and can help resist the lateral deflection.

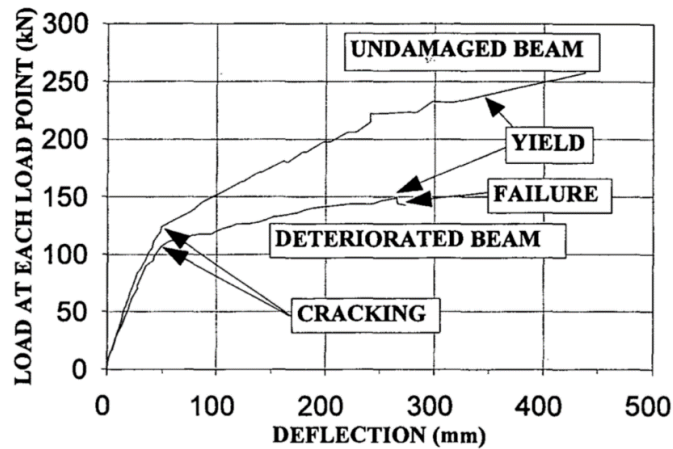


Figure 2-10: Load versus midspan deflection of the damaged and undamaged beams (Miller and Parekh, 1994).

Naito et al. (2008) investigated the cause of deterioration on six prestressed box girders from a bridge that was in service for 12 years. Upon inspection, the girders had several cracks at the supports (pier and abutment). These cracks included flexural shear, flexural, and web shear cracks with majority of the larger cracks extending from the bottom flange. One girder with severe cracking was used for forensic investigation, and it was found that the measured web and the bottom flange dimensions were 15% smaller than the specified dimension at various locations. The authors also found that concrete extracted from the girder showed deficiency of intermediate and finer aggregates sizes. The concrete compressive strength was also 33% larger than the specified 28-day strength. Another girder was tested twice under three-point bending test on both

ends (pier and abutment) 3.56 m away from the supports subjecting the girder to both flexural and shear demands. The goal was to generate positive moments in the damaged region observed from the inspection to evaluate the strand bond condition. Both tests showed early slipping of the strands but the failure mode was strand rupture which indicates that bond strength was sufficient even with the early slipping.

Malumbela et al. (2010) investigated the variation of mass loss of rebar due to deterioration in reinforced concrete beams. Nine beams with a dimension of 153×254×3000 mm were cast. These ‘virgin’ beams were then put under sustained loading up to 12 % of the expected ultimate load capacity. The three tensile reinforcing bars of the beam were then artificially corroded locally at around midspan for a length of 700 mm by placing this region into a 5% NaCl solution combined with an impressed current and different wet and dry cycles (Figure 2-11).

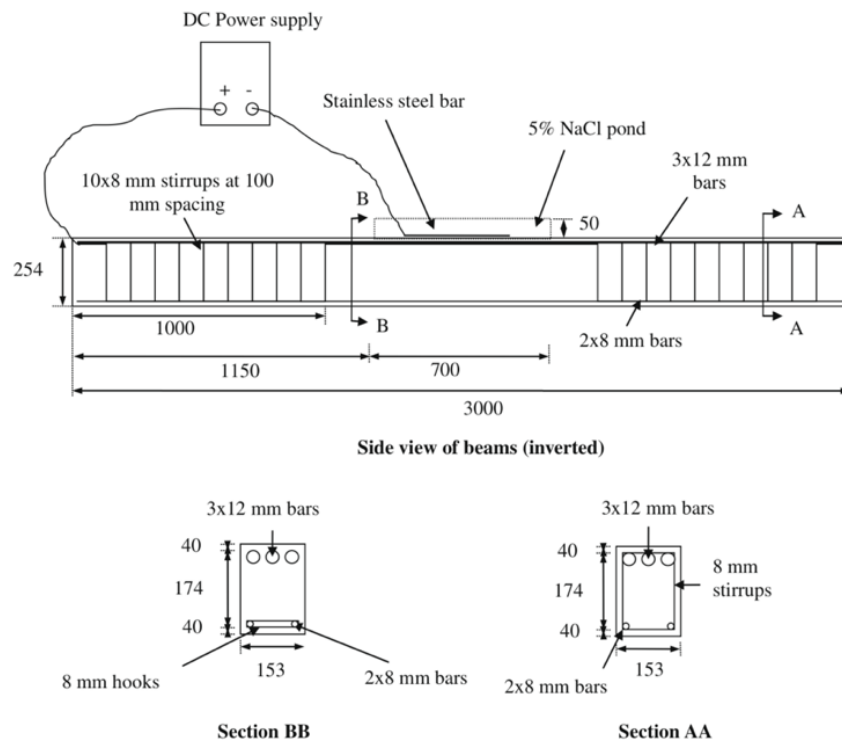


Figure 2- 11: Accelerated corrosion setup and steel configurations for test beams (Malumbela et al., 2010).

The test beams were then loaded to failure under four-point bending with a constant moment region of 1000 mm. The failed beams were then broken to remove corroded reinforcement at least 150 mm beyond the region of corrosion to measure mass loss. Very little corrosion was observed at the end of the corrosion region, highlighting how corrosion can be concentrated at various points along a member. The authors believe that this was due to the fact that concrete at the end region was confined by stirrups helping to reduce crack widths. This result is consistent with the work of Badawi and Soudki (2005) and Soudki and Sherwood (2000) that mass loss of steel is reduced by lateral confinement. Corrosion was most severe on the centre bar. The authors' understanding is that the location of the crack allowed more corrosion agents to penetrate the centre bar compared to the exterior bars. For the ultimate capacity, the test indicated that ultimate moment capacity reduced linearly with corrosion level at a rate of 0.7% for every 1.0% maximum loss of reinforcement area. The failure location was also very close to the region where maximum mass of loss of reinforcement occurred.

There are many studies that evaluated prestressed concrete girder flexural capacity experimentally. Girders with different shapes such as hollow box girder (Naito et al., 2008; Shenoy and Frantz, 1991; Miller and Parekh, 1994) or tee shaped girder (Pettigrew et al., 2016) or girders with different material properties such as lightweight concrete (Pettigrew et al., 2016) were examined and tested under bending. Full-scale testing was often conducted with specimens subjected to increasing monotonic loads until failure (Shenoy and Frantz, 1991; Miller and Parekh, 1994; Pettigrew et al., 2016; Naito et al., 2008).

Sometimes, researchers conduct small scale tests with newly casted beams that did not experience any live loads. These beams can be artificially corroded to investigate deterioration effects (Malumbela et al., 2010). The majority of these studies quantify deterioration effect by

investigating member residual capacity and comparing it with code specifications. However, sometimes code specifications used for comparisons are different than those used when the bridge was built which could lead to inconsistencies in predictions. Shenoy and Frantz's result (1991) was double the calculated 1989 AASHTO specification due to differences in bridge design in 1950s using a lighter design truck. Testing a baseline girder on top of a deteriorated girder test by casting a new girder helps investigate the deterioration effect in a more accurate way (Miller and Parekh, 1994); however, sometimes it is hard to control the material properties (28-day concrete compressive strength or yield and ultimate strength of steel bars and strands) to be exactly the same as the 'as tested' material properties from the bridge girder. This approach may also be impractical for evaluating larger prestressed girders from the research expense and lab capability perspectives.

2.4.2 Testing method: shear test

Shear behaviour needs to be studied to investigate whether deterioration would cause undesired shear failures. Shear test setups create a shear-critical region in the specimen by applying loads near supports. This region is subject to large shear forces and small moments and simulates wheel loading near girder ends. A typical setup is shown in Figure 2-12 with a simply supported girder and point load on top (Floyed et al., 2016). Shear tests allow the study of mechanisms such as diagonal tension cracking, diagonal compression failure, and reinforcement dowel action.

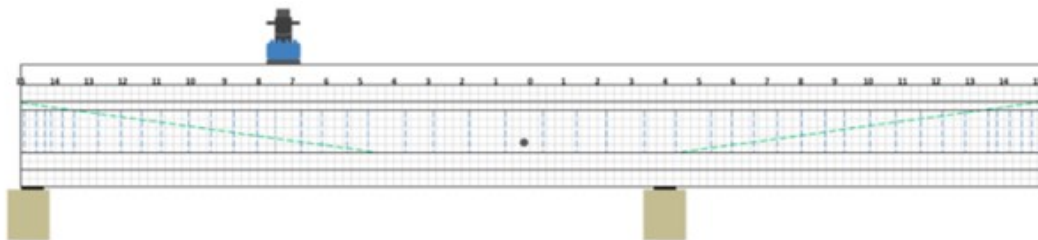


Figure 2- 12: Three-point bending setup (Floyed et al., 2016).

The collapse of de la Concorde overpass in Laval is unfortunate proof that shows the importance of understanding the shear behaviour of deteriorated girders. This overpass collapsed due to shear failure because of a combination of faulty design, deterioration and construction errors (Johnson et al., 2007). Laboratory testing of a specimen constructed with the as-built properties of this bridge without deterioration showed an explosive and sudden shear failure. A horizontal crack at the upper part of the slab extended up to the diagonal bars. This crack later turned into inclined shear crack propagating downward through the slab and created the similar horizontal crack around the lower rebar splitting the member (Figure 2-13). The prototype without deterioration was able to resist loading present on the overpass when it collapsed which indicates that deterioration played a decisive role on load carrying capacity.



Figure 2- 13: Shear failure of the prototype cantilever using the as built properties of the de la Concorde overpass (Johnson et al., 2007).

Osborn et al. (2012) investigated the near support shear capacity of two types of deteriorated AASHTO Type II bridge girders that were in service for around 40 years (Figure 2-14). Girders were prestressed and either 7.1 m or 10.5 m long. These girders were tested under three-point bending with shear spans kept at 1.22 m, with the exception of one girder tested with a shear span of 1.31 m. Results showed that the more deteriorated the girder, the more difficult it was to predict shear response. They found that AASHTO LRFD (2009) predictions were conservative, estimating

between 28% to 55% of the ultimate shear capacity due to the code's assumption of plane sections remaining plane. Strut and tie models more accurately predicted the strength of the tested girders within 2% to 22% of the average measured value Osborn et al. (2012).



Figure 2- 14: Three- point bending test setup (Osborn et al., 2012).

Saqan and Frosch (2009) tested a series of prestressed concrete beams investigating the influence of mild steel bars and prestressing strands on the shear behaviour. The test program consisted of three series of beams. One beam was reinforced with prestressing strands only, whereas the other two were constructed with specific cross-sectional area of steel bars. The test specimens were tested under three-point bending with a constant a/d ratio of 3.33. Results showed that reinforcement had minimal effect on cracking load because concrete primarily controls this portion of the response. Increasing the number of prestressing strands increased the concrete contribution to shear strength and that increasing the number of mild steel bars has a similar effect.

Floyed et al. (2016) investigated the effect deterioration had on two AASHTO Type II bridge girders with corrosion at the ends that were 9.75 m and 14 m long. One girder was prestressed with six straight 12.7 mm strands and four harped strands. The other was prestressed with ten straight strands and six harped ones. Both girders were tested under three-point bending until failure with a/d ratios of 2.0 and 2.5 (Figure 2-12). End corrosion contributed to strand anchorage failure due to bond loss from corrosion and this effect should be considered as an important aspect for

evaluating shear capacities of old bridges. The authors used multiple methods of calculating the shear strength of the girders to investigate the accuracy and conservatism of the methods (Table 2-1). The AASHTO LRFD simplified method (2012) overpredicted the shear capacity of the tested girders while the AASHTO LRFD general method was the most conservative. ACI 318 and AASHTO Modified Compression Field Theory (MCFT) were the most accurate methods predicting shear capacity of the test girders.

Table 2- 1: Normalized predicted capacity by different methods (Floyed et al., 2016).

Method	Average normalized capacity	Coefficient of variation
1973-STD	1.16	9.83%
ACI	1.01	12.1%
2012-SIMP	1.24	8.93%
2012-GEN	0.533	5.01%
2004-AASHTO	0.857	8.44%

Murray (2019) conducted similar experiments on two decommissioned AASHTO Type II bridge girders (9.1 and 14 m respectively) with deterioration on girder ends. Girders were supported at one end with the other end overhanging to avoid damage so that each end could be tested under shear loading. The first girder had a shear span to depth (a/d) ratio of 2.5 and 2.0 whereas the second girder had an a/d ratio of 3.0 and 3.83. Girders with a/d ratios of 2.5 and 3.0 failed in bond shear. The authors believe strands slipping was an anchorage issue caused by cracking from corrosion at the ends. Cracking by corrosion affected the bearing of the girder which led to increased cracking and spalling of concrete. This cracking can become a serious serviceability issue for girders that are still in service and exhibit similar levels of deterioration. The authors found that the AASHTO LRFD modified compression field theory (MCFT) using β - θ expressions was the most conservative with a ratio of 1.23, whereas MCFT using the β - θ table was the most accurate with a ratio of 1.03.

These studies suggested that shear behaviour of a deteriorated girder is crucial to be examined on top of flexural behaviour because material deterioration caused by time, chemical attack, and adverse environmental conditions can reduce shear capacity and lead to tragic events such as the collapse of de la Concorde. However, few studies have focused on the shear behaviour of bridge girders due to the fact that well-designed reinforced or prestressed concrete girders should be able to attain their flexural strength before failing in shear. Shear testing, typically performed under three point bending with load applied close to supports, can be either full scale or small-scale testing depends on the availability of the bridge girders (Johnson et al., 2007; Murray,2019; Floyed et al., 2016; Osborn et al., 2012). Full-scale testing reflects the true structural performance of a specimen over a long period of time but real bridge girders rarely become available for testing. Sometimes researchers use small scale tests with artificial corrosion or changes to find the correlations more accurately since they have more control and knowledge about the degree of deterioration. Many studies used code specifications to predict girder shear capacity (Saqan and Frosch, 2009; Murray,2019; Floyed et al., 2016; Osborn et al., 2012) but code specifications vary and sometimes provide inconsistent results. Osborn et al. (2012) stated that strut and tie led to more accurate result for short shear span girder than the AASHTO LRFD (2009) specifications based on strain compatibility. Testing a control girder helps eliminate this problem and identifies the effect of deterioration more accurately. Often, girders with similar material properties as deteriorated girders was casted and tested; data from this girder is then used as a baseline to investigate the deterioration effect on shear capacity. For instance, laboratory tests on a prototype de la Concorde cantilever with as built properties but without deterioration indicated that the cantilever was in good condition would not fail under the same loading at the time of the collapse (Johnson et al., 2007).

2.5 Research Gaps

Although the majority of existing studies focused on the general behaviour of bridge girders and whether the code's predictions were accurate compared to experimental testing (Shenoy and Frantz, 1991; Pettigrew et al., 2016; Naito et al., 2008; Osborn, 2010; Murray, 2019; Floyed et al., 2016), there was rarely a control girder from the same bridge examined to investigate the behaviour changes from the effect of deterioration. There is also a lack of investigation for both flexural and shear behaviour of severe deteriorated bridge girders which poses concerns on whether an investigated bridge will have sufficient residual strength if only one of the mechanisms is examined. Some researchers have investigated specific deterioration effects on bridge members; however, many focused on either newly casted or small-scale beams instead of real life bridge girders (Malumbela et al., 2010).

Most experimental programs in the literature focus on normal or high-performance concrete used for box or I-shaped girders, while no known studies are available regarding deterioration effects on semi-lightweight prestressed concrete voided slab girders. More research is needed to investigate how different types of deterioration affects the behaviour of light weight prestressed concrete bridge girders. To address this research gap, this thesis investigates the deterioration effect on four full scale semi-lightweight prestressed concrete voided slab bridge girders take from a bridge decommissioned after 28 years in service. These girders were studied under both flexural and shear load effects. The girders in the best rated condition was used as a control for both flexural and shear on top of code predictions to provide a more accurate finding on the deterioration effect of the girders.

CHAPTER 3 : FLEXURAL RESPONSE

3.1 Introduction

Prestressed concrete has advantages over conventional reinforced concrete because of its enhanced stiffness under service loads, which allows for cost-effective cross sections and longer spans. Structural deficiencies during construction or from deterioration are also generally fewer in prestressed concrete bridges than in steel or timber bridges (Dunker and Rabbat, 1995). Prestressed concrete was introduced in the 1950s – nowadays, prestressed concrete bridges constitute more than 50 percent of the bridge inventory in North America, with the most common bridge type being multiple box girder assemblies (Dunker and Rabbat, 1992). Short span bridges outnumber long span bridges – nearly two-thirds have a span in the range of 6 to 18 m (Hurd, 1985).

However, just like with conventional reinforced concrete, prestressed concrete is prone to chemical attacks. The rate of bridge deterioration has accelerated drastically over the past 40 years due to the increased use of deicing salts in winter (Ramseyer and Kang, 2012) combined with the aging of existing infrastructure. Other chemical reactions such as chloride penetration, sulphate attack, or alkali-aggregate reaction are also common causes of concrete deterioration (Hobbs, 1988). Environmental effects such as freeze-thaw cycles cause concrete cracking and spalling. As the concrete spalls, rebar and strands come under attack from corrosion. Bridge deterioration is a serious issue that creates significant public safety concerns as well as economic burdens.

Deterioration occurs under aggressive environments that are conducive to chloride penetration. Chloride penetration happens when the structure is exposed to saltwater or de-icing chemicals. Chlorides penetrate through the concrete or via thin cracks to eventually reach reinforcement.

Brownish bleeding stains on the outer surface of the structure caused by the chloride corrosion product, FeCl_3 , are indicators of chloride induced corrosion. Pitting corrosion, shown in Figure 3-1, is a localized and difficult to detect form of corrosion that results in significant reinforcement cross-section loss. Pitting corrosion is associated with prolonged chloride induced corrosion concentrated in small regions from chemicals accumulated inside the pit (Bertolini et al., 2004).

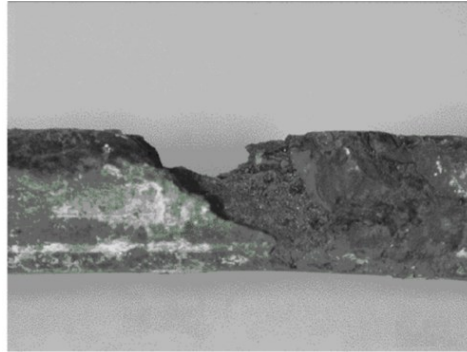


Figure 3- 1: Pitting corrosion of steel reinforcement used in concrete (Bertolini et al., 2004).

Another type of deterioration is caused by freeze-thaw cycling. Deterioration occurs when water volume in concrete pores increases due to freezing, which induces tensile stresses in concrete around the freezing water. This leads to a cascading effect where water further infiltrates these pores and eventually causes damage such as scaling or spalling after undergoing multiple freeze-thaw cycles as shown in Figure 3- 2.



Figure 3- 2: Concrete section loss due to freeze and thaw damage (AT, 2017).

The residual capacity of deteriorated bridges can be determined effectively through testing. Pessiki et al (1996) studied the prestress loss in the strands of two full scale “I” shaped prestressed concrete bridge beams after 28 years in service. Each beam was first loaded a series of flexural cracks formed. These cracks were tracked by cable transducers and strain gauges. Later these beams were repeatedly loaded in a quasistatic manner using the same instrumentation to track crack opening and determine the decompression load (Figure 3-3). The authors found an average prestress loss of 18% for the beams, while design specifications (AASHTO, 1992) only predicted a prestress loss of 10.8%.

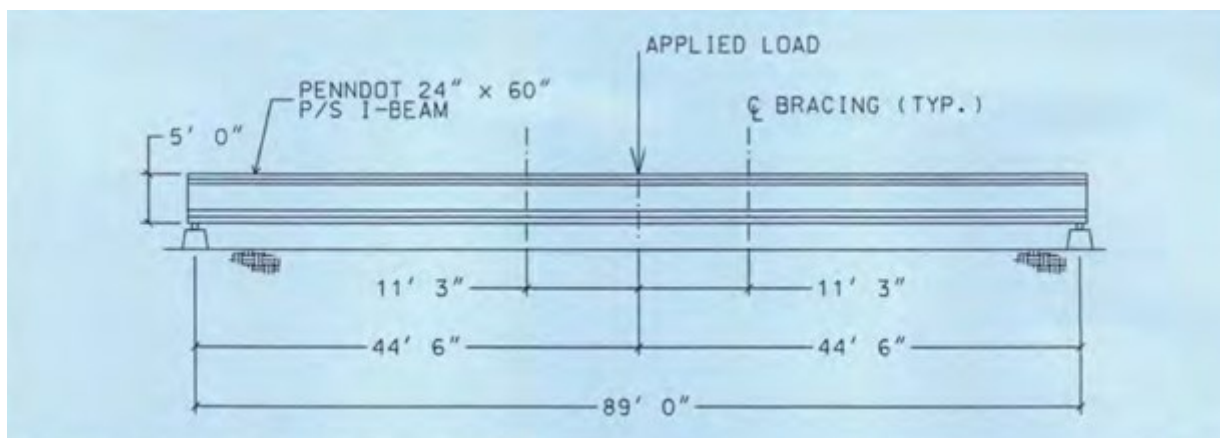


Figure 3- 3: Test setup used by Pessiki et al (1996) to determine cracking and decompression loads in prestressed ‘I’ girders. 1 foot = 305 mm, 1 inch = 25.4 mm (Pessiki et al., 1996).

Pettigrew et al. (2016) tested three 48-year old prestressed double-tee light weight concrete bridge girders with an average unit weight of concrete of 17.6 kN/m^3 (1790 kg/m^3). These girders exhibited localized deterioration and some exposed rebar. The girders were tested under four-point bending to study their residual flexural capacity by performing four-point flexural tests as illustrated in Figure 3-4. The authors found that the AASHTO LRFD approximate method (2012) overestimated girder flexural capacity by 26.2 and 12.5% respectively for using nominal full- and half-deck thickness in the calculation comparing to the measured capacity. This difference was

reduced to 24.1% and 11.6% when strain compatibility was used for the same calculation. The authors believe that the overestimation is due to the deck deterioration reducing the capacity of the compressive block.

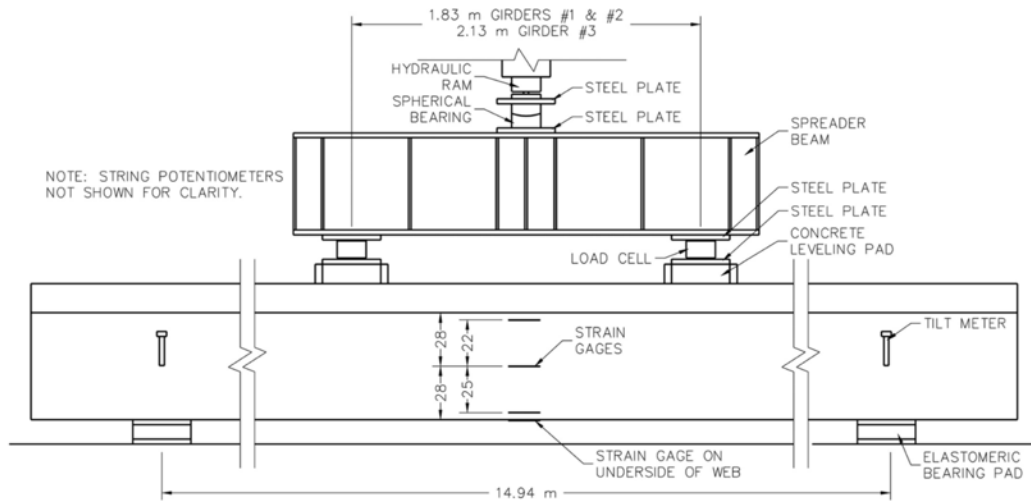


Figure 3- 4: Four-point bending test setup (Pettigrew et al., 2016).

Shenoy and Frantz (1991) tested two 16.5 m long, 27-year old deteriorated prestressed concrete bridge girders, studying their residual strength through four-point bending. Results, shown in Figure 3-5, indicate that flexural cracking was first observed at approximately twice the 1989 AASHTO service limit. The results also show that the girders exceeded the required flexural strength at factored load using 1989 AASHTO specification. The reason for the extra capacity was attributed to design procedures in the 1950s, which were based on the live load of 80% of an HS-20 truck wheel load – this led to higher demands than the design trucks in the 1989 AASHTO specification. Based on the author’s predictions using strain compatibility, the uncracked stiffness, cracking moment, and peak load were well predicted but the tested girders had considerably lower ductility than predicted.

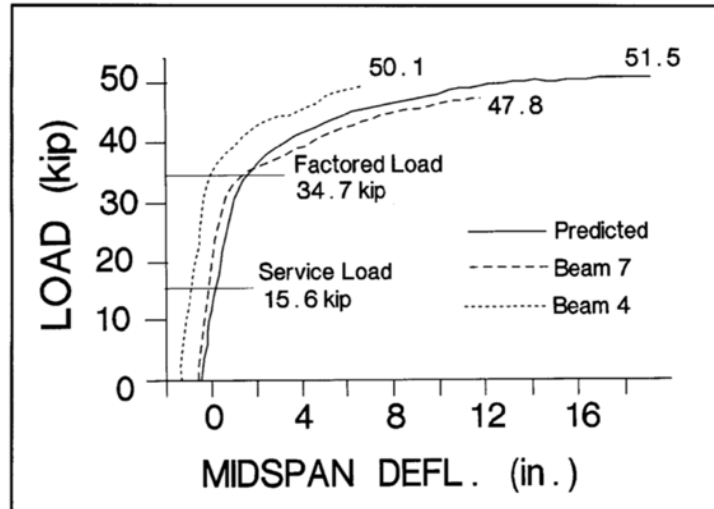


Figure 3- 5: Experimental and predicted load deflection curves from prestressed concrete girders tested by (Shenoy and Frantz, 1991). 1 kip = 4.45 kN, 1 inch = 25.4 mm.

Bridge managers often evaluate the condition of bridges into simple numerical ratings after visual inspections. For instance, Alberta Transportation uses a 1-9 numerical rating system for bridge inspectors (Alberta Transportation, 2018), where a rating of ‘1’ means that the bridge is severely deteriorated with immediate action required and a rating of ‘9’ means that the bridge is in new or almost new condition. Other ratings, including comments and suggested maintenance actions, are shown in Table 3-1.

Table 3- 1: Bridge condition rating system (AT, 2008).

Rating	Assessment	Commentary	Maintenance priority
9	Very Good	New condition.	No repairs in foreseeable future.
8	Very Good	Almost new condition.	No repairs in foreseeable future.
7	Good	Could be upgraded to new condition with very little effort.	No repairs necessary at this time.
6	Good	Generally good condition, functioning as designed with no signs of distress or deterioration.	No repairs necessary at this time.
5	Adequate	Acceptable condition and functioning as intended.	No repairs necessary at this time.
4	Adequate	Below minimum acceptable condition.	Low priority for repairs.
3	Poor	Presence of distress or deterioration. Not functioning as intended.	Medium priority for replacement, repair, and/or signing.
2	Poor	Hazardous condition or severe distress or deterioration.	High priority for replacement, repair, and/or signing.
1	Immediate Action	Danger of collapse and/or danger to users/	Bridge closure, replacement, repair, and/or signing required as soon as possible.

Although numerical rating systems are relatively simple to interpret, they are subjective and ratings depend on the inspector's judgment and experience. An objective assessment tool for bridge girders based on residual strength obtained through full-scale testing can help transportation ministries develop more efficient management systems for deteriorated bridges.

In this study, four girders with different degrees of deterioration from a decommissioned bridge in Alberta were tested under four-point bending to evaluate their residual flexural capacity. The tests included intact girders and specimens that had various types of damage, including artificial damage to simulate different amounts of corrosion.

3.2 Experimental Program

3.2.1 Bridge description

A decommissioned single-span bridge, called "Tiger Lily" bridge near Barrhead, Alberta (approximately 120 km northwest of Edmonton) was examined to investigate its residual flexural response. The bridge was opened in 1990 and taken out of service in 2018 after failing a safety inspection due to severe concrete spalling on the bottom of the bridge and excessive reinforcement corrosion as shown in Figure 3-6. The report from a September 2015 inspection by a different inspector showed that the bridge deteriorated quickly over only eight months after its previous inspection (Table 3-2). Note that inspector bias may be a factor in these different ratings since two different inspectors were involved. Issues with deck drainage were linked to severe deterioration of the superstructure and substructure causing the drainage rating to be changed from seven to three. The deck top, given a rating of 3, was delaminated with evidence of spalling and longitudinal cracks along the centre line exhibited on five interior girders. This bridge did not have asphalt topping or a cast-in-place concrete deck so surface deterioration affects the girders themselves. Three out of nine girders in the bridge were given ratings of 2, meaning they exhibited a hazardous

or severe condition with exposed rebar and strands. The reinforcement had been reported to be in better condition eight months earlier.



Figure 3- 6: (a) Bridge being taken apart, (b) photo of heavily deteriorated girder.

Table 3- 2: Bridge inspection rating and explanations (AT, 2016).

Component	Inspection rating (Jan. 2015)	Inspection rating (Sep. 2015)	Explanation
Deck top	4	3	Delaminated and spalled areas up to 150 x 300 x 50 in three girders Longitudinal cracking along centreline of five interior girders
Deck joints	4	4	Buffer angles have corroded and sections missing
Deck drainage	7	3	Deck drainage causing severe deterioration of superstructure and substructure.
Girders	3	2	Three girders had fallen into the rating category of two with heavily spalling area and exposed rebar and strands.

The bridge consisted of nine, 11 m long, prestressed concrete voided slab girders without topping connected by five steel shear connectors on either side of the girders. The girders had a rectangular section, 0.51 m deep and 1.2 m wide, with three 300 mm diameter holes. The girders were constructed with semi-low-density concrete and a design compression strength of 35 MPa. The girders were pretensioned with twenty 12.7 mm diameter, seven-wire low-relaxation pretensioning strands with a specified ultimate strength, f_{pu} , of 1860 MPa, and seven 10M (100 mm²) steel bars with specified yield strength of 400 MPa (Figure 3-7). The strands had a specified initial prestress

of $0.7f_{pu}$ and a specified effective prestress after losses of $0.58f_{pu}$. (AT, 1988). The tested girders were additionally reinforced with four 25M (500 mm^2) bars that were not indicated in the engineering drawings but that were discovered during forensic examination. After consulting with Alberta transportation, it was found that the 25M bars were placed to reduce long-term camber in the girders. The extra bars for camber control were not included in the drawing at the time of the design (1988), but they were later included in later design specifications for this type of bridge.

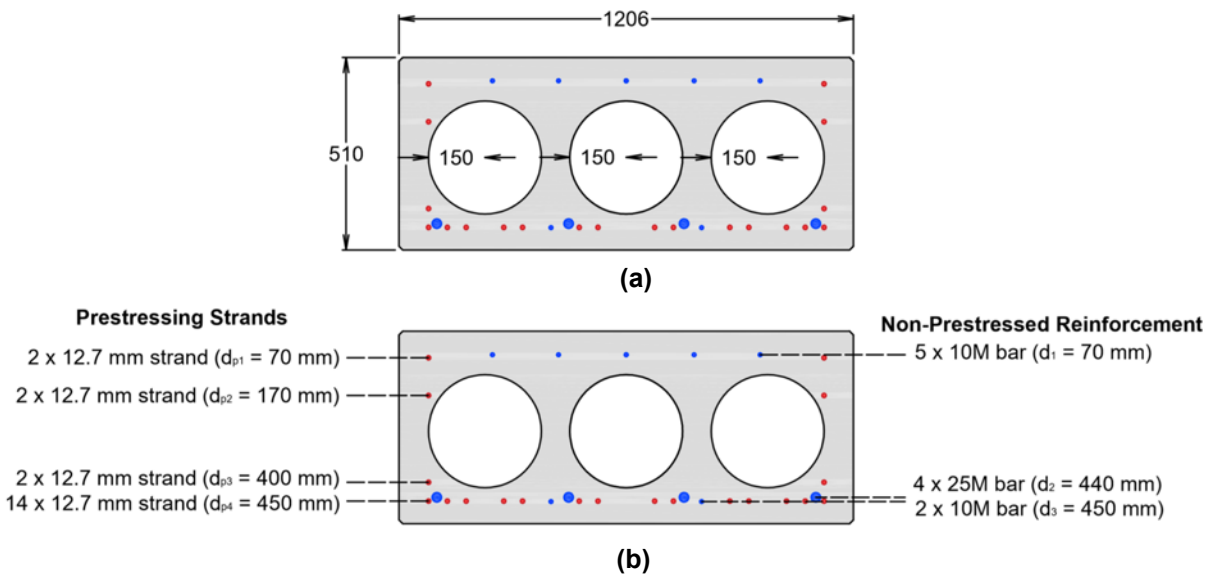


Figure 3- 7: Cross section of test girders showing (a) general geometry and (b) reinforcement details. Stirrups not shown for clarity. All dimensions in mm.

3.2.2 Test girders

Of the nine girders in the bridge, four girders with different degrees of deterioration were selected to investigate their flexural response (Table 3-3).

A girder with limited deterioration (LD) was chosen as a control girder. Girder LD, shown in Figure 3-8a and Figure 3-9a, had no visible concrete spalling on the bottom of the girder or evidence of reinforcement corrosion.

The girder that was the most damaged from deterioration was selected to explore whether this girder was still adequate under design load. Girder HD (heavy deterioration), with significant concrete spalling and corrosion of the bottom layer of reinforcement, was the most damaged girder in the group. As shown in Figure 3-8b, very severe concrete spalling was observed around midspan of the girder which led to significant corrosion of the bottom layer of strands and non-prestressed reinforcement. Around 70% of the bottom cover of the girder was lost causing both severe strand and rebar corrosion (Figure 3-9b).

Girder MD's (moderate deterioration) condition fell between girder LD and HD. Girder MD (Figure 3-9c) exhibited an estimated concrete spalling of 20% with fewer exposed bars and strands. Girder MD was chosen to investigate how a girder with moderate deterioration behaves under flexural loading in comparison to the ones with different level of damage to determine the level of deterioration that the girder's strength would remain sufficient under design load.

To examine the contribution of strands in the girder and how strand corrosion affects flexural capacity, Girder ID (induced deterioration), with similar damage to Girder MD, was selected to investigate the effect of strand loss. Girder ID had an estimated bottom concrete loss of 20% with rebar corrosion and some light strand corrosion as shown in Figure 3-9d. Girder ID was artificially damaged by cutting three strands (amounting to a 21% strand loss in the bottom layer of reinforcement) and removing the clear cover at two locations: 1) at 750 mm from each end, and 2) at midspan, by making 50 mm deep cuts (Figure 3-10). This induced damage was intended to represent severe strand corrosion.

Table 3- 3: Test specimens.

Test name	Deterioration level	Midspan camber (mm)
LD	No visible deterioration	38
HD	Severe concrete spalling and corrosion	28
MD	Intermediate concrete spalling and corrosion	30
ID	21% strands loss at midspan, and 750mm from each end	29

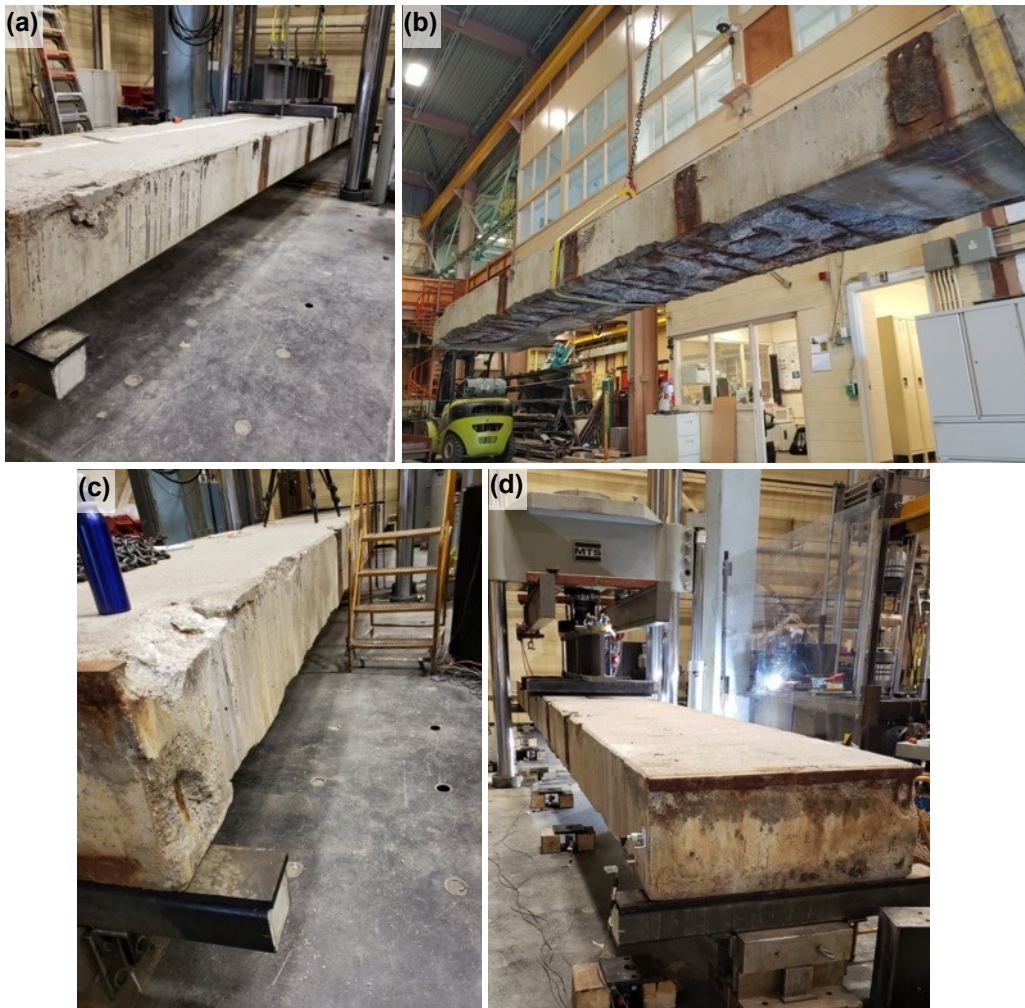


Figure 3- 8: Girder conditions (a)Girder LD with no visible damage (b) Girder HD with severe concrete loss and steel corrosion (c)Girder MD with moderate deterioration (d) Girder ID with moderate deterioration and induced corrosion .

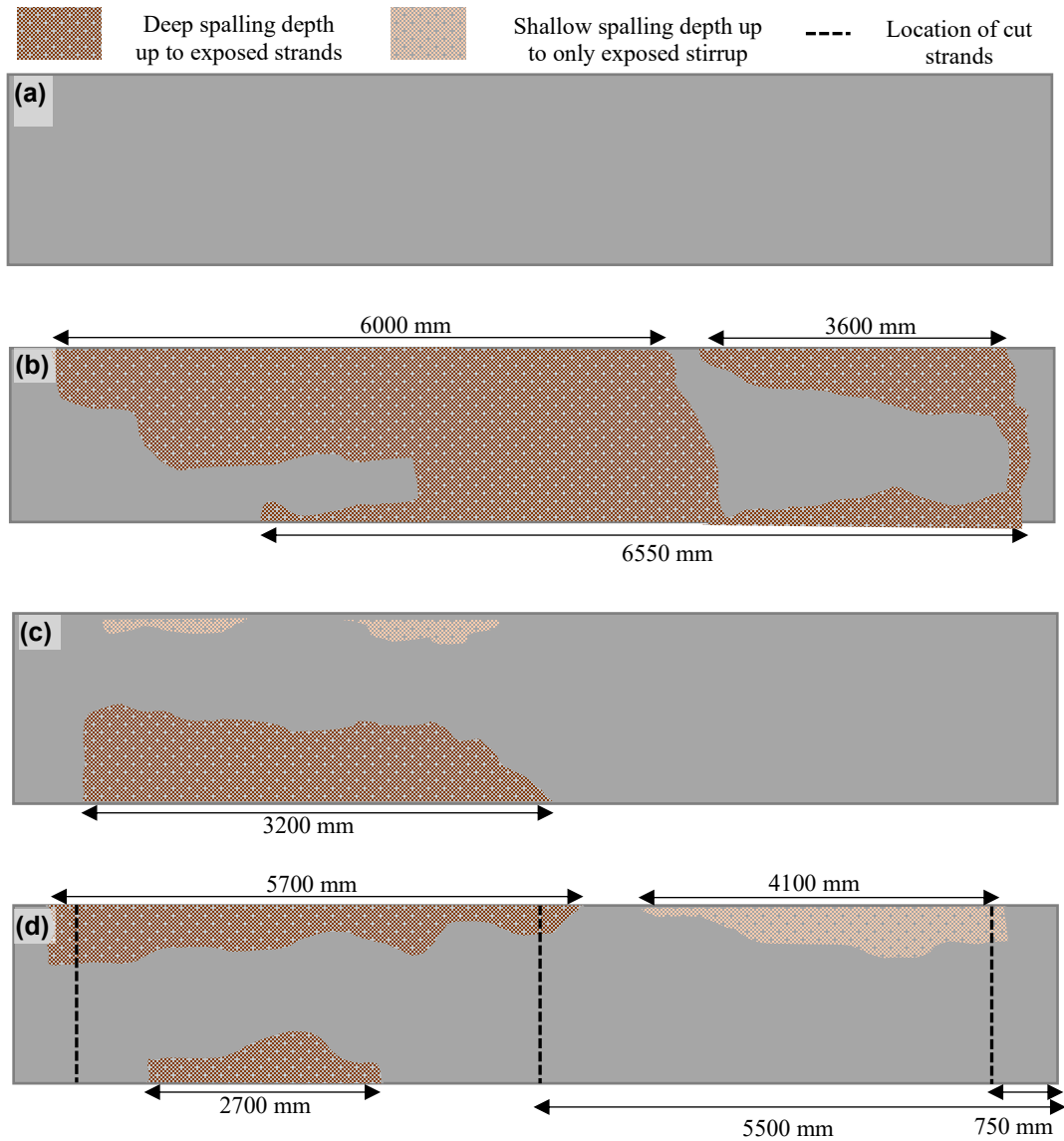


Figure 3- 9: Deterioration mapping on the bottom of the specimens (a) Girder LD without any visible deterioration at 0% concrete spall (b) Girder HD had 70% overall concrete spall with both reinforcement and strand corrosion (c)Girder MD had 20% concrete loss with rebar corrosion and light strand corrosion (d) Girder LD had 20 % concrete loss with rebar corrosion and light strand corrosion.



Figure 3- 10: Induced (cut) strands loss in Girder ID.

3.2.3 Materials

3.2.3.1 Concrete

The girders were constructed with structural semi-lightweight concrete with a nominal density of 1920 kN/m^3 and a specified compressive strength of 35 MPa. After the flexural tests, 100 mm diameter and 200 mm long concrete cores were extracted for compression testing. Three cores were extracted on each girder to ensure a representative value, but some concrete regions were too damaged from testing to properly extract cores. Girder HD had no successful cores and Girder MD only had two successful cores due to the damage sustained from testing.

The weighed density of the cylinder samples was 1980 kN/m^3 . This confirms the girders were built with semi-lightweight concrete. Cylinders were tested as per ASTM C39/C39M-14 (ASTM, 2014) with a 2250 kN capacity load frame. Stress-strain curves (Figure 3-11) indicated a similar compressive strength in all cylinder samples, with an average of 53.9 MPa and standard deviation of 4.15 MPa (Table 3-4). Figure 3-10 also shows a similar modulus of elasticity, calculated as per ASTM C469 (2014), among the cylinder samples with an average of 22.1 GPa and a standard deviation of 2.40 GPa. Note that the elastic modulus of sample D (18 GPa) was significantly lower than the average, but the compressive strength of sample was consistent with the other samples. This difference is attributed to a malfunctioning compressometer sensor during testing.

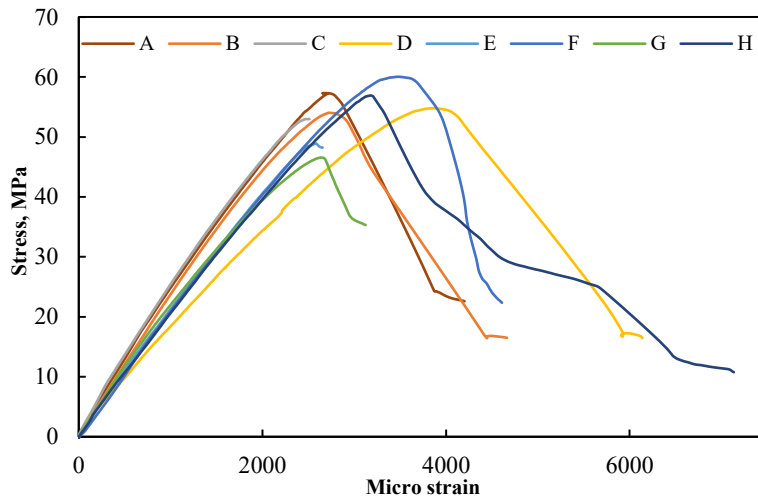


Figure 3- 11: Stress Strain Curves from concrete cylinders extracted from the tested girders.

Two predictions for the concrete modulus of elasticity were completed. The first, $E_{c,ref}$, is based on the ‘reference’ modulus from S6:19 (2019) Clause 8.4.1.5.3 (Eq. 3-1) which accounts for concrete density, γ_c , and compressive strength, f'_c .

$$E_{c,ref} = \left(3300\sqrt{f'_c} + 6900 \right) \left(\frac{\gamma_c}{2300} \right)^{1.5} \quad \text{Eq. 3- 1}$$

For this expression, the measured f'_c from each cylinder was used and a constant value of 1980 kg/m³ was used for γ_c as there were minimal differences in γ_c between cylinders.

The second predicted modulus, $E_{c,design}$ is based on the design strength at 28 days of 35 MPa. S6:19 accounts for time, cement type, and ambient temperature within the elastic modulus calculation. The adjusted time scale, $\tau_E(t)$, accounts for concrete age and ambient temperature and was calculated using Clause 8.4.1.5.4 in S6:19 (Eq. 3-2).

$$\tau_E = t \exp \left(13.65 - \frac{4000}{273 - T_i} \right) \quad \text{Eq. 3-2}$$

Where t is the concrete age in days, and T_i is the average ambient temperature on each day, °C. A value of 10000 days was used for t since the girders were between 9800 and 10500 days old when

tested and there was minimal difference (<0.1%) between these extremes. In lieu of using temperature data from the site, the annual temperature of 3.9 °C taken from the closest weather station (Edmonton - Stony Plain) between 1981 and 2010 was used (Environment Canada, 2021). The overall modulus adjustment coefficient, β_E , was then found using Eq. 3-3.

$$\beta_E = \left(\exp \left\{ s \left[1 - \left(\frac{28}{\tau_E} \right)^{0.5} \right] \right\} \right)^{0.5} \quad \text{Eq. 3-3}$$

Where s accounts for cement type and assumed to be 0.25 (normally hydrating cement) in lieu of specific concrete mix details. Though assumed, there was less than 2% difference in β_E from normally hydrating and rapidly hydrating cements. The approximate modulus of elasticity based on S6:19 Clause 8.4.1.5.2 was then calculated as $E_{c,design} = \beta_E E_{c,ref}$ where $E_{c,ref}$ was calculated using the design f'_c of 35 MPa. The value obtained from this calculation is 23.7 GPa and the ratio between test and predicted moduli are reported in Table 3-4.

Table 3- 4: Material properties of concrete for each specimen.

Cylinder ID	Length (mm)	Diameter Average (mm)	Maximum compressive stress (MPa)	Measured Elastic Modulus, $E_{c,test}$ (ASTM C469), GPa	Reference Elastic Modulus, $E_{c,ref}$, GPa	$\frac{E_{c,test}}{E_{c,ref}}$	$\frac{E_{c,test}}{E_{c,design}}$
A	202	94.3	57.3	24.6	25.5	0.96	1.04
B	201	94.4	54.0	23.7	24.9	0.95	1.00
C	203	94.4	53.0	25.3	24.7	1.02	1.07
D	185	93.8	54.8	-- ^a	25.0	-- ^a	-- ^a
E	200	94.5	48.9	21.2	23.9	0.90	0.90
F	200	94.4	60.0	21.1	25.9	0.81	0.89
G	187	93.8	46.6	22.3	23.5	0.95	0.94
H	200	94.5	56.9	20.5	25.4	0.81	0.86
		S.D.	4.15	1.87	0.81	0.08	0.08
		Average	53.9	22.7	24.9	0.92	0.96

^a – sensor error in test led to inaccurate elastic modulus, test not considered in average or deviation for $E_{c,test}$

The predicted $E_{c,ref}$ had an average of 24.9 GPa with a standard deviation of 0.81 GPa. The ratios between the tested ($E_{c,test}$) and the predicted moduli ($E_{c,ref}$ and $E_{c,design}$) were used to investigate which method more accurately predicted the concrete elastic modulus. Both methods were generally within 10% of the test value. The ratio between the tested and the predicted

reference modulus $E_{c,ref}$ had an average ratio of 0.92 with a standard deviation of 0.08. The accuracy increased when the prediction method accounted the age and the temperature factors of the concrete which are very important factors to consider for the 28-year service life of the Tiger Lily bridge. The average ratio between the tested and the predicted design modulus was 0.96 with a standard deviation of 0.08.

3.2.3.2 Non-prestressed steel

After each flexural test, the girders were cut and remaining pieces were used to extract samples of the stirrups and mild steel reinforcement shown in Figure 3-12a. Non-prestressed steel was comprised of both bars with the ‘bamboo’ ribbing which dominates current practice as well as ‘X’ ribbing which was more popular in the 1980’s. In some cases, both rib types were used in the same girder (Figure 3-12b). For 25M bars, the ‘X’ ribbing was only used in Girder LD (Figure 3-12c) while the other girders were reinforced with ‘bamboo’ ribbed 25M bars (Figure 3-12d). The material properties of the rebar were determined based on ASTM A370 provision (ASTM, 2016).

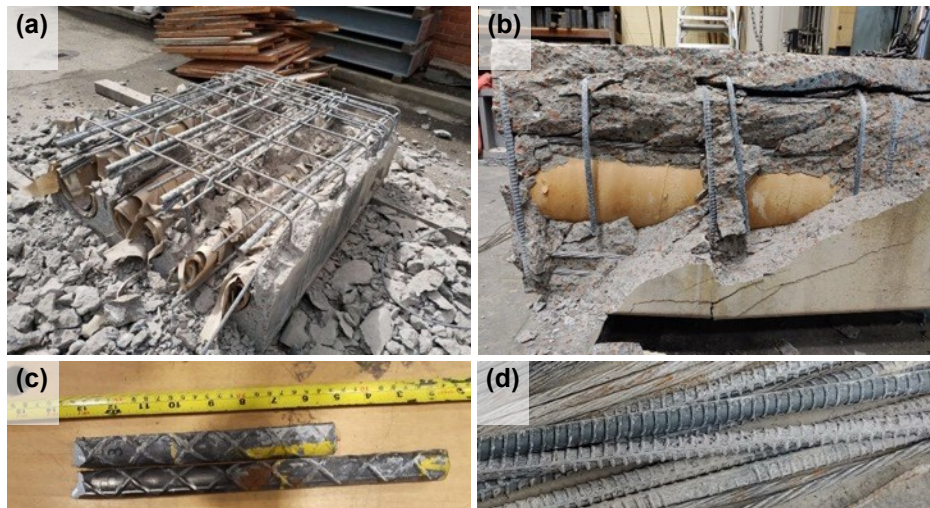


Figure 3- 12: (a) Extraction of rebar from Girder LD (b) Failed Girder MD with both types of bars visible (c) ‘X’ ribbing in Girder LD’s 25M bars and (d) ‘bamboo’ ribbing on 25M bars from other girders.

For the 10M rebar, both transverse and longitudinal bars were extracted and tested with results shown in Figure 3-13. All stresses, including those for corroded bars, were calculated assuming a nominal bar area of 100 mm². Results are split between bars with ‘X’ ribbing and those with ‘bamboo’ ribbing as there were observed differences between these bar performances attributed more so to differences in the steel used to make the bars and cross-sectional area rather than the ribbing type. Tests on corroded bars are also shown in Figure 3-13. For each type of bar, neglecting corroded bar tests, there were similar moduli of elasticity, yield strengths, and ultimate strengths. Yield strengths were determined using the 0.2% offset method from ASTM A370 (2016). After the bars yielded, strain hardening occurred followed by fracture. The average yield strength of ‘X’ ribbed and bamboo ribbed bars were 430 MPa and 492 MPa, with a standard deviation of 19.0 MPa and 8.0 MPa respectively. The average ultimate strength of the ‘X’ ribbed bars was 667 MPa with a standard deviation of 30.5 MPa. For the bamboo ribbed 10M bars, the average ultimate strength is 663 MPa with a standard deviation of 14.5 MPa. The modulus of elasticity of ‘X’ and bamboo ribbed 10M bars were 200 GPa and 215 GPa, with a standard deviation of 6.46 GPa and 7.23 GPa respectively. Note that modulus of elasticity results from three tests (one with bamboo ribbing and two with ‘X’ ribbing) were not used because of extensometer malfunction or slipping.

The corroded bars had slightly lower elastic moduli values than their non-corroded counterparts. However, these bars had considerably lower yield and ultimate strengths, an absence of a yield plateau, and were considerably more brittle than their non-corroded counterparts.

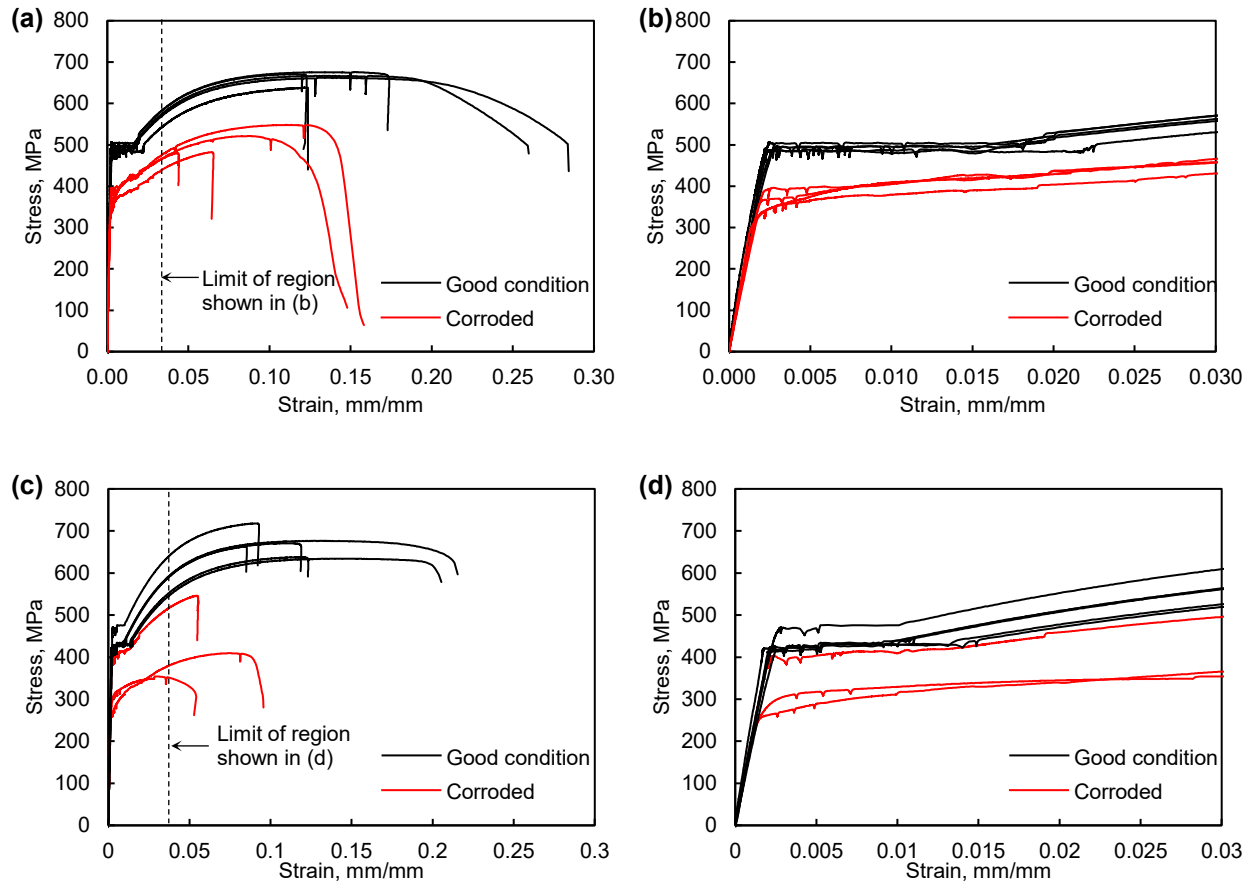


Figure 3-13: Stress and strain curve from 10M bars (a) full curve for bamboo ribbed bars (b) zoomed in curve for bamboo ribbed bars showing elastic region and yield plateau (c) full curve for 'x' ribbed bars (d) zoomed in curve for 'x' ribbed bars showing elastic region and yield plateau, (b) X-ribbed.

The results from twelve tests on longitudinal 25M bars are shown in (Figure 3-14). All bar stresses were calculated using a nominal area of 500 mm^2 . The average yield and ultimate strength of 25M bars with 'X' ribbing were 412 MPa and 640 MPa, with a standard deviation of 4.5 MPa and 6.1 MPa, respectively. The average yield and ultimate strength of 25M bars with 'bamboo' ribbing were 466 MPa and 630 MPa, with a standard deviation of 10.3 MPa and 3.7 MPa, respectively. Both rib types had essentially the same elastic modulus of 202 GPa with a standard deviation of 11.2 GPa. Unlike what was observed in the 10M bars and strands, there was negligible evidence of corrosion on any of the 25M bars even in girders with severe corrosion in other bars.

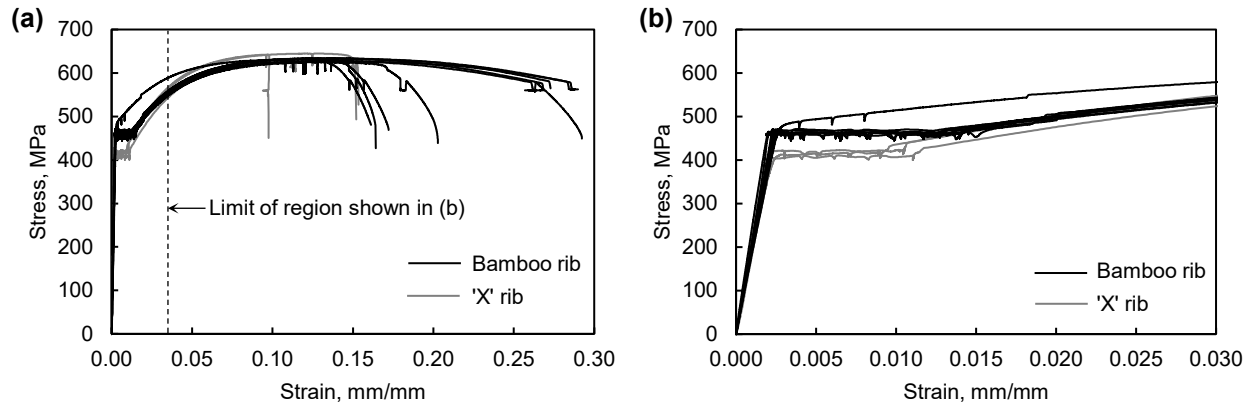


Figure 3- 14: Stress and strain curves from longitudinal 25M bars (a) entire curve (b) zoomed in region showing elastic region and yield plateau.

Table 3- 5: Material properties of rebar.

Reinforcement	Average yield strength (MPa)	Average ultimate strength (MPa)	Average elastic modulus (GPa)
10M 'X' rib	430	667	200
10M bamboo rib	492	663	215
25M 'X' rib	412	640	202
25M bamboo rib	466	630	202

3.2.3.3 Prestressing strands

Samples of the prestressing strands were also obtained from the demolished girders after testing. Both 'healthy' strands without visible corrosion and corroded strands were tested to investigate the effect of deterioration effect on the strand response. The material properties were determined based on ASTM A1061 (ASTM, 2016). The stress-strain curves were obtained from the tensile tests are shown in Figure 3-15. Stresses were calculated using a nominal area of 99.7 mm².

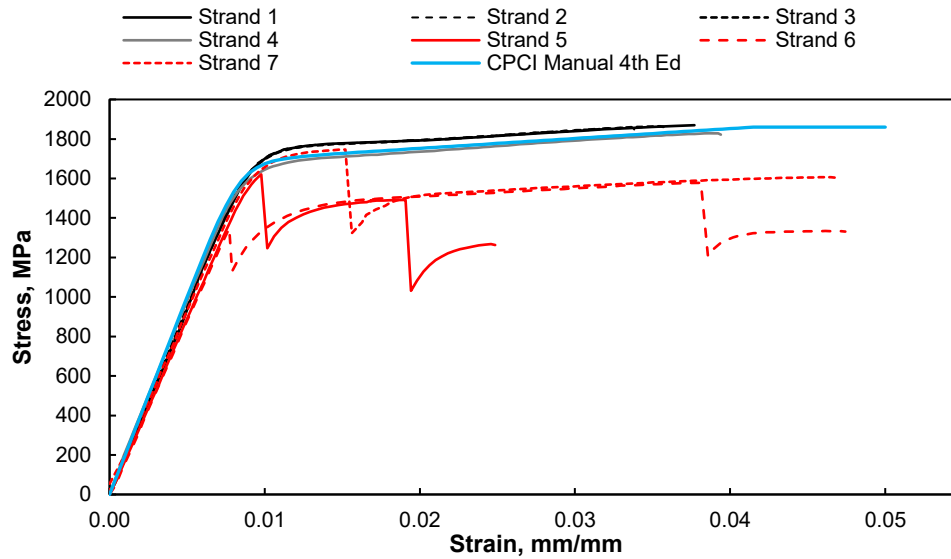


Figure 3-15: Stress and strain curve for prestressing seven wire strands.

The yield strength of the prestressing strands was determined based on the measured strain at 1% elongation and accounting for any toes observed early in the test following procedures from ASTM A1061.

Seven strands with different level of corrosion were used as samples to investigate the corrosion effect as shown in Table 3-6. The healthy strands had an average yield strength of 1700 MPa with no standard deviation. They also had an average ultimate strength and elastic modulus of 1860 MPa and 192 GPa with a standard deviation of 5.77 MPa and 1.15 GPa respectively. As seen in Figure 3-15, corrosion negatively affected the yield and ultimate strength. The more severe the corrosion exhibited on the strands, the less residual strength. Only one corroded strand yielded while the others experienced individual wire fracture prior to yielding. The corroded strands were more brittle and ruptured with a capacity drop for each wire rupture. Sudden drops in the response of the corroded strands in Figure 3-15 reflect individual wire snapping, with the corresponding sudden drop in strength. As expected, the first drop in strength is close to $\frac{1}{7}$ of the load carried by as each strand since they each have 7 wires. Strands 5, 6 and 7 did not yield before one of the

seven wire strands snapped. The average elastic modulus had a slight reduction: 183 MPa with a standard deviation of 5.44 GPa. The curves also plotted against stress calculated using Eq. 3-4 given in the CPCI Manual (2007). Figure 3-15 indicated that strands (strand 1, 2 and 3) in good condition followed very similar trends as the CPCI curve.

$$f_{ps} = 200 \times 10^3 \varepsilon_{ps} \left\{ 0.25 + \frac{0.975}{[1 + (118\varepsilon_{ps})^{10}]^{0.1}} \right\} \leq 1860 \text{ MPa} \quad \text{Eq. 3-4}$$

Where f_{ps} is the stress in the strand and ε_{ps} is the strain in the strand.

Table 3- 6: Material properties of prestressing 7 wire strands.

Prestressing 7 wire tendons	Condition	Yield strength (MPa)	Ultimate strength (MPa)	Elastic Modulus, GPa
1	No visible corrosion	1700	1870	193
2	No visible corrosion	1700	1860	193
3	No visible corrosion	1700	1860	191
	Average	<i>1700</i>	<i>1860</i>	<i>192</i>
	S.D.	<i>0</i>	<i>5.77</i>	<i>1.15</i>
4	Lightly corroded	1640	1830	191
5	corroded	-- ^a	1620	180
6	corroded	-- ^a	1580	179
7	corroded	-- ^a	1750	183

^a*This strand ruptured before it yielded.*

3.2.4 Test setup and instrumentation

Four-point bending tests were carried out using a hydraulic actuator load frame with a capacity of 6100 kN. After decommissioning the girders, they were stored in an open yard until they were delivered to the Morrison Structural Lab at the University of Alberta for testing (approximately one year after decommissioning). The girders were simply supported on 152 mm × 152 mm hollow steel sections resting on steel pedestals to distribute loads across the width of the girder. Neoprene pads with a thickness of 25 mm were used on top of each HSS to simulate the support condition of the girders in service. The centre-to-centre span between supports was 10800 mm. A spreader beam with load points spaced 1.5 m apart on centre was used to convert the actuator force to four-point bending (as shown in Figure 3-16).

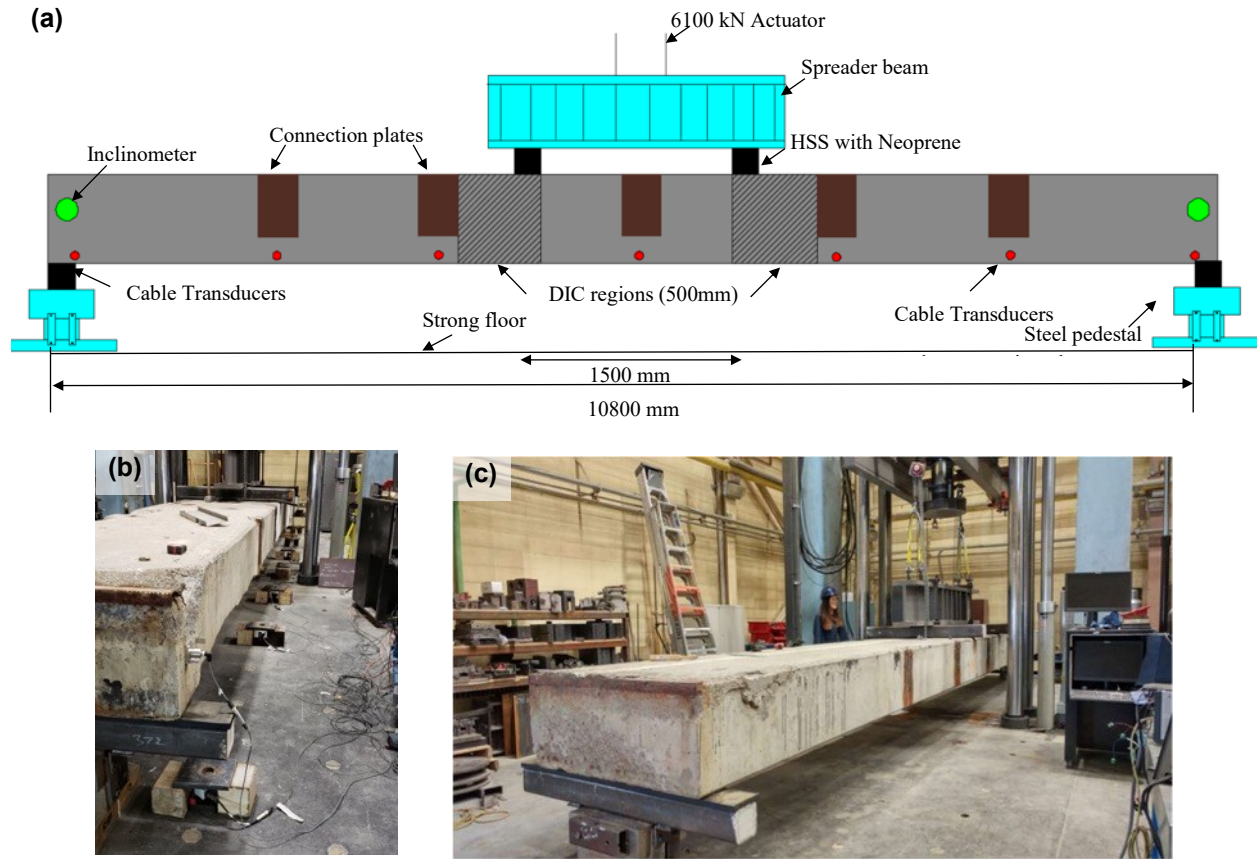


Figure 3-16: Test setup and instrumentation (a) Elevation view of test setup showing location of load points and instrumentation (b) Photo showing placement of sensors (c) photo showing overall girder in place.

Service Limit State (SLS) and Ultimate Limit State (ULS) loads were calculated using appropriate loads from the Canadian Highway Bridge Design Code (CSA S6:19, 2019). As shown in Figure 3-17, an 18 m long CL-625 truck (total truck weight, W , of 625 kN) with one-wheel line was used to determine the critical midspan moment. Only one-wheel line was applied because the truck (1.8 m) is wider than the girder. Two load cases with different axle positions were used to determine the critical midspan moment: Case 1 was when the first three axles of the truck were positioned on the girder as shown in Figure 3-18a; Case 2 is when the heaviest axle (no.4) was positioned on midspan (Figure 3-18b). An additional lane load (Figure 3-19a) was also considered by adding a uniformly distributed load of 9 kN/m on top of the truck load, as shown in Figure 3-19b.

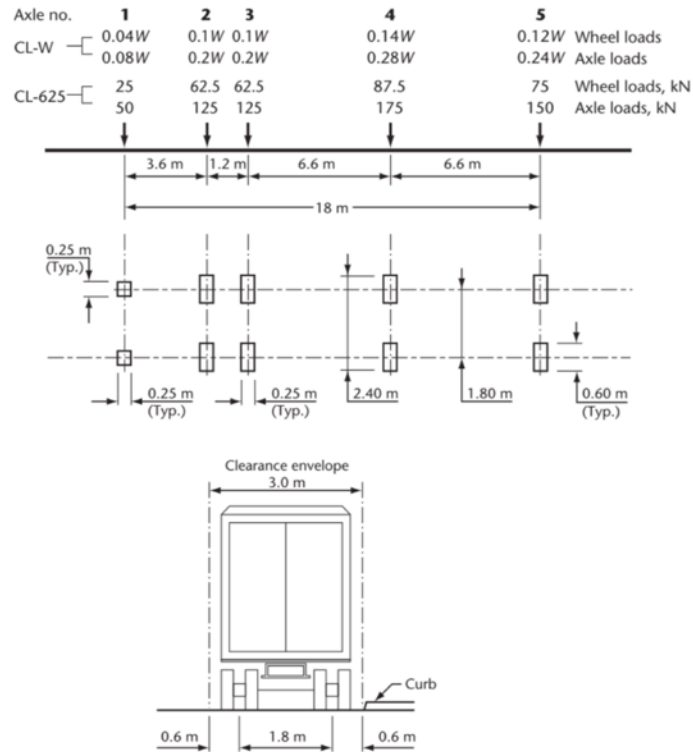


Figure 3- 17: CL-W truck load (CSA S6:14, 2014)

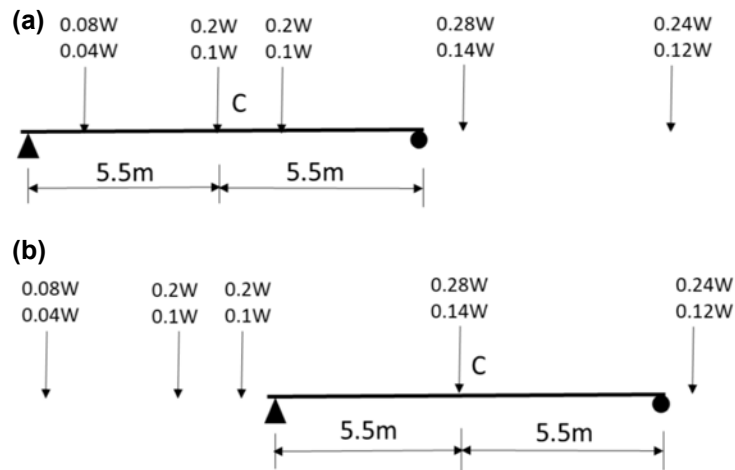


Figure 3- 18: possible critical midspan moment cases using truck load (a) first three axle numbers of the truck are on the bridge girder (b) the heaviest axle (no.4) is located at midspan of the girder (Huang, 2020).

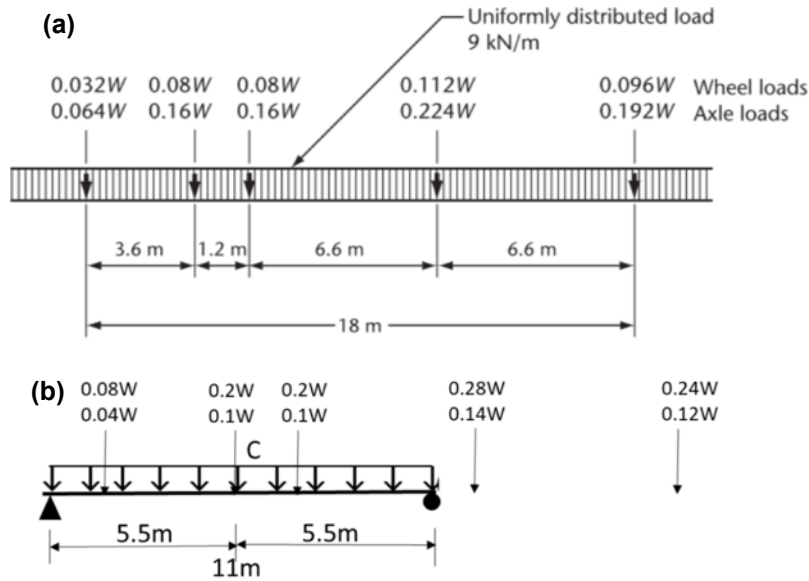


Figure 3- 19: Lane load considered (a) CL-W lane load (CSA S6:14,2014) (b) possible critical midspan moment (Huang, 2020).

Dynamic load factors and multiple-lane load factor were considered when determining the possible critical midspan moment. A dynamic load allowance of 0.3 was applied to the truck axle load no.1 to no. 3 of Case 1, to account for the dynamic amplification effect. A multiple-lane factor was applied to account for the load distribution among girders. A factor of 0.9 was considered assuming a highway class A (CSA S6:14, 2014).

The critical midspan moment, M , from live loads only was calculated to be 579 kNm using Case 1. The dead load was accounted for by using the measured density of concrete in the girder and considered later. The critical moment was back calculated into an equivalent total live load force, P , that the load frame needs to apply using Eq. 3-5:

$$P = \frac{2M}{a} \quad \text{Eq. 3-5}$$

Where a is the distance between the support and load point (4.65 m). Using Eq. 3-5, P , was calculated as 249 kN. The governing service and ultimate limit states were determined using the

appropriate load combination factors for live load from CSA S6:19. The service load using SLS combination 2 and ultimate load using ULS combination 1 were 210 kN and 410 kN respectively.

Each girder was tested at a rate of 5 mm/min. Girders were first loaded to the Serviceability Limit State (SLS) load of 210 kN and then unloaded to zero. Next, they were loaded to the Ultimate Limit State (ULS) load of 410 kN and then unloaded back to SLS. Girders were then loaded until failure, considered to be the point where the test specimen lost 50% of its strength after peak load.

Eight cable transducers with sample rate of 1 Hz were used on each girder to record the deflection of the girders under loading (as shown in Figure 3-16a). The cable transducers were placed on both ends of the girder (to measure support deformation), at each shear connection plate and at both sides of the girder at midspan to track deflection. Inclinometers were placed on each end of the girder to measure support rotation.

Images were collected from each girder to allow for Digital Image Correlation (DIC) analysis to be used to help future studies investigate crack propagation and prestress loss of the girders. Formal DIC analysis is beyond the scope of this thesis but images were used to qualitatively aid in identifying cracking moments. Images for future DIC analysis were taken of regions located between either load point and a point 500 mm away from load points towards the supports. Canon Rebel T6 and T7 cameras with resolution of 18.7 megapixels and 24.1 megapixels shooting at 15 second intervals were used to capture the crack formations within these regions. DIC images were not collected at midspan because the test frame did not have enough space to set up DIC cameras at that location.

3.3 Results and Discussion

3.3.1 Load-deflection relationship

The relationship between load and deflection is shown in Figure 3-20. The deflection measured by cable transducers corresponds to the displacement of the girder during the test, and as such it does not include the deflection due self-weight or the initial camber due to prestress. The load included the weight of the spreader beam (16 kN) used to transfer the loads from the actuator to the girder but does not include the self-weight of the girder. The self-weight of the girder was calculated to be 7.59 kN/m. The midspan moment from self-weight of the girder was 111 kNm, calculated using the measured density of the concrete in the girder. General test results are displayed in Table 3-7. Figure 3-21 shows the deflected profile of the girders at three response milestones: service limit state, ultimate limit state, and failure.

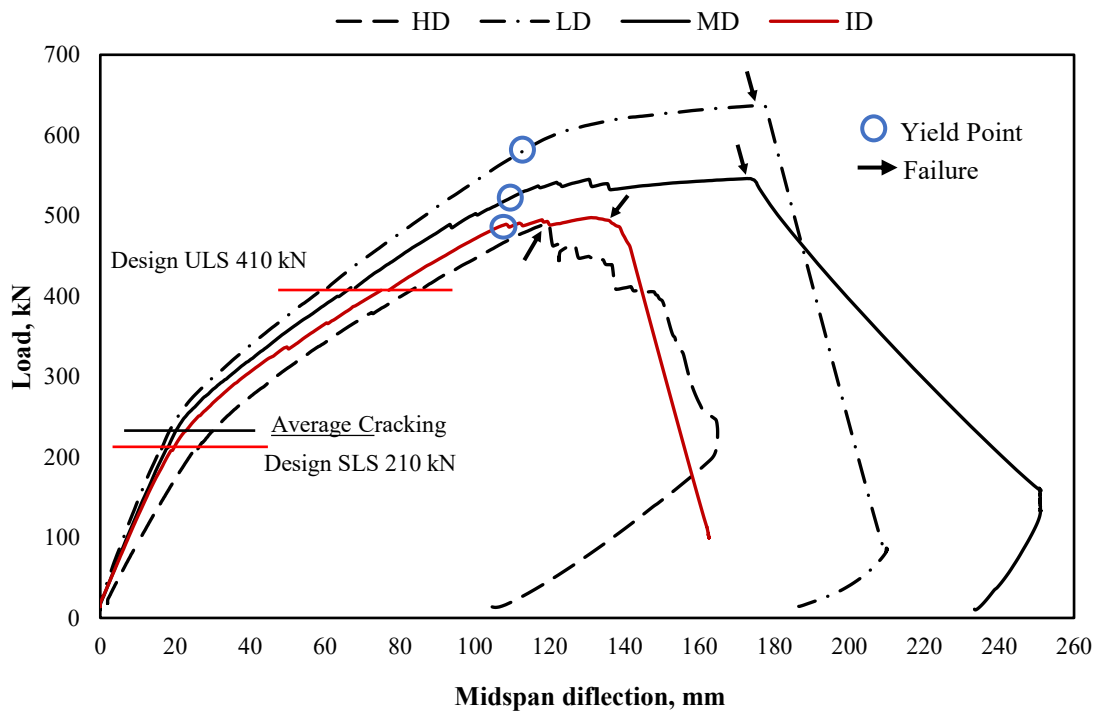


Figure 3- 20: Load deflection curves.

Table 3- 7: General test results for each specimen.

Test name	Deflection at SLS, mm	Deflection at ULS, mm	Cracking load, kN	Yield load, kN	Peak load, kN	Midspan moment at yield (includes self-weight), kNm	Midspan moment at peak (includes self-weight), kNm	Failure mode
LD	16.1	59.8	240	590	637	1480	1590	Concrete crushing after steel yielded
HD	25.3	84.1	230	-- ^a	491	-- ^a	1250	Strand rupture
MD	17.6	67.0	237	535	546	1350	1380	Concrete crushing after steel yielded
ID	19.6	75.1	231	486	498	1240	1270	Strand rupture

^a – Yielding not observed in HD prior to reaching peak load

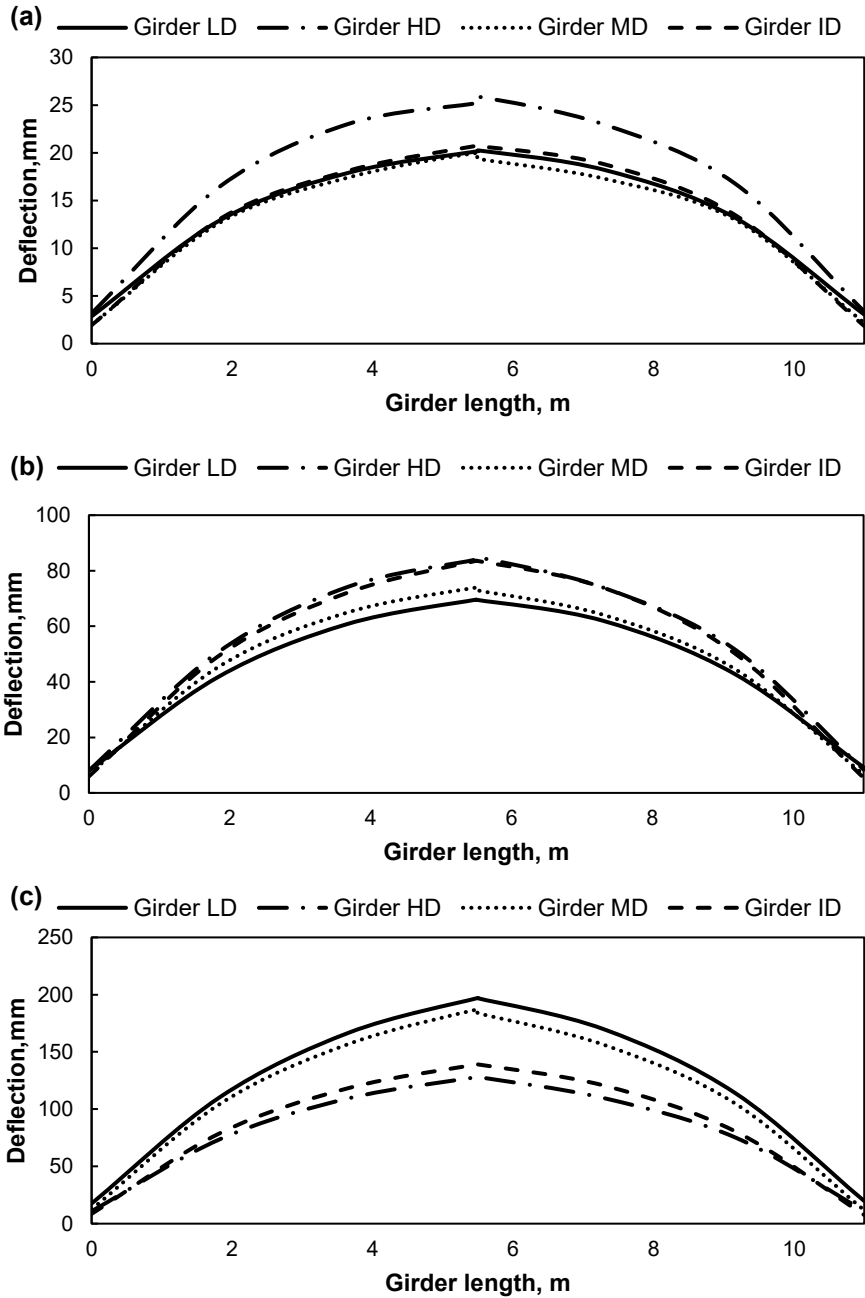


Figure 3- 21: Deflected shapes at (a) SLS, (b) ULS, (c) failure.

3.3.2 SLS performance and initial cracking

All four girders showed satisfactory SLS performance in terms of cracking. Cracking was not observed on any girder specimens under service load regardless of deterioration level. Using the information given in Table 3-8, the uncracked stiffness of each girder was calculated by taking the midspan deflection at service, Δ_{max} , and back calculating the flexural stiffness EI using elastic deflection equations for a simply supported beam under four-point bending (Eq. 3-6):

$$\Delta_{max} = \frac{Pa}{24EI} (3l^2 - 4a^2) \quad \text{Eq. 3-6}$$

where l is the span of the test specimen, a is the distance from the girder support to the load point centreline, and P was taken as half the total applied load. The baseline girder LD, with limited damage, had the largest stiffness (3.00×10^{14} Nmm²). The ratio of uncracked stiffness from each specimen to that of Girder LD was used to evaluate the deterioration effect. Girder HD had the smallest stiffness, 66.7% that of LD, which is attributed to the significant loss of concrete section in girder HD. The stiffness of Girder MD was similar to that of Girder LD, with a ratio of 93.7%. Girder ID was 85.3% the stiffness of Girder LD. Girder ID had 91% of the stiffness of Girder MD, although Girder ID was in a similar deteriorated condition as Girder MD when the girders were extracted from the bridge. This is because of the induced damage done to Girder ID before testing.

Table 3- 8:Uncracked stiffness of each specimen and percentage of baseline.

Test name	Uncracked stiffness (Nmm ²)	Percentage of baseline, LD
LD	3.00×10^{14}	N/A
HD	2.00×10^{14}	66.7%
MD	2.81×10^{14}	93.7%
ID	2.56×10^{14}	85.3%

Figure 3-21a shows deflections up to cracking consistent with Table 3-7, with Girder HD exhibiting the largest deflection (25mm) and Girder LD the smallest (16.1 mm). Girder MD and ID had similar deflected shapes, with deflections of 17.6mm and 19.5mm respectively.

For a bridge under vehicular load, a historical deflection limit under live load only of $l/800$ where l is the bridge span is used as a comparison. This bridge had a span of 10800 mm, so the deflection limit is 13.5 mm. As shown in Table 3-9, all girders under service live loads exceeded the deflection limit. Girder LD had the least excess deflection, 19.3% above the limit. Girder MD and ID followed with 30.4 % and 45.2 % above the limit respectively. Girder HD had the largest deflection, 85.2% above the limit. With all girders exceeding the deflection limit, results indicate that the design of the bridge was likely deflection controlled. A possible reason for the violation of deflection could be that the truck load used for calculating the design SLS and ULS is heavier than the ones used when the bridge was designed in 1990.

The load required to violate the deflection limit was also determined for each girder. Girder LD reached a load of 184 kN at the deflection limit of 13.5 mm which was 12.4% below the service load of 210 kN. Girder MD and ID followed reaching a load of 168 kN and 161 kN which is 20.0% and 23.3 % below the service load respectively. Girder HD had the lowest load (122 kN) which is 41.9% below the service limit.

Table 3- 9: Deflection of each specimen and percentage increase to the deflection limit.

Test name	Deflection at service (mm)	Percentage increase to deflection limit	Load required to violate deflection limit, kN
LD	16.1	19.3%	184
HD	25.0	85.2%	122
MD	17.6	30.4%	168
ID	19.6	45.2%	161

As expected, the cracking load is correlated with the degree of damage. The least damaged girders cracked at higher loads and the most damaged girders cracked at lower loads. However, despite

the different degrees of deterioration, the change from largest cracking load (Girder LD) to smallest (Girder HD) was within 5 percent. The initial cracking load was not visible to the naked eye, but observed with qualitative DIC analysis and correlated with a change of slope on the load deflection curve in Figure 3-20.

3.3.3 ULS performance

When girders were loaded to the design ULS, wide cracks formed on all girders. After the girders were unloaded, the cracks were still visible which indicated that these girders were never loaded to the expected design ULS when they were in service.

An effective cracked stiffness of each girder at ULS was calculated with the same procedure used to determine the uncracked stiffness (Eq. 3-6) but using deflections and loads measured at the ULS load. As expected, the most damaged girder (HD) had the smallest effective cracked stiffness (1.25×10^{14} Nmm²) while Girder LD had the largest (1.78×10^{14} Nmm²). Girder ID, which was purposefully damaged to simulate strand area loss, had a stiffness close to that of Girder HD (1.41×10^{14} Nmm²), while Girder MD had a slightly larger cracked stiffness (1.59×10^{14} Nmm²). In terms of deflection at the ULS load, Figure 3-21b confirms that Girder HD was the least stiff, with the largest deflection (85 mm) at the ULS. Girder ID followed with a deflection of 77.9 mm. Girder MD had a deflection of 66.9mm and girder LD had the smallest deflection, at 60.6 mm.

The yielding point in each girder was identified as the starting point of a plateau on the load and deflection curve (Figure 3-20) marked as circle. Girder LD started yielding under a load of 590 kN while Girder MD yielded at 535 kN and Girder ID started yielding at 486 kN. Girder HD failed suddenly by strand rupture without yielding due to its high degree of deterioration.

Compared to Girder LD, Girder MD had 9.32% lower yield load, and Girder ID had a 17.5% lower yield load.

Girder HD was the only girder that did not show signs of yielding before failure due to its high level of steel corrosion and concrete spalling. The sudden failure without entering into the nonlinear stage is consistent with the performance of corroded tendons (Figure 3-15) present in Girder HD. As indicated in Figure 3-20, girders with less damage from deterioration exhibited a larger yield load and provided more warning with a longer plateau than the ones with higher degree of deterioration.

The performance of the girders at the design ULS showed differences attributed to their differing degrees of deterioration. Girder LD and MD showed significant reserves of strength after they were loaded to design ULS. The load displacement response (Figure 3-20) shows that Girders LD and MD both exhibited a sustained plateau after yielding and before failure. As deterioration level increased, Girder ID (with 21% strand loss) had a very short plateau and Girder HD showed no signs of yielding after the ULS and had a sudden failure.

Despite differences in capacity and failure modes, even with varying levels of deterioration all girders had capacities above the design ULS load, including Girder HD. However, the lack of yielding in Girder HD is undesirable in the context of the ductile design philosophy followed for a bridge.

3.3.4 Failure

Girder LD had the largest peak load of 637 kN. Girder LD had a sustained plateau after the steel yielded, failing at a deflection of 197 mm. The failure mode of this baseline girder was concrete crushing at the top fibre after steel yielded (Figure 3-22a).

Girder HD had the lowest peak load (491 kN) and the smallest peak load deflection (128 mm). The strands in Girder HD were too corroded to yield and HD failed by strand rupture (Figure 3-22b), signaled by a loud snapping during testing. This point is seen on the load deflection curve (Figure 3-20) as a sudden load drop. This failure mode was consistent with the material tests performed on the corroded strands (Figure 3-15).

Girder MD showed a similar response as Girder LD but had a slightly lower failure load (546 kN). Girder MD also showed significant post-yield deformation (56.9 mm additional deflection after yielding) before failure. The failure mode for Girder MD was concrete crushing at the top after steel yielded (Figure 3-22c).

Girder ID failed at 498 kN, a load slightly larger (1.4%) than that of Girder HD. Girder ID had a relatively short post-yield deformation (21.9 mm) and failed due to the rupture of the strands afterwards (Figure 3-22d). This indicates that the induced damage in Girder ID was representative of a high damage state, such as that observed in Girder HD.



Figure 3- 22: Failure modes of tested girders (a) Girder LD – concrete crushing, (b) Girder HD– strand rupture, and (c) Girder MD – concrete crushing, (d) Girder ID – strand rupture.

The ductility of the girders was quantified by taking the ratio of deflection at failure and deflection at yielding for all the specimens. As shown in Table 3-10, deterioration had direct effects on

ductility. Girder LD had the largest ductility ratio of 1.70. As the deterioration level increased, the ductility of the girders decreased (Table 3-10). Girder MD with moderate deterioration had a slight decrease with a ductility ratio of 1.63. Girder HD with severe corrosion did not have the ability to yield before sudden failure, therefore does not have a reported ductility value.

Table 3-10: Girder ductility.

Test name	Deflection at yielding (mm)	Deflection at failure (mm)	Deflection at failure/deflection at yielding
LD	116	197	1.70
MD	115	187	1.63
ID	106	139	1.31
HD	-- ^a	-- ^a	-- ^a

^a Girder HD did not yield before failure

3.3.5 Comparison to design code predictions

CSA S6:19 (2019) was used as the design guideline to calculate the flexural strength of the girder. Reasonable assumptions were made whenever design, material, and construction information were missing. The flexural strength of the girder was calculated based on the basic principles of compatibility of strains and equilibrium, and used appropriate constitutive relationships for the concrete, mild steel, and prestressing steel.

In the strain compatibility analysis according to CSA S6, strain is assumed to vary linearly through the section depth, with a maximum usable strain at the extreme concrete compressive fibre of 0.0035. The tensile contribution of the concrete was neglected in this study for simplicity. The mild and prestressed reinforcement are assumed to be fully bonded in the calculations. The material reduction factor for concrete and steel, ϕ , is set to 1.0 to compare against test predictions. To determine the flexural strength, the neutral axis c is determined using trial and error until the equilibrium is satisfied as shown in Eq. 3-7:

$$\sum C = \sum T \qquad \text{Eq. 3-7}$$

$$\Sigma a_1 \phi_c f'_c \beta_1 c b = \Sigma \phi_s f_s A + \Sigma \phi_s f_{ps} A$$

$$c = \Sigma \frac{\phi_s f_s A}{a_1 \phi_c f'_c b_1 b}$$

Where C refers to concrete compressive force at the desired concrete fibre, T is the steel or strands tensile force at the desired reinforcement layer, f'_c is the concrete strength, b is the cross section width, f_s is the actual rebar stress at the desired location, f_{ps} is the actual prestressing strands stress at the desired location and A is the total area of steel or strands at the desired location. For these calculations the neutral axis at failure was found to remain above the voids so calculations did not need to account for varying section width in the compression zone.

The stresses in the mild steel rebar were determined with Eq. 3-8. The measured yield strength and Young's modulus of elasticity were used in the calculations. E_s is the steel rebar modulus of elasticity which was assumed to be 200 GPa, ϵ_s is the strain of rebar, and f_y is the yield strength of rebar:

$$f_s = E_s \epsilon_s \leq f_y \quad \text{Eq. 3-8}$$

Strain hardening was also considered in the calculation by using a trilinear stress-strain curve fitted against the tested mild steel bars. The post strain hardening modulus of the steel reinforcement was found to be 5833 MPa and the strain where strain hardening began was 0.008 mm/mm.

The stress of prestressing strands at desired locations f_{ps} were determined by using Eq. 3-9 given in the CPCI Design Manual 4 (2007) for low relaxation seven wire prestressing strands. In Eq. 3-9, where ϵ_{ps} is the total prestressing strain at ultimate.

$$f_{ps} = 200000 \epsilon_{ps} \left\{ 0.025 + \frac{0.975}{(1 + (118 \epsilon_{ps})^{10})^{0.10}} \right\} \quad \text{Eq. 3-9}$$

The moment capacity is finally calculated by summing up all the moments generated by the concrete forces and steel forces at an arbitrary point in the cross-section.

Flexural calculations were conducted using the “as-designed” properties and “as-constructed properties” (Table 3-11). The “as-constructed” properties were taken from healthy material samples. The yield strength of 25M bars was taken as 412 MPa to be more conservative since demolition presented a mix of ‘X’ ribbed and bamboo ribbed 25M bars in the girders and material tests indicated that ‘X’ ribbed 25M bars had lower yield strength than bamboo ribbed bars. Using the resulting moment capacity, the equivalent load capacity in a 4-bending test setup was determined by statics. Table 3-11 and 3-12 shows comparisons of predicted load capacity at the cracking stage and the ultimate stage, and the uncracked stiffness, with the measured capacity of Girder LD. The cracking moment was calculated using Eq. 3-10,

$$M_{cr} = \frac{(f_r + \frac{P}{A} + \frac{Pe\bar{y}}{I})I_g}{\bar{y}} \quad \text{Eq. 3-10}$$

where f_r is the modulus of rupture of concrete, taken as $0.34\sqrt{f'_c}$ as per CSA S6:19 requirements for semi-low density concrete, A is the girder cross-section area, I_g is the girder gross moment of inertia, \bar{y} is the distance from the gross centroid to the extreme tension fibre, e is the lumped prestress eccentricity relative to the gross centroid, and P is the effective prestress force, based on the nominal specified values after losses (107 kN per strand and 2140 kN total). Later, cracking load was back calculated by dividing the cracking moment by the shear span of the girder.

Table 3- 11: Test predictions comparison of crack and peak load compared to Girder LD.

	Description	Predicted cracking load, kN	Ratio to LD	Predicted peak load, kN	Ratio to LD
As designed	35 MPa concrete	209	0.871	459	0.721
As constructed-1	53 MPa concrete, as per original drawings (25M bars not included)	218	0.908	483	0.758
As constructed-2	53 MPa concrete, with the 25M bars, elastic plastic mild steel	218	0.908	607	0.953
As tested	53 MPa concrete, 25M bars, and strain hardening	218	0.908	620	0.973

Table 3- 12: Test predictions comparison of uncracked stiffness.

	Description	Uncracked stiffness, Nmm²	Difference compared to LD
As designed	35 MPa concrete	2.76x10 ¹⁴	8.00%
As constructed-1	53 MPa concrete, as per original drawings (25M bars not included)	3.07x10 ¹⁴	2.33%
As constructed-2	53 MPa concrete, with the 25M bars, elastic plastic mild steel	3.07x10 ¹⁴	2.33%
As tested	53 MPa concrete, 25M bars, and strain hardening	3.07x10 ¹⁴	2.33%

It is seen that the accuracy of the prediction increased as more of the “as-tested” properties were considered. The cracking load (Table 3-11) was not greatly affected by the updated reinforcement characteristics since the cracking load depends largely on the concrete properties. For peak load, the strength in concrete changing from 35 MPa to 53.9 MPa did not impact the peak load significantly for the “as constructed-1” calculation, since the moment capacity of tension controlled sections is more strongly correlated with the tension forces and their moment arms than with the concrete compressive strength. Importantly, there was a 25% increase in peak strength when the 25M bars placed in the girders for camber control were taken into account. Including strain hardening behaviour in the mild steel properties had minimal influence on peak strength. At failure predictions indicate that strain hardening was taking place but only slightly with the maximum stress in the 25M bars only be 7% larger than the yield strain.

Overall, the “as-tested” girders were about 33% stronger, in terms of peak load, than the “as-designed” girders – the implication being that there was a significant increase of strength from the updated material properties, particularly the addition of the 25M bars for camber control. The calculations of flexural strength using test material properties, however, indicate that CSA S6:19 (2019) can accurately predict the flexural capacity of the undamaged girders. The ratios between the code prediction using as tested properties and measured baseline value were 0.908 and 0.973

respectively for crack and peak load. As shown in Table 3-12, general principles of mechanics work well the uncracked stiffness of the girder.

3.4 Chapter conclusions

A prestressed concrete bridge was decommissioned after 28 years in service in Barrhead, Alberta due to severe deterioration. This bridge consisted of nine prestressed semi-lightweight concrete girders with different degrees of deterioration. Four bridge girders with different degrees of deterioration were tested under four-point bending to investigate the corrosion effects on the strength capacity of these bridge girders.

1. The “as-built” material properties of the girder were significantly different than the “as-designed properties”. The average concrete strength was 51% larger than the design value. The measured elastic moduli were close (within 10%) compared to the predictions from CSA S6:19, but the accuracy of the predictions slightly increased when age of the concrete and the temperature were considered. Four extra 25M reinforcement bars were found after extraction with the purpose of camber control, which significantly influenced the peak flexural strength. The predicted flexural strength of the girder increased by 5% with the updated concrete strength and another 25% with the extra 25M reinforcement. The flexural methods in CSA S6:19 can accurately predict the ultimate strength capacity of a girder that is in good condition with no visible damage if the material properties are known.
2. All girders, regardless of deterioration level, showed satisfactory service performance in terms of uncracked behaviour. The measured cracking loads for all girders were higher than the design service load. However, none of the girders met the live load deflection limit of $1/800$. The deteriorated girders had lower stiffness than the baseline specimen

Girder LD. The most deteriorated girder HD had a 33.3% decrease in uncracked stiffness compared to the baseline girder LD without deterioration.

3. All girders sustained significant damage with visible cracks after being loaded to the expected design ultimate load which indicated that the bridge never experienced this level of load when it was in service. All girders failed at higher loads than the design ultimate load. In Girders LD and MD, the failure mode was the expected concrete crushing at the top after steel yielded; in girders with a higher degree of actual and simulated deterioration (ID and HD) the failure was sudden with strands snapping. Girder HD and ID had a reduction in flexural strength of 22.9% and 21.8%, respectively, failing suddenly due to strand rupture. Girder MD, with less deterioration, closely followed the behaviour of girder LD with a slight decrease in flexural strength (14.3%) and stiffness (6.3%).
4. The sudden failure mode in deteriorated girders (strand rupture) is attributed to steel corrosion. Steel tensile tests confirmed that strand corrosion greatly affected the post-yield deformation capacity of the strands. Strands with a higher degree of corrosion were more brittle and ruptured suddenly; some even ruptured before they yielded.
5. Assuming the total applied load is equally distributed to all girders through the shear connector and the rest of the untested girders exhibited similar or less deterioration as Girder HD, the average capacity of the bridge girders would still satisfy the design ULS. For bridges with similar design and material properties that sustained resembling degrees of deterioration, the flexural result indicated that these bridges could satisfy the ULS. However, as indicated by the results from Girder HD, the potential mode of failure of a damaged girder is brittle – not desirable for a bridge structure.

CHAPTER 4 : SHEAR RESPONSE

4.1 Introduction

Shear failures are often sudden and can cause catastrophic structural collapses. A well-designed reinforced or prestressed concrete girder should be able to attain its flexural strength, exhibiting ductility via reinforcement yielding, before failing in shear. This is accomplished by proportioning the cross section such that shear stresses are kept low (typically by enlarging the section), and by using transverse reinforcement (stirrups). However, even in members in which shear failures are precluded by design, material deterioration caused by time, chemical attack, and adverse environmental conditions may reduce the shear capacity. The infamous collapse of *De La Concorde* overpass in Laval, QC, killed five people and injured six due to a combination of faulty design, construction errors and deterioration (Johnson et al., 2007). Low quality concrete, more susceptible to freeze-thaw, and the effects of deicing salt over the years exacerbated construction defects on the stirrup anchorage and caused severe deterioration that led to collapse of the bridge.

Investigating the response of reinforced concrete structures subjected to shear is complex, as highlighted in Section 4.2.1. There is scant data on the shear behaviour of full-scale bridge girders subjected to deterioration. Osborn et al. (2012) investigated the near support shear capacity of two types of deteriorated AASHTO Type II bridge girders that were in service for around 40 years (Figure 4-1). The girders were either 7.1 m or 10.5 m long. Both girders were prestressed with 11.1 mm diameter seven-wire prestressing strands. These girders were tested under three-point bending with shear spans kept at 1.22 m, with the exception of one girder tested with a shear span of 1.31 m. Results showed that the more deteriorated the girder, the more difficult it was to predict shear response. They found that predictions per AASHTO LRFD (2009) were conservative and predicted between 28% to 55% of the ultimate shear capacity due to the code's assumption of

plane sections remaining plane. They found that strut and tie models more accurately predicted the strength of the tested girders within 2% to 22% of the average measured value.



Figure 4- 1: Three- point bending test setup (Osborn et al., 2012).

Saqan and Frosch (2009) tested nine 4.67 m long prestressed concrete beams with a shear span to depth ratio of 3.33 to investigate the influence of mild steel bars and prestressing strands on shear response (Figure 4-2). Increasing the cross-sectional area of prestressing strands and mild steel bars increased the shear strength contributed by the concrete in the beam since more reinforcement is better able to control crack widths and maintain aggregate interlock. They found that the total amount of prestressing and steel reinforcement affected the members' behaviour and strength up to the formation of shear cracks, meaning for specimens with the same total amount of reinforcement, the same shear strength contributed by concrete, V_c , was observed.

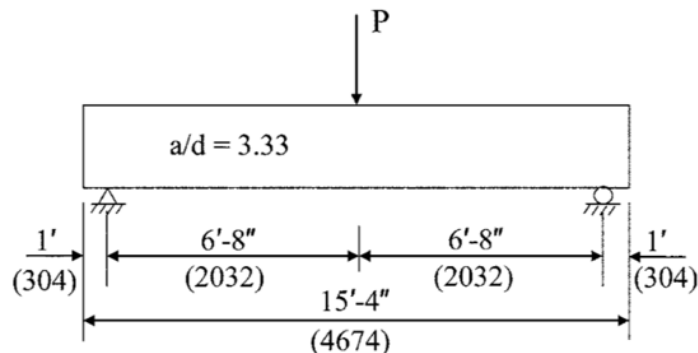


Figure 4- 2: Three- point bending test setup. Dimensions in parenthesis are in mm. (Saqan and Frosch, 2009).

Floyed et al. (2016) investigated the effect of deterioration on two AASHTO Type II bridge girders with corrosion at the ends that were 9.75 m and 14 m long. One girder was prestressed with six straight 127 mm strands and four harped strands. The other was prestressed with ten straight strands and six harped ones. Both girders were tested under three-point bending at both ends with different shear span to depth ratios of 2.0 and 2.5 to create B regions (Figure 4-3). The girder was loaded under 22.3 kN increments until failure. Results show that end corrosion contributed to the observed strand anchorage failure due to bond loss from corrosion and this should be considered an important aspect for evaluating the shear capacity of old bridges.

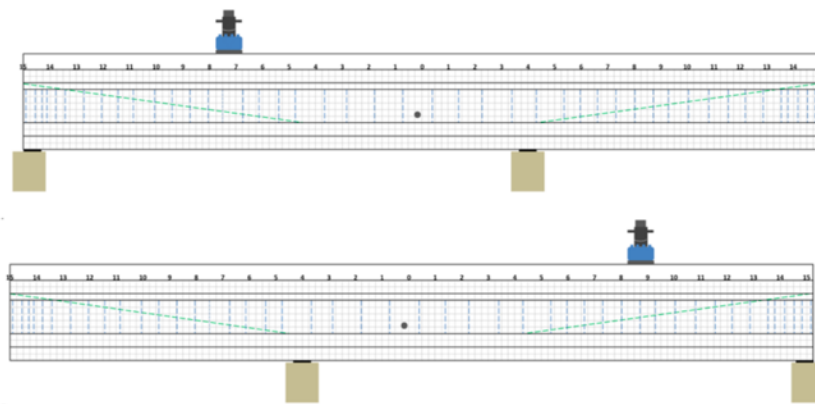


Figure 4- 3: Three- point bending test setup (Floyed et al., 2016).

4.2 Experimental Program

4.2.1 Testing rationale

The shear response of reinforced and prestressed concrete is sensitive to the shear span (a) to effective depth (d) ratio of the member, commonly referred to as the a/d ratio. Girders tested in this program were loaded under two different a/d ratios to evaluate how the shear resistance and failure mode of deteriorated girders is affected by the change in the location of the load point.

The a/d ratio affects the shear transfer mechanism within a member. Members with $a/d < 2.5$ are typically referred to as deep beams, while members with $a/d > 2.5$ are typically referred to as

slender beams (Wight and MacGregor, 2012). In this context, a slender beam is one in which Bernoulli-Euler beam theory is applicable, with plane sections remaining plane (i.e., exhibiting a linear strain profile) under loading. In a deep beam, beam theory cannot be applied as the distribution of strains is nonlinear.

In slender beams ($a/d > 2.5$), shear is transferred to the supports by a combination of elements in compression and tension within the member that resemble a truss. As shown in Figure 4-4, when a beam is loaded relatively far from the support, it develops a compressive force, C , in the top chord, a tensile force, T , in the bottom chord, tension forces in the stirrups, and compressive forces in the concrete between the inclined cracks.

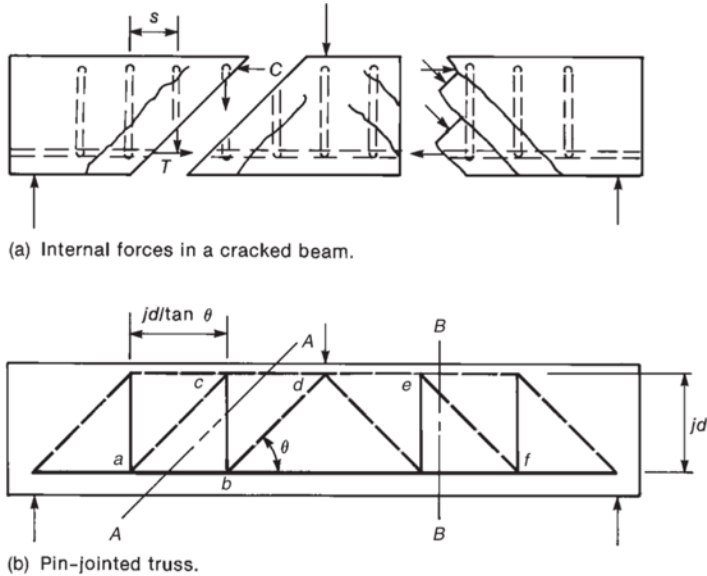


Figure 4- 4: Truss analogy (Wight and MacGregor, 2012).

If the external load is far from the support, external loads cannot transfer directly from the load point to the support through a single compressive strut, since the small angle requires a very large force on the strut that would not satisfy equilibrium. This is why intermediate “elements”, such as stirrups, are required to transfer forces.

If flexural capacity exceeds shear capacity, failure of a slender beam may be caused by shear. For a beam with few stirrups, vertical tension forces cannot be effectively resisted, leading to a shear failure mode called “diagonal tension failure”. This failure mode is characterised by excessive stirrup yielding leading to wide diagonal cracks and loss of aggregate interlock and capacity (Figure 4-5c). With sufficient stirrups present, slender beams are more likely to fail in shear-compression (Figure 4-5a), where concrete crushes at the top of the shear crack in the compression zone. In these members, diagonal crack widths are restrained by the stirrups which maintains aggregate interlock through the crack. Shear tension failure may also occur when the bond between longitudinal reinforcement and concrete fails due to shear cracking along the shear reinforcement (Figure 4-5b).

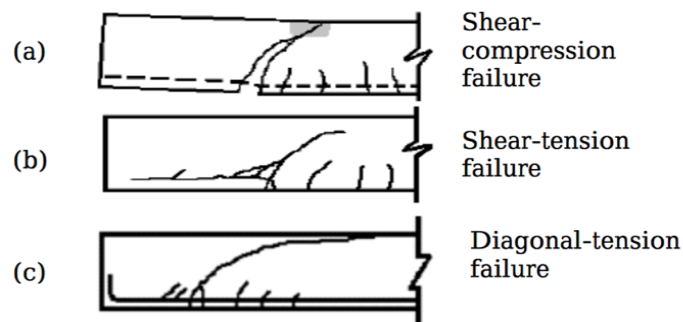


Figure 4- 5: Different types of shear failures (Sinha, 2002).

Short shear span ($1.0 < a/d < 2.5$) members exhibit deep beam behaviour. In these members, load transfer is via the so-called arch action or strut-and-tie action. This mechanism is associated with a diagonal compression strut tied by the flexural tension reinforcement (Figure 4-6).

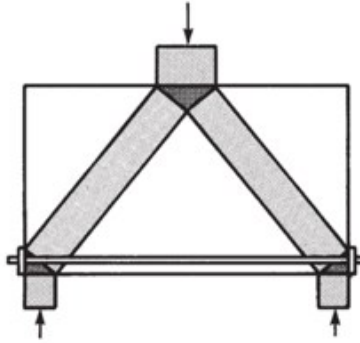


Figure 4- 6: A strut and tie model of a deep beam (Sinha, 2002).

Shear force is transferred to the end support via an inclined compression strut, with cracks often forming parallel to the strut (Figure 4-6). This mechanism is different than beam action in a sense that it transfers the load to the support through the shortest path, so it does not involve transfer of forces through the stirrups. Depending on the amount of crack control reinforcement provided to the beam, these types of beam may fail by the crushing of the compression strut (Figure 4-7), or their strength may also be governed by yielding or anchorage failure of the tension tie.

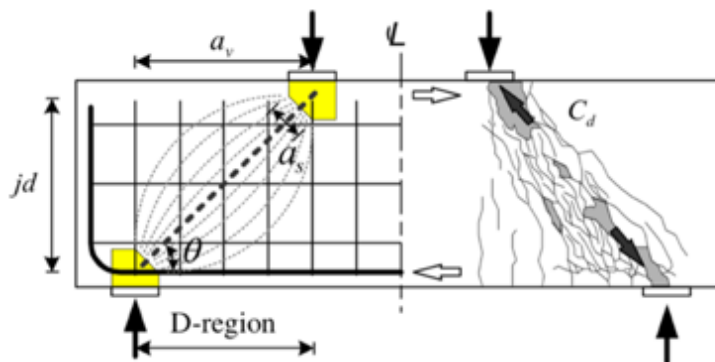


Figure 4- 7: A strut and tie model of a deep beam (Kuo et al., 2010).

Crack control reinforcement is used to prevent failures related to the formation of diagonal cracks in strut and tie models. CSA S6:19 requires the ratio of reinforcement area to gross concrete area shall not be less than 0.003. This reinforcement need not be more than 1500 mm²/m in each face and each direction. The crack spacing parameter s_z shall be assumed to be equal to either the shear

effective depth, d_v , or the distance between layers of crack control reinforcement. The area of crack control reinforcement must satisfy Eq. 4-1:

$$A_s > 0.003b_w s_z \quad \text{Eq. 4- 1}$$

Where b_w is the sectional width. In these tests, both beam and strut-and-tie action were investigated. This was achieved by testing girders under three-point bending with load applied at different locations relative to the closest support (1.0 m and 1.5 m). Girders with a 1.0 m load scheme have an a/d ratio of 1.96 which falls into the category of a deep beam where strut-and-tie action governs. Girders with a 1.5 m load scheme have an a/d ratio of 2.95, falling into the category of a slender beam where beam action governs.

4.2.2 Test girders

The shear specimens were prepared from segments cut from the girders originally tested under flexure, as discussed in Chapter 3. Previous studies used shortened (cut) PC girders to investigate the shear behaviour of full-scale girders (Pei et al., 2008). Limited lab space and the limited number of available girders also made testing full length girders to assess shear response impractical. For reference, flexural tests were performed on four girders, selected from a total of nine girders used in the bridge. After the flexural tests, the ends of the four girders were cut into 3.8 m long segments (Figure 4-8). Damage, including cracking, strand rupture, and crushing that was observed in the flexural tests occurred within the midspan region of each tested girder; therefore, the end segments did not exhibit flexural damage. The shorter segments allowed for a load arrangement where shear forces experienced by the girders were more critical than the bending moments, enabling the study of the shear response of the specimens. The girders were tested under three-point loading using a loading rate of 0.50 mm/min with a point load located either 1.0 m or 1.5 m from one of the ends. Details on test procedures and instrumentation are presented in Section 4.2.3.



Figure 4- 8: Flexural girder cutting.

The nomenclature used to identify specimens is based on the primary identifier presented in Chapter 3 (LD – limited deterioration, MD – moderate deterioration, and HD – high deterioration, and ID – induced deterioration), and a number representing the shear span, in metres (Table 4-1). Figure 4-9 shows the deterioration mapping of the shear specimens. More details on observed deterioration is given in Section 3.2.2. Figure 4-10 shows the stirrup layout from the elevation view of the girder up to 1.5 m. The girder had a solid section about 300 mm from the end. The stirrups were four-legged 10M rebar with spacings ranging from 75 to 200 mm.

Table 4- 1: Test specimens for shear loading.

Test name	Test region shear span, m	Induced damage	Girder description
LD-1	1.0	None	Limited deterioration (no evidence of corrosion staining on girder surface, some longitudinal cracking in concrete at level of bottom reinforcement)
HD-1	1.0	None	Heavily deteriorated (spalling of soffit concrete, noticeable pitting corrosion on stirrups and prestressing strands)
HD-1.5	1.5	None	Heavily deteriorated
MD-1.5S	1.5	Cut stirrups at bottom corner within shear span	Moderately deteriorated (assessed condition between limited and heavily deteriorated cases)
MD-1.5	1.5	None	Moderately deteriorated
ID-1	1.0	Saw cut concrete soffit, cut through 3 strands 750 mm from girder end	Moderately deteriorated
ID-1.5	1.5	Saw cut concrete soffit, cut through 3 strands 750 mm from girder end	Moderately deteriorated

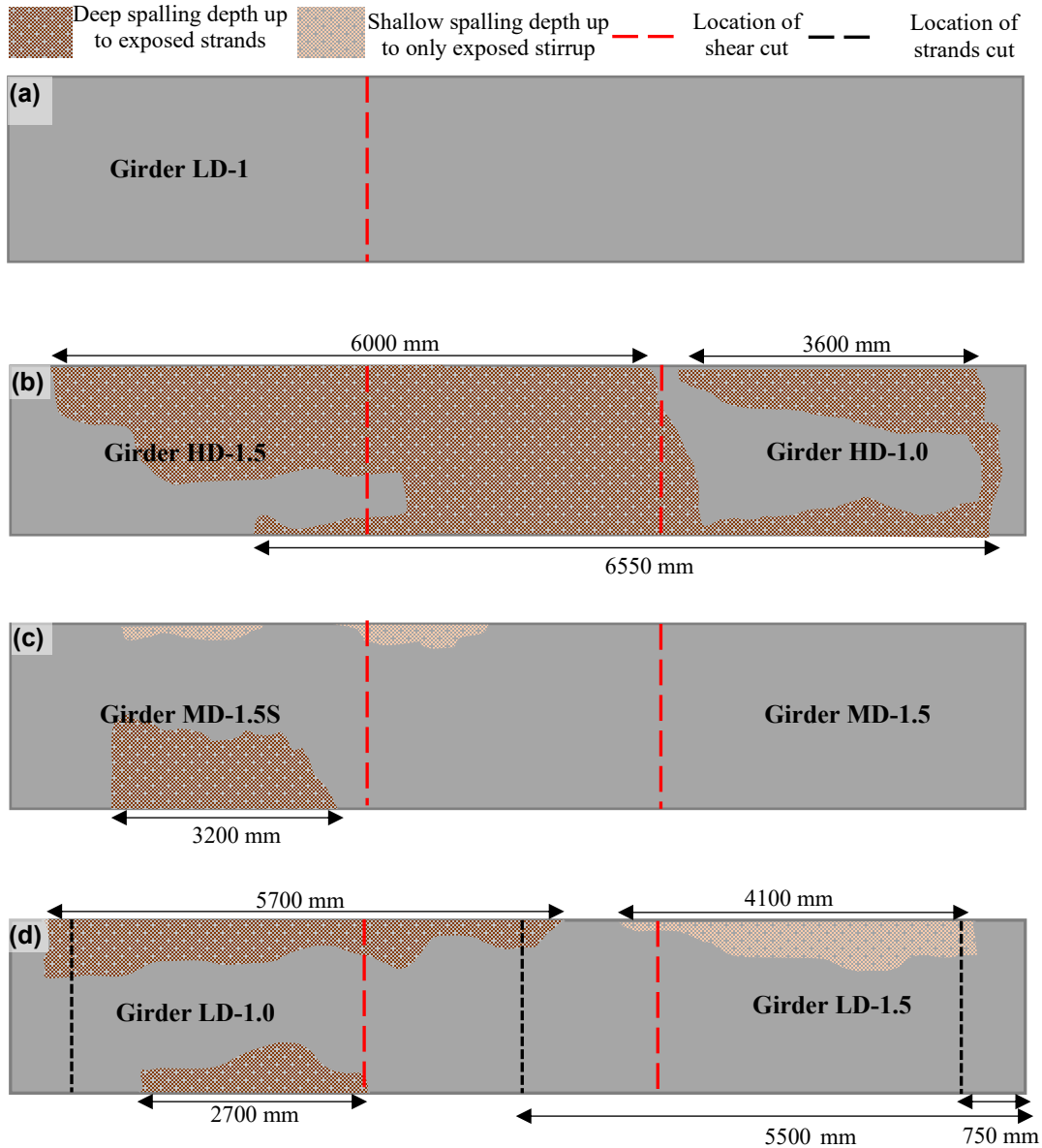


Figure 4- 9: Shear girders from the original flexural girders and their deterioration mapping (a) LD-1 (b) HD-1.5 and HD-1.0 (c) MD-1.5S and MD-1.5 (d) ID-1.5 and LD-1.0.

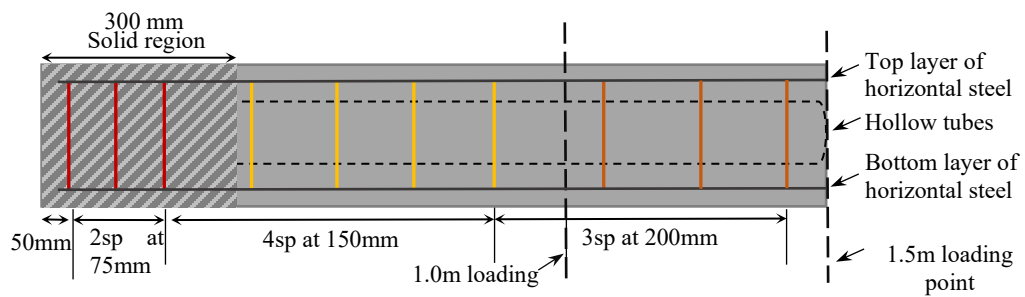


Figure 4- 10:Stirrups layout on the girder up to 1.5m load point.

4.2.2.1 Girder LD-1

Initially, only arch action was to be investigated and only one shear specimen (LD-1) was extracted from Girder LD and tested with 1.0 m load scheme (Figure 4-11a). The other end of the girder was demolished to confirm properties such as concrete strength, bar layout, and to study deterioration within the girder so testing with a 1.5 m loading scheme was not possible for this girder. LD-1 was chosen as the baseline girder because it exhibited limited visible damage from deterioration. As shown in Figure 4-9, LD-1 had no visible concrete loss on the bottom or steel and strand corrosion.

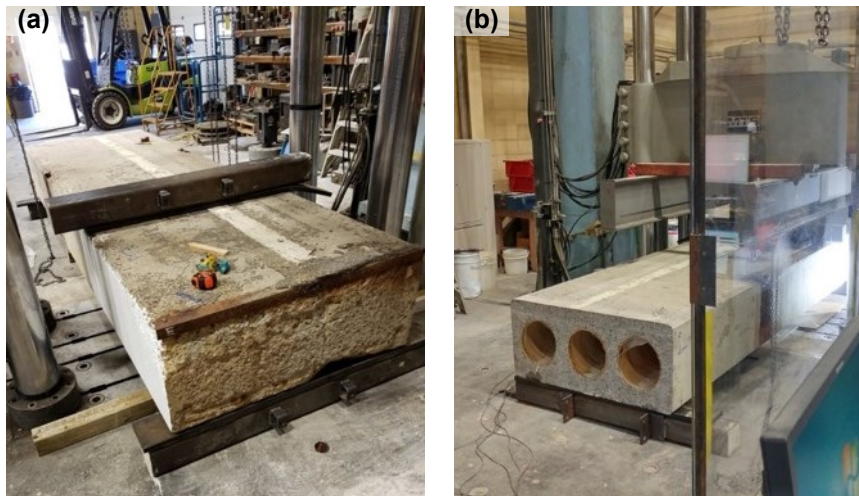


Figure 4- 11: Girder LD-1 with no visible deterioration damage (a) tested shear span region (b) other end.

4.2.2.2 Girders HD-1 and HD-1.5

After testing LD-1, it was decided that 1.5 m load scheme with a larger a/d ratio was needed to investigate a slender beam response that involves more stirrups; therefore, 1.0 m and 1.5 m load schemes were implemented for the ends of Girder HD (Figure 4-9b). Both girders had severe concrete spalling in the bottom, with some spalling on top as well (in particular, HD-1.5). HD-1.5 and HD-1.0 had an estimated 50% and 40% bottom cover concrete loss respectively with both rebar and strands corrosion clearly visible. However, Figure 4-13 shows that HD-1.5 and HD-1, cut from the ends of the Girder HD, presented less severe corrosion than the midspan region of

their parent girder. Although corrosion was observed in the shear reinforcement (Figures 4-13e), the majority of the strands were still well embedded and intact at the girder ends, while at midspan (Figure 4-13a) multiple strands had snapped as mentioned in Section 3.2.3.3 and Figure 3-15. In consequence, HD-1 and HD-1.5 were not the most deteriorated specimens in the shear series, due to their limited strand corrosion, compared to the tests that are discussed next. However, HD-1 and HD-1.5 did have the most concrete loss among all the test specimens.



Figure 4- 12: (a) Girder HD-1 and (b) Girder HD-1.5.

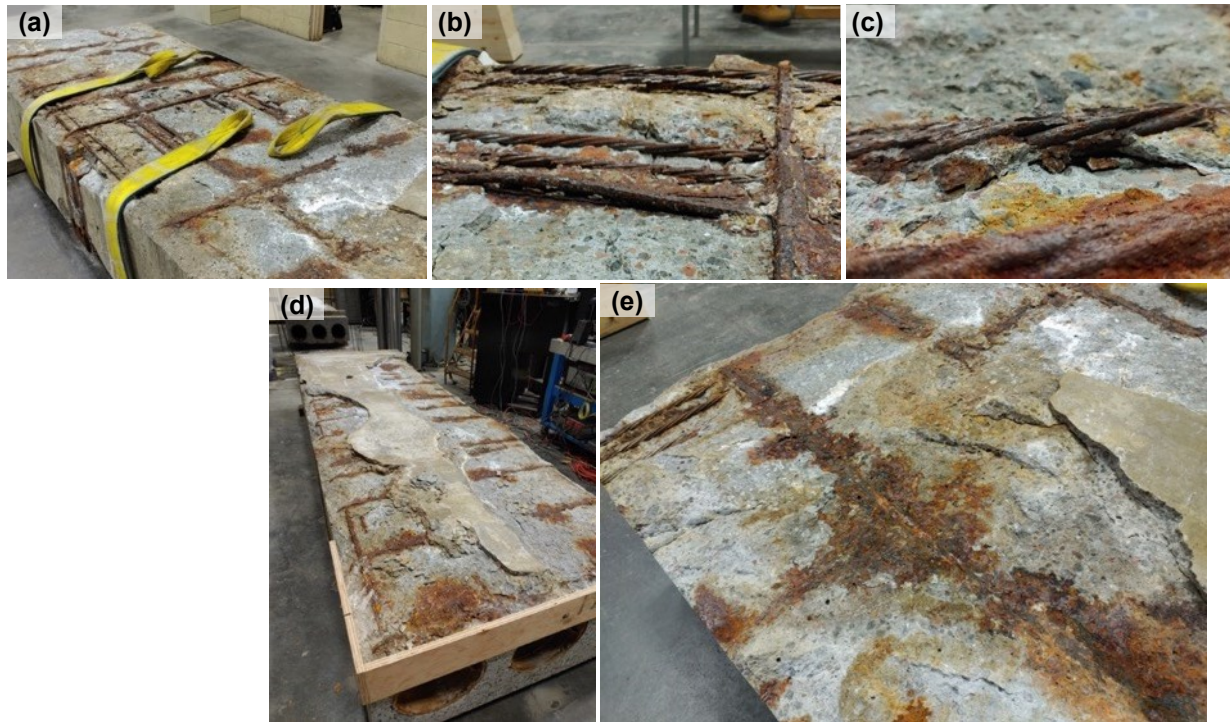


Figure 4- 13: Location of deterioration on the tension side of Girder HD (a) midspan region of girder with most severe corrosion (b) strands in midspan region showing evidence of pitting corrosion (c) photo of single strand showing damage at midspan (d) significant spalling and reinforcement corrosion but limited strand corrosion for Girder HD-1 (e) significant spalling and reinforcement corrosion but limited strand corrosion for Girder HD-1.5.

4.2.2.3 Girders MD-1.5 and MD-1.5S

Both ends of Girder MD were tested under 1.5 m loading after they were cut from Girder MD (intermediate deterioration) to investigating how bottom shear reinforcement loss affected the truss mechanism for load transfer. Girders MD-1.5S and MD-1.5 had moderate level of deterioration (Figure 4-9c). MD-1.5, even though the concrete cover was still intact, had large horizontal cracks on the side along the bottom concrete cover, indicating corrosion and spalling risk (Figure 4-14b). MD-1.5S had an estimated 30% concrete spalling on the bottom. However, in their original condition, the stirrups were relatively healthy in both specimens. To investigate how stirrup loss affects the truss mechanism for load transfer, MD-1.5S was modified to simulate the loss of bottom shear reinforcement. Seven stirrups were cut, at both legs, in the bottom of MD-1.5S to simulate

severe stirrup corrosion (Figure 4-15) similar to that observed at the bottom and corners of each stirrup in other tests. MD-1.5 was used as a reference for MD-1.5S as it had its stirrups intact.



Figure 4- 14: (a) Girder MD-1.5S (b) Girder MD-1.5.



Figure 4- 15: Cut stirrups (cuts circled) on girder MD-1.5S. These stirrups had limited deterioration as evidenced by their colour and lack of pitting corrosion.

4.2.2.4 Girders ID-1 and ID-1.5

As shown in Figure 4-16 Girder ID-1 and ID-1.5 showed signs of moderate deterioration. The side profile of the girders indicated that there was some concrete spalling with ID-1.0 and 1.5 having an estimated 40% and 20% of cover concrete loss respectively. Both ID-1 and ID-1.5 had visible rebar and strand corrosion.

In this girder, the parameter investigated was the effect of the strand loss on the arch and truss mechanisms for load transfer. A 21% strand loss was simulated by cutting three strands 750 mm from the end in both specimens (Figure 4-16c). Strand cutting required removing the concrete cover at the ends. Exposing the reinforcement revealed that the steel reinforcement and strands were in fairly good condition, with the majority of the reinforcement having adequate embedment in the concrete.

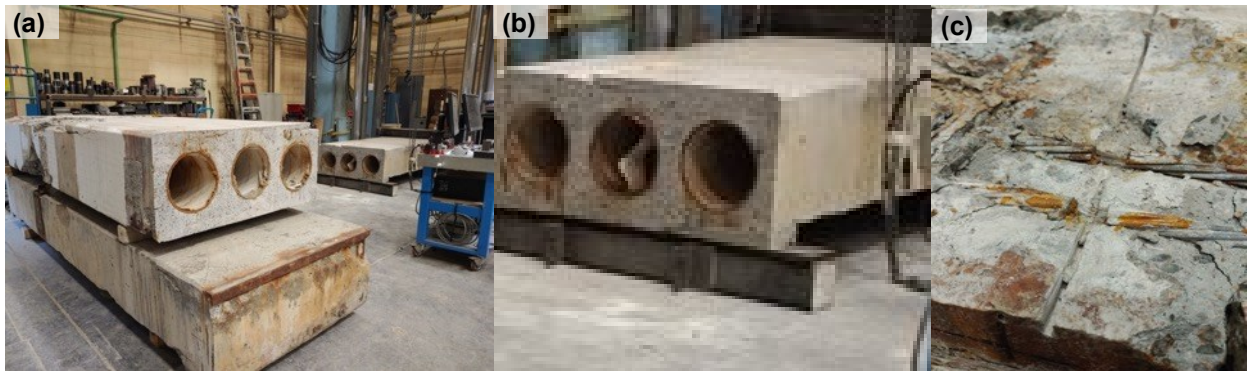


Figure 4- 16: (a) Girder LD-1, (b) Girder LD-1.5, and (c) Cut strands for Girder ID for induced deterioration.

4.2.3 Test setup and instrumentation

Three-point bending tests were carried out using a hydraulic actuator load frame with a capacity of 6100 kN (Figure 4-17). The shear girders were cut and tested in the Morrison Structural Lab at the University of Alberta after the flexural tests presented in Chapter 3 were completed. The 3.8 m girder segments were simply supported on two 152 mm by 152 mm rectangular hollow steel sections (HSS) acting as supports. To achieve even loading surfaces and simulate the girder supports in practice, the ends of the beams in contact with the HSS with concrete spalling were grouted with a fast curing concrete mix (Figure 4-18).

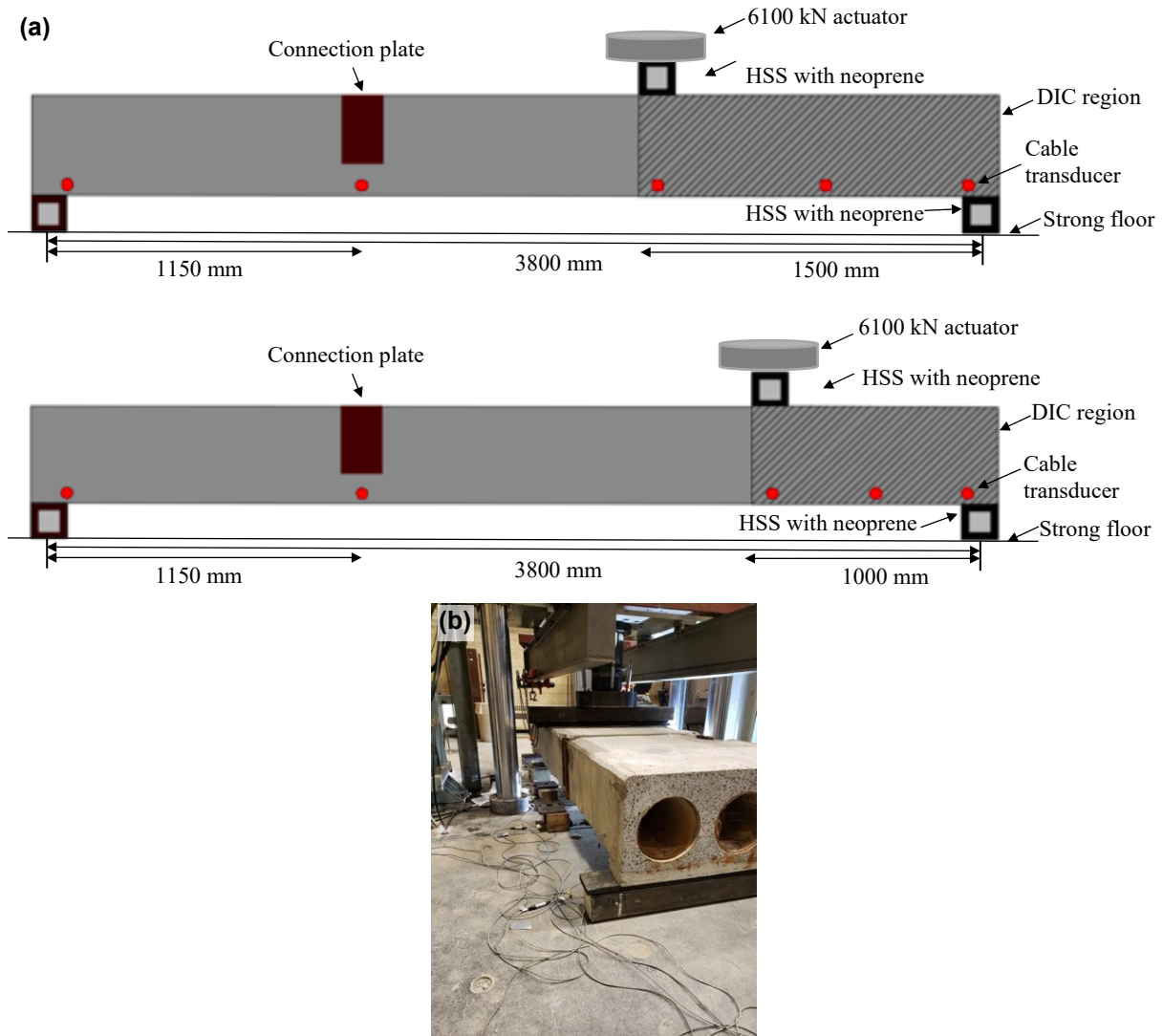


Figure 4- 17: Test setup and instrumentation (a) Elevation view of test setup showing location of load points and instrumentation (b) Photo of test specimen.

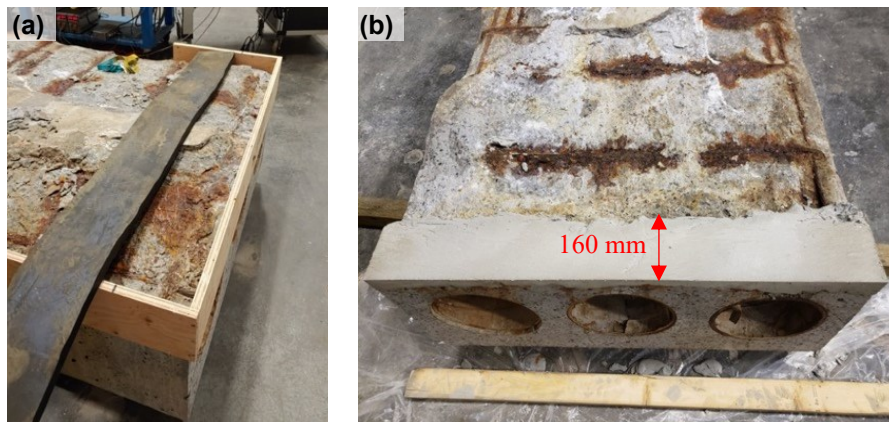


Figure 4- 18: Grouting of girder end with damage (a) before grouting (b) after grouting.

Another HSS placed across the top of the girder to distribute loads across the girder width to achieve three-point bending. A 25.4 mm thick neoprene pad was placed on top of each support to simulate the actual bridge support conditions. Two loading schemes were used. In LD-1, HD-1, and ID-1, load was applied one metre from the end, while the rest of the tests (HD-1.5, MD-1.5, MD-1.5S and ID-1.5) were loaded at 1.5 m from the end. Each specimen was tested to failure at 0.5mm/min. Tests were stopped once the specimen lost 50% of its strength. Tests were occasionally paused to investigate girder responses, particularly crack formation and angles.

Five cable transducers with a sample rate of 1 Hz were used to measure deflection. The cable transducers were placed on both ends of the specimen, below the connection plate, load point, and at midpoints between the load point and supports. Cameras were placed focusing on the shortest shear span of each test to capture the crack formation and pattern during testing. Photos were taken every 15 seconds for each test. Detailed DIC analysis to measure crack widths and deformations was not completed in this thesis, but qualitative (i.e. no formal measurements but using the software to identify crack locations) DIC analysis was used to identify crack formation.

4.3 Results and Discussion

4.3.1 Load-deflection relationship

The relationship between shear force, calculated from statics based on the actuator load and locations of loading and reaction points, and deflection at the loading point is shown in Figure 4-19. The force reported in the load deflection curves is the largest shear force carried by the specimens along their span. Deflections shown in Figure 4-19 do not include the initial upward camber, and the shear force reported does not include the self-weight. The self-weight contribution to shear, based on a self-weight of 7.65 kN/m as specified by standard AT drawings (1988) is estimated to be around 14 kN which is around 2% of the required shear force to cause failure in

these girders. Deformation in the supporting neoprene pads was factored out of Figure 4-19 using the deformations measured at either end of the girder so the reported deflection at the load point is based on the actual deflection of the specimen itself at the load point.

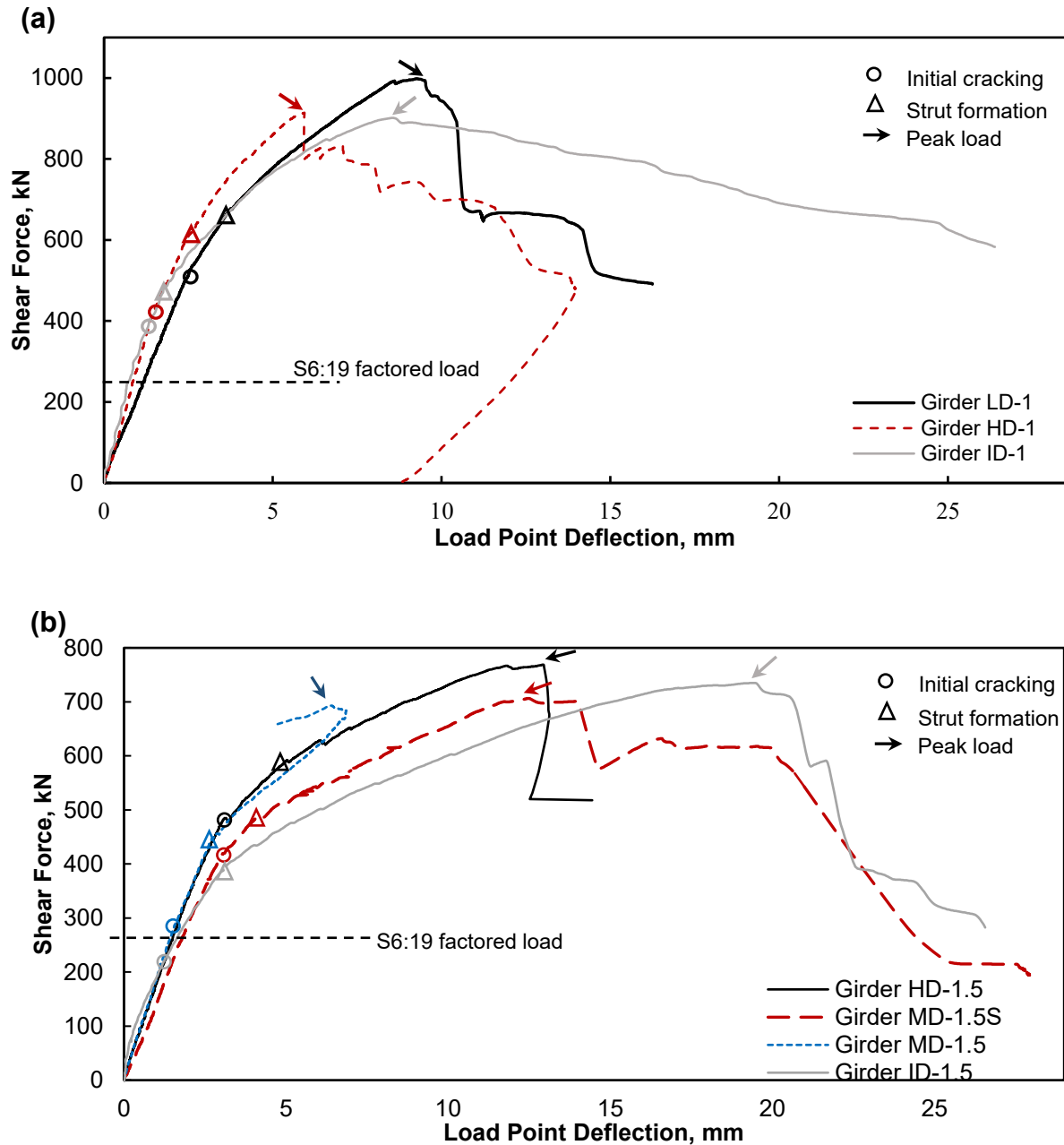


Figure 4- 19: Load deflection curves for (a) tests with 1.0 m shear span and (b) tests with 1.5 m shear span.

Before testing, expected ultimate limit state (ULS) load demands on the girder were calculated from the Canadian Highway Bridge Design Code (CSA S6, 2019). CSA S6:19 CL-W 625 kN is used for the design truck. The most critical case for shear was calculated through an influence line analysis using a CL-W 625 truck axle load on a 10.8 m span. One line of wheels was assumed to be applied on the girder, with no load sharing between girders. The maximum shear under this loading was 142.4 kN. The most critical shear as per S6:19 occurs when including a lane load (a uniformly distributed load of 9 kN/m) in the calculation for shear force and reducing the truck load to 80%. Using this calculation, the maximum unfactored shear force was 162.5 kN. The factored shear, treating the entire load as live load, is 276 kN (using a live load factor of 1.7).

Table 4-2 shows the shear force at the first cracking, strut formation, and peak load. Cracking was identified as the first change of slope on the load deflection curve as shown in Figure 4-19. Identification was made in the load curve because the cracks were not visible to the naked eye from the safe stand-off distance during the test. Qualitative DIC analysis confirms that the first slope change corresponds to initial crack formation.

Strut formation was identified as the slope change after initial cracking was observed in the load-displacement curve. Strut formation is characterized by noticeable damage in the girders, where inclined cracks formed on the side of the girder (such as Figure 4-20). The peak load is the maximum load in the shear force – displacement curve.

Table 4- 2: General test results.

Test name	Cracking, kN	Strut formation, kN	Maximum shear force, kN	Failure mode
LD-1	517	668	998	Strut crushing
HD-1	435	611	914	Strut crushing
ID-1	411	474	901	Strut crushing accompanied by anchorage failure
HD-1.5	485	585	769	Shear compression failure
MD-1.5S	417	483	706	Diagonal tension failure
MD-1.5	295	435	693	Anchorage Failure
ID-1.5	219	398	735	Shear compression failure

4.3.2 1.0 m load scheme

4.3.2.1 Initial cracking

Girder LD-1 had the highest cracking load due to its relatively healthy, undamaged condition, cracking at 517 kN. HD-1 followed, cracking at 435 kN, and ID-1 cracked at 411 kN. Cracks were not visible to the naked eye due to the prestressed nature of the girders, but initial cracking was identified as a slope change in Figure 4-19. All specimens remained uncracked after they were loaded to the designed ULS (276 kN). Girder HD-1, that had a major loss of concrete cover, showed a 15.9% reduction in cracking shear force compared to the baseline LD-1. ID-1, with 21% strand loss, had a decrease in cracking shear force reduction of 20.5% compared to LD-1.

4.3.2.2 Strut formation

DIC analysis identifying the crack formation was used to capture the strut formation as visible inclined cracks on the girder web; it can also be identified as a second slope change in the load deflection curve. Girder LD-1, the baseline specimen with no visible deterioration, formed a visible inclined crack (Figure 4-19) at 668 kN (Figure 4-20a). Girder HD-1 (Figure 4-20b) followed, with strut formation at a load of 611 kN. Girder HD-1 had an 8.5% reduction in strut formation load compared to LD-1, due to severe concrete loss. DIC did not capture the initial strut formation of Girder ID-1, because struts first formed on the opposite face of the girder where the cut strands were located. This asymmetry is attributed to the way the strands were cut; the strands were only cut on one side of the girder, which caused the first struts to form on the side where the cut strands were located. Strut formation for ID-1 was identified by using the load deflection curve (Figure 4-19). ID-1 formed struts at the lowest load level, 474 kN, which indicated that the simulated strand loss had a considerably negative impact on the girder's ability to form struts, given the fact that it originally had a relatively healthy state, similar to that of LD-1.

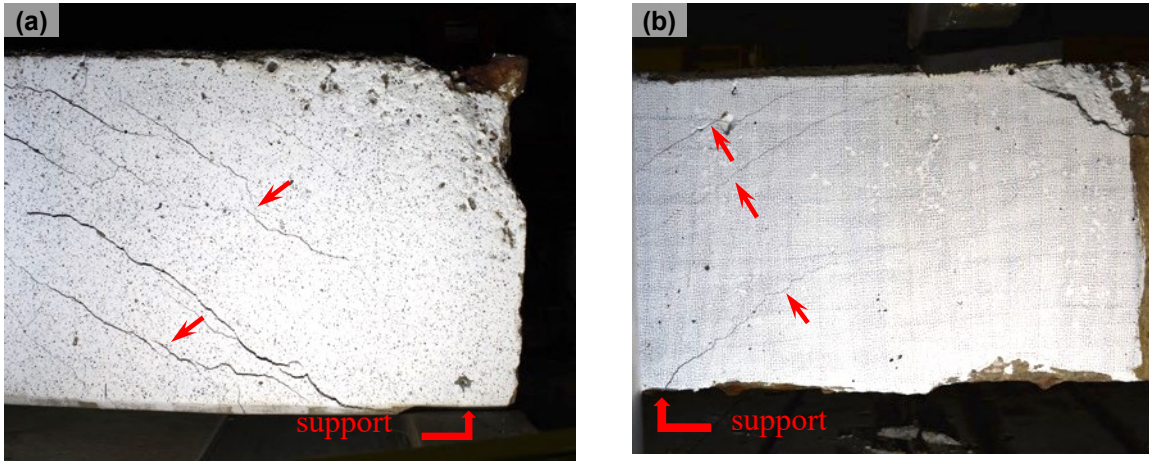


Figure 4- 20: Strut formation on shear girders with diagonal cracking indicated with arrows (a) Girder LD-1 (b) Girder HD-1.

4.3.2.3 Peak load

As expected, the baseline LD-1 had the largest peak load (998 kN). HD-1 had a slightly lower (8.4%) peak load, at 914 kN. Both specimens failed as shown in Figure 4-21 by crushing of the compressive struts, which was expected for girders with such low span to depth ratio. Since stirrups were less involved in the force transfer due to arch action, corrosion of the shear reinforcement (Figure 4-7) in Girder HD-1 did not have a major impact on the shear capacity.

Girder ID-1, with cut strands, showed a 9.6% lower capacity compared to LD-1, failing at 901 kN. ID-1 failed in strut crushing accompanied by signs of strand debonding at the support. Horizontal cracks at the level of the strands formed at the support, accompanied by a loud snapping sound. The cutting of 21% of the strands, simulating severe strand corrosion, did not have a significant influence in the peak load capacity of the girder, as it led to only a 9.6% reduction. The reason for this could be the remaining strands still maintained a satisfactory bond, as the cover was observed to be in good condition.




Test name	Failure mode	Description
Girder LD-1		strut crushing under load point
Girder HD-1		strut crushing under load point
Girder ID-1		Strut crushing accompanied with some anchorage failure at support

Figure 4- 21: Failure modes of shear girder with 1.0 m load scheme.

4.3.2.4 1.0-m loading scheme – summary of experimental performance

As shown in Section 4.3.1, a factored ULS load of 276 kN was calculated using the CL-625 truck from CSA S6:19 (2019) for the 1.0 m load scheme. All specimens with 1.0 m shear spans had capacities well above the design ULS shear load at all stages as shown in Table 4-3. Despite the 21% strand loss and negative effects (29%) on strut formation, ID-1 was still 3.26 times stronger than the designed ULS at peak load. This shows that strand loss had a more negative impact on the load when the compressive strut formed (29% decrease) than the peak load at failure (9.6%

decrease). This is attributed to the wider cracks observed in the girder when the strands were cut, causing the loss of prestress. The reduced prestress means that there was less compressive stress to overcome before cracking, leading to earlier formation of the compressive strut in ID-1 compared to the other girders

Table 4- 3: Peak load of the shear girders and ratios to designed ULS.

Test name	Peak load (kN)	Ratio to designed ULS
Girder LD-1	998	3.62
Girder HD-1	914	3.31
Girder ID-1	901	3.26

4.3.3 1.5 m load scheme

4.3.3.1 Initial cracking

Like with the 1.0 m tests, cracking was identified as a change in the initial slope in the load deflection curve in Figure 4-19 and corroborated with qualitative DIC. HD-1.5 first cracked under a shear force of 485 kN, while MD-1.5S (stirrup corners cut) showed initial cracking at 417 kN. MD-1.5 cracked at 295 kN, while ID-1.5 (with 21% strand loss) cracked at 219 kN.

As shown in Figure 4-9, HD-1.5 was not the most deteriorated specimen (due to the modifications that were done on MD-1.5S and ID-1.5 with the cut stirrups and strands); however, HD-1.5 did have the most concrete spalling. HD-1.5 had the lowest stiffness as shown in Figure 4-19. Strand corrosion (ID-1.5) and inadequate development length (MD-1.5) seemed to have a larger impact on the crack formation of the shear girders more than corrosion of the stirrups (MD-1.5S) and concrete spalling (HD-1.5).

4.3.3.2 Strut formation

All girders formed visible inclined cracks with a second slope change (Figure 4-19). As shown in Table 4-4, HD-1.5 carried the largest shear before strut formation (Figure 4-22c) followed by MD-1.5S, with simulated stirrup loss (Figure 4-22a). The results showed a higher load at strut

formation from HD-1.5 than MD-1.5S, indicating that stirrup corrosion played a more significant part in negatively affecting the shear strength of these girders than concrete loss.

Table 4- 4: Strut formation of the shear girders and ratios to designed ULS.

Test name	Strut formation (kN)	Ratio to designed ULS
HD-1.5	585	2.12
MD-1.5	435	1.58
MD-1.5S	483	1.75
ID-1.5	398	1.41

For MD-1.5, the strut formed at an even lower load (435 kN). With a moderate damage condition and no induced damage, it was unexpected that MD-1.5 would have the least shear force at strut formation. One cause for this behaviour could be the fact that the anchorage on the cut side was damaged, causing the reduction in shear strength regardless of the deterioration condition of the girder. The bond damage is evidenced by the failure mode exhibited by the beam which consisted in anchorage failure as shown in Figure 4-23. The bond damage may have been caused by the previous flexural tests conducted on the beam, since MD-1.5 exhibited no severe damage from deterioration as shown in Figure 4-9c. Initial strut formation was not captured by DIC because it was suspected that struts first formed on the opposite side with the inadequate anchorage.

As shown in Table 4-4, ID-1.5 formed a strut at the lowest load and indicated a 32% reduction of strut formation load compared to HD-1.5, which suggests that loss of prestress area (from cut strands or corrosion) plays a more significant role than concrete spalling, stirrup loss, and development length issues in negatively affecting strut formation. Loss of prestress area means lower prestressing force which lead to lower compression force on the concrete therefore less stress to overcome to form struts.

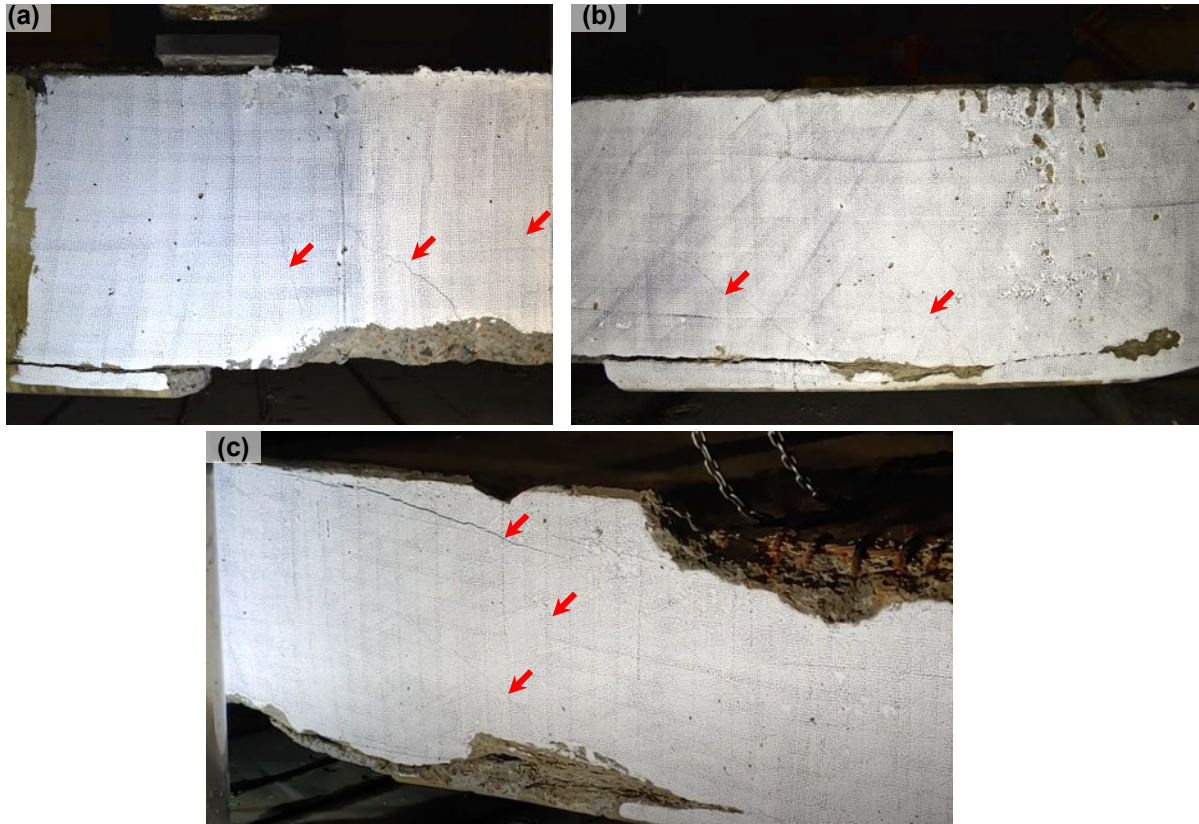


Figure 4- 22:Strut formation with crack location indicated by arrows (a) Girder MD-1.5S (b) Girder ID-1.5 (c) Girder HD-1.

4.3.3.3 Peak load

Girder HD-1.5 reached a peak shear force of 769 kN and then failed under shear compression with crushing at the top of the shear crack beside the load point (Figure 4-23). This failure indicates that, with the beam action shear transfer mechanism, the stirrups were sufficient to resist the tension forces. HD-1.5 was 2.79 times stronger than the design ULS load.

ID-1.5 had the second largest peak shear force of 735 kN. It failed due to shear compression failure with the crushing of the concrete at load point. Even with the 21% strand loss, with the tendons being cut at 750 mm from the end, no horizontal cracks associated to strands pullout were observed. ID-1.5 was 2.66 times stronger than the ULS design load (Table 4-5).

Girder MD-1.5S followed, with a peak strength of 706 kN. The failure mode of MD-1.5S was diagonal tension failure where a large diagonal crack across the girder accompanied by some flexural shear cracks propagating toward the bottom as shown in Figure 4-23. The cut stirrups loss in MD-1.5S could not sufficiently resist the shear load which led to yielding of the stirrups hence the diagonal tension failure. However, MD-1.5S still had a capacity exceeding the S16:9 factored shear load by 2.56 times (Table 4-5).

Girder MD-1.5 had the lowest peak load, at 693 kN. Instrumentation did not properly capture the load displacement relationship of MD-1.5 at failure because this specimen had a sudden anchorage failure (Figure 4-23) on the end located away from the load point. The load-deflection curve (Figure 4-19) indicates a change in direction in the girder's deflection once MD-1.5 reached a shear force of 683 kN. The deflection of the girder started to decrease even though MD-1.5 had not yet reached peak load. The deflection at the failing end of the girder increased drastically, which caused changes in the midspan deflection in the load deflection curve. MD-1.5 failed at 693 kN with a sudden drop in capacity followed by strands pulling out. Slippage of the strands was also observed. As shown by the photo of MD-1.5 from Figure 4-23, strands and the 25M bars slipped and recessed into the girder due to the insufficient development length and bond strength on the cut side. Horizontal cracks at the failed end are indicative of anchorage failure as well. Figure 4-23 shows that the anchorage failure also led to strut crushing. Despite this, MD-1.5 still resisted 2.51 times the design ULS load.





Test name	Failure mode	Failure type
Girder HD-1.5		<p>Shear compression failure with crushing of concrete beside load point at the top of the shear crack</p>
Girder MD-1.5		<p>Anchorage failure of horizontal reinforcement on the cut side of the girder which also led to strut crushing. The cross section indicated that reinforcement and strands slipped and retracted into the girder</p>
Girder MD-1.5S		<p>Diagonal tension failure due to insufficient stirrups</p>
Girder ID-1.5		<p>Shear compression failure</p>

Figure 4- 23: Failure modes of shear girders with 1.5m load scheme.

Table 4- 5: Peak load of shear girder and ratio to Designed ULS.

Girder name	Peak load (kN)	Ratio to designed ULS
Girder HD-1.5	769	2.79
Girder MD-1.5S	706	2.56
Girder ID-1.5	735	2.66
Girder MD-1.5	693	2.51

4.3.3.4 1.5-m loading scheme – summary of experimental performance

Even with induced damage, ID-1.5 (with 21% of strands cut) and MD-1.5S (with the bottom stirrups cut) still performed well above the ULS loading (Table 4-5). Specimens with reduced corrosion or no induced damage failed with a typical slender beam failure: shear-compression failure. Specimens with more severe stirrup loss failed with diagonal tension failure and the specimen with inadequate development length failed by anchorage failure. However, the difference in peak load was only 9.9% between the largest and smallest peak loads. The deterioration appears to have affected the loads causing crack formation more than the peak load. ID-1.5 cracked at a lower load, 54.8% less than HD-1.5. HD-1.5 is used as a reference in this section because of its fair condition, with reduced concrete spalling and moderate degree of shear reinforcement corrosion (Figure 4-9) without any induced damage. Anchorage and bond issues also caused considerable decreases in cracking load, with MD-1.5 cracking at loads 39.2% lower than HD-1.5. When compared to the factors discussed above, stirrup loss played a minor role, with MD-1.5S cracking at a load 14% below that of HD-1.5. The strut formation load was more affected by strand loss than other kinds of deterioration seen in the specimens. ID-1.5 had the lowest load at strut formation (Table 4-4) which was 32% lower than HD-1.5's load at strut formation.

4.3.4 Comparison to design code predictions

CSA S6:19 (2019) provisions were used to calculate the flexural strength of the girders in Chapter 3 SECTION 3.3.5. The general method for shear resistance in CSA S6:19 was used to calculate

the shear capacity of the girders with both 1.0 m and 1.5 m load schemes. The general method for shear in S6:19 is based on Modified Compression Field Theory (MCFT). Even though MCFT has been proven to be conservative in predicting shear strength of a specimen with a/d ratio less than two due to the assumption of plane section remain plane (Murray, et al., 2019), its effectiveness to predict the shear strength for the 1.0 m load scheme (a/d ratio of 1.96) will be assessed in this study. Since the strut and tie method is highly variable at predicting shear strength depending on the sectional geometry model the designer has chosen, it is not used for this investigation.

In S6:19 the shear resistance of a concrete specimen, V_r , is shown in Eq. 4-2,

$$V_r = V_c + V_s + V_p \quad \text{Eq. 4-2}$$

Where V_c and V_s are the shear resistances provided by the concrete and transverse reinforcement respectively, and V_p is the vertical component of the prestressing force. V_p is zero in this study since strands were not harped or draped. The shear resistances given by the concrete and transverse reinforcement were calculated using Eq. 4-3 and 4-4. The material reduction factors for concrete and steel, ϕ , were set to one to compare against test predictions.

$$V_c = 2.5\beta f_{cr} b_v d_v \quad \text{Eq. 4-3}$$

$$V_s = \frac{f_y A_v d_v \cot \theta}{s} \quad \text{Eq. 4-4}$$

Where β is a factor accounting for the force resisted by the concrete, calculated to be 0.224 for 1.0 m and 0.236 for 1.5 m load scheme; f_{cr} is the tensile strength of the concrete, calculated to be 2.5 MPa, and cannot exceed 3.2MPa using $f_{cr} = 0.34f'_c{}^{0.5}$ (used for semi-low density concrete) where f'_c is the concrete compressive strength; b_v is the width of the section within the shear span accounting the reduction caused by the voids which calculated to be 306 mm; and d_v is the effective shear depth of the section, calculated to be 396 mm.

In Eq. 5, f_y is the yield strength of the transverse steel reinforcement which is 400 MPa, A_v is the area of transverse steel per spacing which is 400 mm² for four legged stirrups, θ is the crack angle measured from the bottom surface of the specimen, calculated to be 32.7 degrees and 32.3 degrees for 1.0 m and 1.5 m load scheme respectively and s is the spacing of the transverse steel reinforcement which is 150 mm for 1.0 m and 200 mm for 1.5 m load scheme. To calculate the crack angle θ and factor β , the longitudinal strain at mid-depth of the section, ε_x , was determined first using Eq. 4-5:

$$\varepsilon_x = \frac{\frac{M_f}{d_v} + V_f - V_p + 0.5N_f - A_{ps}f_{po}}{2(E_S A_S + E_p A_{ps})} \quad \text{Eq. 4- 5}$$

Where M_f , V_f , and N_f are the moment, shear force and axial load at the considered section. N_f and V_p are zero because of the straight strands and no external axial loading. A_{ps} and A_S are the area of reinforcing bars and prestressing tendons in the flexural tension zone which are 1994 mm² and 2700 mm² respectively. f_{po} , the stress corresponding to the locked-in strain in the strands, is assumed to equal f_{pr} and is calculated using Eq. 4-6:

$$l_d = 0.145(f_{pr} - 0.67f_{pe})d_b \quad \text{Eq. 4- 6}$$

where d_b is taken as 12.7 mm for the diameter of the seven-wire strands, l_d , the development length, was taken as the distance from the end of girder to the location of the point of application of the load, f_{pe} , the effective stress in the tendons after losses, was taken as 1073 MPa given by the stock drawing (AT, 1988). Assuming that f_{pr} is equal to f_{po} at ultimate (CPCI, 2017) as suggested in the stress corresponding to the locked-in strain in the strands is 1262 MPa and 1533 MPa for 1.0 m and 1.5 m load scheme respectively; The stress loss was calculated according to

the stock design (AT, 1988) with 22 kN/strand loss and f_{pr} , the stress in the tendons at factored resistance, represented the locked-in stress.

For the general method, θ and β are determined by using Eq. 4-7 and 4-8:

$$\beta = \left[\frac{0.4}{1 + 1500\varepsilon_x} \right] \left[\frac{1300}{1000 + s_{ze}} \right] \quad \text{Eq. 4-7}$$

$$\theta = 29 + 7000\varepsilon_x \quad \text{Eq. 4-8}$$

Where s_{ze} is crack space factor taken as 300 mm for these girders since the minimum required amount of transverse reinforcement was provided to mitigate the shear size effect.

The shear resistances of girders with 1.0 m and 1.5 m load schemes were calculated using as-built material properties (Table 4-6) with predictions from CSA S6:19 shown in Table 4-7. Table 4-8 indicates that when compared with the test result, the CSA S6:2019 (2019) is conservative in predicting the shear strength of the girder. The accuracy of the code equation increases when the span to depth ratio increases from 1.0 m to 1.5 m load scheme, as the strain distribution becomes more linear. Regarding the effect of damage on the predicted shear strength, it is seen that reductions in A_p and A_v (loss in strand area and stirrup area, respectively, due to corrosion) lead to smaller shear strengths, as seen during the tests.

Table 4- 6: Material properties of the as tested shear girder.

	f'_c (MPa)	AS_{10M} (mm ²)	AS_{25M} (mm ²)	f_y (MPa)	E_s (MPa)	A_p (mm ²)	f_{pu} (MPa)	E_p (MPa)
As tested	53.9	700	2000	400	200000	1994	1860	200000

Table 4- 7: Shear resistances of different load schemes using CSA S6:19 (2019).

Load scheme	Shear resistance $V_{r_{predicted}}$ (kN)
1.0 m	797
1.5 m	656

Table 4- 8: Test prediction comparison.

Test name	$V_{r_{test}}$ (kN)	$V_{r_{test}}/V_{r_{predicted}}$
LD-1.0	998	1.25
HD-1.0	914	1.15
ID-1.0	901	1.13
HD-1.5	769	1.17
MD-1.5S	706	1.08
MD-1.5	693	1.06
ID-1.5	735	1.12

4.4 Chapter Conclusion

A prestressed concrete bridge was decommissioned after 28 years in service near Barrhead, Alberta, due to severe deterioration. The bridge consisted of nine prestressed semi-lightweight concrete girders with different degrees of deterioration. Three shear specimens were tested with three point bending at 1.0 m load scheme and another four specimens were tested with a 1.5 m shear span after flexural testing to investigate the deterioration effect on the shear capacity.

1. Span to depth ratio (a/d) affected failure modes. For 1.0 m load scheme with an a/d ratio of 1.96, all specimens failed by struts crushing, because less stirrup reinforcement is involved in the arch action mechanism. For the 1.5m load scheme with an a/d ratio of 2.94, the failure mode depended on various factors. When the girder was in fair condition where stirrups, flexural reinforcement, and strands were sufficient to resist the tension forces in the truss mechanism, shear compression failure governed (Girder HD-1.5). However, when stirrups were damaged from corrosion, diagonal tension failure can occur since the stirrups are not enough to resist the tension loads, which led to excessive yielding and wide cracks (Girder MD-1.5S). Anchorage failure may occur when the anchorage length of the

longitudinal reinforcement is inadequate which led to sudden failure from reinforcement or strands pulling out (Girder MD-1.5).

2. Deterioration did not greatly affect the peak load of the girders, but played a larger role in negatively affecting other stages of shear responses for both load schemes. For 1.0 m load scheme, all specimens had capacities well above the factored design load. There was only a 9.6% decrease from the baseline LD-1 to ID-1 with 21% strand loss. However, the effect of strand loss was more significant at the strut formation stage. The strut formed at a lower load by 29% for ID-1 compared to LD-1. This is due to the fact that strand corrosion led to decreased prestressing force in the concrete which means that there was less stress in the concrete to overcome in order to form struts. For the 1.5 m load scheme, there was only a 9.9% difference between the highest and the lowest shear capacities. However, at cracking, strand loss in ID-1.5 reduced the cracking load by 54.8% compared to HD-1.5. Anchorage issue (MD-1.5S) negatively impacted the cracking load by 39.2% compared to HD-1.5. The ability to resist shear before strut formation dropped 32% for ID-1.5 with strand loss.
3. Girder MD-1.5 with failed suddenly with anchorage failure away from the load point with the lowest peak load. Compared to the other tests, anchorage issue played a larger role in affecting the strength of this specimen. Corrosion that leads to anchorage issues, such as end cracking, needs to be carefully examined by bridge inspectors.
4. Even neglecting shear transfer between girders, the shear tests indicated that the strength of the deteriorated girders exceed the shear demands from S6:19 (CSA, 2019). For bridges with similar design and similar levels of deterioration, the bridge safely resisted the design load in service. Moreover, given the flexural result, this bridge was flexural dominant and could safely hold the design load in service under flexure. However, as the rate of

deterioration was not investigated, this observation is only valid for the deterioration conditions exhibited by the girders.

The shear tests showed promising results using three-point bending to investigate the deterioration effect on the shear capacity of the girders. Combined with flexural tests, it allows the investigation of how different types of corrosion such as strand loss, concrete loss or stirrup loss affected the capacity of the girder as a whole. However, the tests showed that it is challenging to investigate the effects of deterioration when there are different levels and types of deterioration at random locations. The authors recommend further investigation with different types and degrees of deterioration on these girders using modeling software, so a more detailed correlation can be investigated on how different degrees of deterioration on different parts of the bridge affect the capacity of the girders. Another future study could focus on the unanalyzed DIC results from the shear test to investigate crack propagation and width which can give a more in depth understanding of how different parts of the girder contributed to the capacity.

CHAPTER 5 : SUMMARY AND CONCLUSIONS

5.1 Summary

Four girders (LD, HD, MD, and ID) with different levels of deterioration were selected from a decommissioned semi-lightweight voided slab prestressed concrete bridge (Tiger Lily Bridge) near Barrhead, Alberta. By analyzing the flexural (Chapter 3) and shear (Chapter 4) response of the deteriorated girders, this thesis shows how different types of deterioration affect girder capacity and failure mode. This work is intended to aid transportation ministries to better understand and anticipate the structural behaviour in girders with similar deterioration conditions.

5.2 Flexural Testing

Chapter 3 showed that tested properties and reinforcement layout of the girders were different than designed. There were four extra 25M bars added for camber control. The average concrete strength (57 MPa) was 51% larger than the specified value (35 MPa). The measured elastic moduli were close (within 10%) to predictions from CSA S6:19, but the accuracy of the predictions slightly increased when concrete age and average air temperature were considered. The predicted nominal flexural strength increased due to the changes in material properties: 5% due to the increase in concrete strength and an extra 25% due to the extra 25 M bars. This indicates that the additional strength of camber-control reinforcement is significant, and should be taken into account if its presence is adequately documented in the construction and design drawings.

The serviceability and ultimate strength of the girders were evaluated. Even though all the girders cracked after they were loaded to the Service Limit State, none of the girders satisfied the deflection limit at service. A possible reason for the deflection limit violation could be that the truck load used for calculating the design SLS and ULS is heavier than the ones used when the bridge was constructed in 1990.

All tested girders failed at loads exceeding the factored ULS loading from CSA S6:19 despite their deterioration. However, deterioration highly affected girder ductility and failure. In Girders LD and MD, the failure mode was the expected concrete crushing at the top after steel yielded; in girders with a higher degree of actual (HD) and simulated (ID) deterioration the failure was sudden with strand rupture before steel yielding. HD and ID had a reduction in flexural strength of 22.9% and 21.8%, respectively compared to the baseline girder LD. Girder MD, with less deterioration, closely followed the behaviour of LD with a slight decrease in flexural strength (14.3%) and stiffness (6.3%). The sudden failure mode in deteriorated girders is attributed to steel corrosion. Steel tensile tests confirmed that strand corrosion greatly affected the post-yield deformation capacity of strands. Strands with a higher degree of corrosion were more brittle and ruptured suddenly with some rupturing before they yielded.

For girders with similar material properties and deterioration, flexural tests indicated that it is possible for these bridges to safely hold the design load in service with the condition that the load is distributed evenly to all girders. However, as indicated by the results from Girder HD, the potential mode of failure of a damaged girder is brittle – not desirable for a bridge structure.

5.3 Shear Testing

Shear testing followed after flexural testing to investigate the shear behaviour of the deteriorated girder because of the likelihood of premature shear failure due to deterioration damage is of concern. As expected, the shear tests indicated that span to depth ratio (a/d) affected the failure modes. For the 1.0 m load scheme with an a/d ratio of 1.96, all specimens failed by strut crushing because less stirrup reinforcement is involved in the arch action mechanism and the longitudinal reinforcement was able to resist the applied load without yielding or catastrophic pullout. For the 1.5m load scheme with an a/d ratio of 2.94, the failure mode depended on various factors. When

the girder was in fair condition where stirrups, flexural reinforcement, and strands were sufficient to resist tension forces in the truss mechanism, shear compression failure governed (Girder HD-1.5). However, when stirrups were damaged from corrosion, diagonal tension failure occurred since the stirrups were not able to resist the tension loads, which led to excessive yielding and wide cracks (Girder MD-1.5S). Anchorage failure may occur when the anchorage length of the longitudinal reinforcement is inadequate which leads to sudden failure from reinforcement or strands pulling out (Girder MD-1.5); however, results indicated that anchorage issue played a larger role in affecting the strength of the girders. Girder MD-1.5 with failed suddenly with anchorage failure away from the load point with the lowest peak load. Corrosion that leads to anchorage issues, such as end cracking, needs to be carefully examined by bridge inspectors.

All specimens performed well by failing after they were loaded to design ULS. Deterioration did not have a large impact on the peak strength of the girders, but it influenced the strength of the girders needed to resist cracking and strut formation. For 1.0 m load scheme, there was only a 9.6% decrease in peak load between baseline LD-1 and Girder ID-1 with 21% strand loss. In contrast, the 21% strand loss affected strut formation more significantly where the strut formed at a lower load by 29% for ID-1 compared to LD-1 due to the fact that strand corrosion led to decreased prestressing force in the concrete meaning there was less stress for the concrete to overcome in order to form struts. For the 1.5 m load scheme, there was only a 9.9% difference between the highest and the lowest shear capacities. However, at cracking, 21% strand loss in ID-1.5 reduced the cracking load by 54.8% compared to HD-1.5.

In summary, though the flexural tests showed that the bridge girders were flexurally controlled (they would fail first in flexure rather than shear), the shear tests indicate that all girders regardless of deterioration state were able to resist the design shear ULS loads at the time of testing.

Although these results are encouraging, the rate of deterioration was not investigated in this study so these observations are only valid for the specific deterioration conditions exhibited by the tested girders.

5.4 Recommendations

The experimental program studied the deterioration effect of a deteriorated decommissioned bridge. As it is initial work of more studies to come, there are several recommendations for future works that are based on the outcome of this thesis.

Further investigation is recommended for different types and degrees of deterioration. This could be accomplished by testing more girders, with various degrees of deterioration, as they are decommissioned by the bridge authority in the province, and using approaches such as finite element modeling to simulate different degrees, localization, and type of deterioration on a validated model.

Another future study could focus on interpreting the unanalyzed DIC results collected in this study from the flexural and shear tests to investigate deformations, strains, and crack development, which can give a more in depth understanding on how the deterioration affected the load transfer mechanisms in the girders.

The rate of deterioration is also recommended to be studied due to the rapid deterioration process of the Tiger Lily Bridge. This work will provide insight on important aspects, such as possible changes in flexure versus shear controlling mechanisms, failure modes, deformation, and residual capacity.

REFERENCES

- ACI Committee 318, (1989). "Building Code Requirements for Reinforced Concrete (ACI 318-89)," *American Concrete Institute*, Detroit, MI, 353 pp.
- Alberta Transportation, (1988). "Prestressed concrete 11 m type SM-510 interior girder".
- Alberta Transportation, (2015). "Bridge inspection and maintenance system 72343-1 bridge".
- Alberta Transportation, (2017). "BIM Advisory Bulletin #6 – May 2017." Alberta Transportation.
- Alberta Transportation, Loo, T., Roberts, G., Atkin, L., Shalagan, R., Chelak, B., Saunders, D., & Herrick, B., (2008). "Bridge Inspection and Maintenance System Inspection Manual version 3.1". Alberta Transportation.
- Alberta Transportation. (2008). "Bridge Inspection & Maintenance System- Inspection Manual." Alberta Transportation.
- Alberta Transportation. (2016). "Bridge Inspection & Maintenance System- Inspection Report." Alberta Transportation.
- American Association of State Highway and Transportation Officials. (2012). *AASHTO LRFD bridge design specifications*, 6th Ed., Washington, DC.
- American Association of State Highway and Transportation Officials. (2009). *AASHTO LRFD bridge design specifications*. 4th edition, 2009 Interim. Washington DC.
- American Association of State Highway and Transportation Officials, (1989). *Standard Specifications for Highway Bridges*, 14th Edition, Washington, D.C., 420 pp
- American Society of Civil Engineers, (2017). "2017 report card for America's infrastructure". Reston, VA.
- ASTM A1061 / A1061M-16, (2016). "Standard Test Methods for Testing Multi-Wire Steel Prestressing Strand", *ASTM International*, West Conshohocken, PA, www.astm.org

- ASTM A370-16, (2016). “Standard Test Methods and Definitions for Mechanical Testing of Steel Products”, *ASTM International*, West Conshohocken, PA, www.astm.org
- ASTM C39 / C39M-14, (2014). “Standard Test Method for Compressive Strength of Cylindrical Concrete Specimens”, *ASTM International*, West Conshohocken, PA, 2014, www.astm.org
- ASTM C469 / C469M-14e1, (2014). “Standard Test Method for Static Modulus of Elasticity and Poisson's Ratio of Concrete in Compression”, *ASTM International*, West Conshohocken, PA, 2014, www.astm.org
- Badawi M, Soudki K. (2005). “Control of corrosion-induced damage in reinforced concrete beams using carbon fiber-reinforced polymer laminates”. *Journal of Composites for Construction* 2005;9(2):195–201.
- Barker, R. M., & Puckett, J. A. (2013). *Design of Highway Bridges: an LRFD Approach*, 3rd Ed. John Wiley & Sons, Inc.
- Bertolini, L., Elsener, B., Pedferri, P., Polder, R. (2004). *Corrosion of Steel in Concrete, Prevention, Diagnosis, Repair*, 1st Ed. Wiley, Weinheim, 409 pp
- Birhane, F. N., Kim, S.-I., & Jang, S. Y. (2020). “Long-Term deflection of prestressed concrete Bridge Considering Nonuniform Shrinkage and Crack Propagation by equivalent load approach”. *Applied Sciences*, 10(21), 7754. <https://doi.org/10.3390/app10217754>
- Bolen, W. P., & Barnes, L. M., (2016). *2016 Minerals Yearbook*. Washington, D.C.; U.S. Dept. of the Interior, Bureau of Mines.
- Canadian Infrastructure Report Card (CIRC), (2019). *Canadian infrastructure report card (roads and bridges)*. <http://canadianinfrastructure.ca/en/municipal-roads.html>

- Canadian Precast Prestressed Concrete Institute. (2007). *CPCI Design Manual*, 4th. Ed. Ottawa, Ontario.
- Canadian Precast Prestressed Concrete Institute. (2017). *CPCI Design Manual*, 5th Edition. Ottawa, Ontario.
- Canadian Standards Association. (2014). *CSA S6:14 Canadian Highway Bridge Design Code*. Mississauga, Ontario.
- Canadian Standards Association. (2016). *CSA S6:16 Canadian Highway Bridge Design Code*. Mississauga, Ontario.
- Canadian Standards Association. (2019). *CSA S6:19 Canadian Highway Bridge Design Code*. Mississauga, Ontario.
- Cullington, D. W., & Raggett, S. J. (1991). *Shear strength of some 30-year-old prestressed beams without links*. Transport and Road Research Laboratory, Transport Planning Division.
- Dasar, A., Irmawaty, R., Hamada, H., Sagawa, Y., & Yamamoto, D. (2016). "Prestress loss and bending capacity of pre-cracked 40-year-old PC beams exposed to marine environment". *MATEC Web of Conferences*, 47, 02008. <https://doi.org/10.1051/mateconf/20164702008>
- Dunker, K. F., and Rabbat, B. G. (1992). "Performance of Prestressed Concrete Highway Bridges in the United States- The First 40 Years." *PCI Journal*, 37(3), 48–64.
- Dunker, K. F., and Rabbat, B. G. (1995). "Assessing Infrastructure Deficiencies: The Case of Highway Bridges." *Journal of Infrastructure Systems*, 1(2), 100–119. [https://doi.org/https://doi.org/10.1061/\(ASCE\)1076-0342\(1995\)1:2\(100\)](https://doi.org/10.1061/(ASCE)1076-0342(1995)1:2(100))
- Federal Highway Administration, (2018). *Bridge preservation guide: maintaining a resilient infrastructure to preserve mobility*.

- Floyd, R.W., Pei, J., Tang, P., & Murray, C. (2016). *Understanding the Behavior of Prestressed Girders after Years of Service*. Final Report. Oklahoma Department of Transportation
- Gash, M. (2007). *The collapsed 35W bridge in Minneapolis*. National Public Radio.
- Goodwin, P. (1977). Habit and Hysteresis in Mode Choice. *Urban Studies* 14(1), 95–98.
- Government of Canada. (2021). *Temperature and Precipitation Graph for 1981 to 2010 Canadian Climate Normals EDMONTON STONY PLAIN*. Retrieved September 17, 2021, from https://climate.weather.gc.ca/climate_normals/results_1981_2010_e.html?searchType=stnName&txtStationName=edmonton&searchMethod=contains&txtCentralLatMin=0&txtCentralLatSec=0&txtCentralLongMin=0&txtCentralLongSec=0&stnID=1870&dispBack=0.
- Hobbs, D.W. (1988). *Alkali-Silica Reaction in Concrete*, 1st Ed. Thomas Telford, London, 183 p.
- Huang, L. (2020). *Finite Element-based Parametric and Probabilistic Analysis of Structural Deterioration in Corroded Pre-stressed Concrete Girders*. MSc, University of Alberta, Edmonton, Alberta.
- Hurd, M. K. (1985). “Economical Short Span Concrete Bridges.” *Concrete Construction*, <https://www.concreteconstruction.net/how-to/construction/economical-short-span-concrete-bridges_o> (May 25, 2021).
- IDVIA. (2020). “Reasons for the collapse of a bridge: Morandi Bridge”. <https://www.idvia.es/en/reasons-for-the-collapse-of-a-bridge-morandi-bridge> (August 18, 2021).
- Jayaseelan, H., and Russell, B. W., (2007). “Prestress losses and the estimation of long-term deflections and camber for prestressed concrete bridges,” *Final Report*, School of Civil Environmental Engineering, Oklahoma State University.

- Johnson, P.M., Couture, A., Nicolet, R., Trudeau, N., & Desprez, M., (2007). *Commission of inquiry into the collapse of a portion of the de la Concorde overpass*, October 3, 2006-October 15, 2007: report. Montréal, Québec.; Commission d'enquête sur le viaduc de la Concorde Québec.
- Koch, G. H., Brongers, M. P. H., Thompson, N. G., Virmani, Y. P., & Payer, J. H. (2002). “Corrosion Cost and Preventive Strategies in the United States”. *Final report*.
- Kuo, W. W., Cheng, T. J., & Hwang, S. J. (2010). “Force transfer mechanism and shear strength of reinforced concrete beams”. *Engineering Structures*, 32(6), 1537–1546. <https://doi.org/10.1016/j.engstruct.2010.02.002>
- Lane, D. S., (1994). *Alkali Silica Reactivity in Virginia*. Charlottesville; Virginia Transportation Research Council.
- Lukschová, Š., Příkryl, R., & Pertold, Z. (2009). “Petrographic identification of alkali–silica reactive aggregates in concrete from 20th century bridges”. *Construction and Building Materials*, 23(2), 734–741. <https://doi.org/10.1016/j.conbuildmat.2008.02.020>
- Mahoney, J. (2006). *An aerial view of the de la Concorde overpass collapse hours after it happened on Sept. 30, 2006*. Montreal Gazette. <https://montrealgazette.com/news/local-news/10-years-since-de-la-concorde-overpass-collapse>.
- Malumbela, G., Alexander, M., & Moyo, P. (2010). “Variation of steel loss and its effect on the ultimate flexural capacity of RC beams corroded and repaired under load”. *Construction and Building Materials*, 24(6), 1051–1059. <https://doi.org/10.1016/j.conbuildmat.2009.11.012>
- Miller, R., & Parekh, K. (1994). “Destructive Testing of Deteriorated Prestressed Box Bridge Beam”. *Engineering Research Record*.

- Moore, M., Phares, B., Graybeal, B., Rolander, D., & Washer, G., (2001). *Reliability of visual inspection for Highway Bridges, Volume I: Final report*. McLean, VA; U.S. Department of Transportation.
- Murray, C. D., Cranor, B. N., Floyd, R. W., & Pei, J.-S. (2019). "Experimental Testing of Older AASHTO Type II Bridge Girders with Corrosion Damage at the Ends". *PCI Journal*, 64(1).
<https://doi.org/10.15554/pcij64.1-02>
- Naito, C., Sause, R., & Thompson, B. (2008). "Investigation of Damaged 12-Year Old Prestressed Concrete Box Beams". *Journal of Bridge Engineering*, 13(2), 139–148.
[https://doi.org/10.1061/\(asce\)1084-0702\(2008\)13:2\(139\)](https://doi.org/10.1061/(asce)1084-0702(2008)13:2(139))
- Naito, C., Sause, R., Hodgson, I., Pessiki, S., & Desai, C., (2006). *Forensic Evaluation of Prestressed Box Beams from the Lake View Drive over I-70 Bridge*. Bethlehem, Pennsylvania; ATLSS.
- National Transportation Safety Board, (2008). *Collapse of I-35W highway bridge Minneapolis, Minnesota, August 1, 2007*. Washington, D.C.
- Nowak, A. S., & El-Hor, H. H. . (1995). "Serviceability Criteria for Prestressed Concrete Bridge Girders". *Forth International Bridge Engineering Conference*, 2(7), San Francisco, California.
- Nürnberg, U. (1996). "Stainless Steel in Concrete- State of the Art Report", *European Federation of Corrosion Publications*, No. 18.
- Office of Research & Implementation, Floyd, R., Pei, J.-S., Murray, C., Cranor, B., & Tang, P., (2016). *Understanding the Behavior of Prestressed Girders after Years of Service*. Oklahom; Oklahoma Department of Transportation.

- Ohno, M., Chijiwa, N., Suryanto, B., & Maekawa, K. (2012). “An Investigation into the Long-Term Excessive Deflection of PC Viaducts by Using 3D Multi-scale Integrated Analysis”. *Journal of Advanced Concrete Technology*, 10(2), 47–58. <https://doi.org/10.3151/jact.10.47>
- Osborn, G. P., Barr, P. J., Petty, D. A., Halling, M. W., & Brackus, T. R. (2012). “Residual Prestress Forces and Shear Capacity of Salvaged Prestressed Concrete Bridge Girders”. *Journal of Bridge Engineering*, 17(2), 302–309. [https://doi.org/10.1061/\(asce\)be.1943-5592.0000212](https://doi.org/10.1061/(asce)be.1943-5592.0000212)
- Panchak, P. (2005). *Pittsburgh Post-Gazette*. <https://www.post-gazette.com/local/washington/2005/12/28/Westbound-I-70-reopens-after-overpass-collapses/stories/200512280148>.
- Pape, T.M. and Melchers, R.E., (2013). “Performance of 45-year-old corroded prestressed concrete beams”. *Proceedings of the Institution of Civil Engineers-Structures and Buildings*, 166(10), pp.547-559.
- PCI Industry Handbook Committee (2010). *PCI Design Handbook – Precast and Prestressed Concrete*, 7th Edition. Precast/Prestressed Concrete Institute, Chicago, Illinois.
- PCI Industry Handbook Committee (2011). *PCI Design Handbook – Precast and Prestressed*, 7th Edition. Chicago, Illinois.
- Pei, J. S., Martin, R. D., Sandburg, C. J., and Kang, T. H.-K. (2008). “Rating precast prestressed concrete bridges for shear.” Report No. ODOT SPR ITEM 2186, University of Oklahoma.
- Pessiki, S., Kaczinski, M., and Wescott, H. H. (1996). “Evaluation of Effective Prestress Force in 28-Year-Old Prestressed Concrete Bridge Beams.” *PCI Journal*, 41(6), 78–89.

- Pettigrew, C. S., Barr, P. J., Maguire, M., and Halling, M. W. (2016). "Behavior of 48-Year-Old Double-Tee Bridge Girders Made with Lightweight Concrete." *Journal of Bridge Engineering*, 21(9), 04016054.
- Rajabipour, F., Giannini, E., Dunant, C., Ideker, J. H., & Thomas, M. D. A. (2015). "Alkali-silica reaction: Current understanding of the reaction mechanisms and the knowledge gaps". *Cement and Concrete Research*, 76, 130–146.
<https://doi.org/10.1016/j.cemconres.2015.05.024>
- Ramseyer, C., & Kang, T. H.-K. (2012). "Post-damage repair of prestressed concrete girders". *International Journal of Concrete Structures and Materials*, 6(3), 199–207.
<https://doi.org/10.1007/s40069-012-0019-7>
- Rinaldi, Z., Imperatore, S. and Valente, C., (2010). "Experimental evaluation of the flexural behaviour of corroded P/C beams". *Construction and Building Materials*, 24(11), pp.2267-2278.
- Saqan, E., & Frosch, R. (2009). "Influence of Flexural Reinforcement on Shear Strength of Prestressed Concrete Beams". *ACI Structural Journal*, 106(1).
<https://doi.org/10.14359/56284>
- Shenoy, C. V., and Frantz, G. C. (1991). "Structural Tests of 27-Year-Old Prestressed Concrete Bridge Beams." *PCI Journal*, 36(6), 80–90.
- Sinha, S.N., (2002). *Reinforced Concrete Design*, 2nd Ed. Tata McGraw-Hill.
- Soudki, K., Sherwood, T.G., (2000). "Behaviour of reinforced concrete beams strengthened with carbon fibre reinforced polymer laminates subjected to corrosion". *Canadian Journal of Civil Engineering*, 27(5).

- The Department BIM Committee, Loo, T., Roberts, G., Atkin, L., Shalagan, R., Chelak, B., Saunders, D., and Herrick, B. (2018). *Bridge Inspection and Maintenance System Inspection Manual*, Government of the Province of Alberta.
- Thomas, M. D. A., Fournier, B., & Folliard, K. J., (2013). *Alkali-aggregate reactivity (AAR) facts book*. Final Report.
- Wight, J. K., & MacGregor, J. G (2012), *Reinforced Concrete Mechanics and Design*, 6th Ed., pp. 243–310. Essay Pearson Education, Inc.
- Zhu, S., & Levinson, D. M., (2010). *Traffic flow and road user impacts of the collapse of the I-35W Bridge over the Mississippi River*. St. Paul, MN; Minnesota Department of Transportation, Research Services Section